TECHNISCHE UNIVERSITÄT MÜNCHEN

Fakultät für Medizin

Identification, isolation and characterization of T cell receptors for adoptive T cell therapy in tumor and viral infections

Karolin Isabel Wagner

Vollständiger Abdruck der von der Fakultät für Medizin der Technischen Universität München zur Erlangung eines

Doctor of Philosophy (Ph.D.)

genehmigten Dissertation.

Vorsitz: Prof. Dr. Stefan Lichtenthaler

Betreuer*in: Prof. Dr. Dirk H. Busch

Prüfer*innen der Dissertation:

1. Prof. Dr. Markus Gerhard
2. Prof. Dr. Radu Roland Rad
3. Prof. Dr. Marion Subklewe

Die Dissertation wurde am 13.06.2022 bei der Fakultät für Medizin der Technischen Universität München eingereicht und durch die Fakultät für Medizin am 30.07.2022 angenommen.

Institut für Medizinische Mikrobiologie, Immunologie und Hygiene
Fakultät für Medizin
Technische Universität München

Identification, isolation and characterization of T cell receptors for adoptive T cell therapy in tumor and viral infections

Karolin Isabel Wagner

Vollständiger Abdruck der von der Fakultät für Medizin der Technischen Universität München zur Erlangung des akademischen Grades eines

Doctor of Philosophy (Ph.D.)

genehmigten Dissertation.

Vorsitz:
Prof. Dr. Stefan Lichtenthaler

Betreuer*in:
Prof. Dr. Dirk H. Busch

Prüfer*innen der Dissertation:
1. Prof. Dr. Markus Gerhard
2. Prof. Dr. Roland Rad
3. Prof. Dr. Marion Subklewe

Die Dissertation wurde am 13.06.2022 bei der Technischen Universität München eingereicht und durch die Fakultät für Medizin am 30.07.2022 angenommen.

Abstract

The transfer of T cell immunity for the treatment of viral infections and tumor malignancies by the adoptive transfer of, respectively, donor- and patient-derived autologous T cells has been therapeutically exploited in different disease settings, and has shown safety and clinical efficacy. The generation of less patient-individualized cell sources for adoptive T cell therapy, for example by genetic engineering to express tumor-specific T cell receptors (TCRs), represents a promising development in cancer immunotherapy. Especially, T cells targeting neo-epitopes derived from frameshift (fs)-mutations of tumor suppressor genes are of highest interest, as antigen expression is exclusive to the tumor and on-target/off-tumor toxicity would be minimized. A source for the identification of neo-epitope-specific TCRs can be the naive repertoire of healthy donors, due to its huge diversity that should encompass all kinds of specificities. In addition, having passed central tolerance, natural peripheral TCR repertoires show a high safety profile for therapeutic application. However, naive neo-antigen-specific T cells with high functionality are extremely low in frequency, and therefore difficult to isolate.

Here, we focus on neo-epitopes derived from Ring Finger Protein 43 (RNF43), a tumor suppressor gene that upon loss of function enhances tumor growth, and is frequently fs-mutated in pancreatic ductal adenocarcinoma (PDAC), among other gastro-intestinal cancers. PDAC is a cancer with very poor prognosis and limited treatment options for the patient. Thus, novel PDAC therapies are urgently needed and open the opportunity to explore new strategies.

We developed a platform for the isolation of extremely rare epitope-specific naive $CD8^+$ T cells from peripheral blood of healthy donors via single cell sorting on combinatorial peptide major histocompatibility complex (pMHC) multimer staining. Sequencing of sorted epitope-specific T cells revealed the TCR sequence for re-expression and functional characterization. We used the recently by our group developed CRISPR/Cas9-mediated orthotopic TCR replacement for knockout of the endogenous TCR and knockin of the transgenic TCRs into the endogenous TCR locus for physiological re-expression in donor T cells. In subsequent *in vitro* functional assays, we assessed TCR specificity via pMHC multimer staining and T cell functions by the measurements of TCR structural avidity (k_{off}-rate), peptide sensitivity and cytotoxicity.

As proof of principle, we successfully isolated highly functional TCRs specific for HLA-A*02:01 and HLA-B*07:02 restricted RNF43 neo-epitopes, which may already serve as candidates for clinical translation. More broadly, the presented workflow can be applied to any tumor antigen and entity, and we propose an outlook to platform adaptations for high-throughput identification of highly functional TCRs.

In light of the Coronavirus Disease 2019 (COVID-19) pandemic, we transferred the methodology and expertise in the identification and characterization of antigen-reactive

Abstract

T cells also to the field of viral infection. With such interdisciplinary approach, we identified transcriptional signatures of severe acute respiratory syndrome corona virus 2 (SARS-CoV-2)-reactive T cells and identified immunogenic epitopes. Further, we describe long-lasting, polyclonal and highly functional $CD8^+$ T cell response in mild convalescent donors.

Zusammenfassung

Die Übertragung von T-Zell-Immunität zur Behandlung von Virusinfektionen und bösartigen Tumorerkrankungen durch den adoptiven Transfer von Spender T-Zellen oder autologen T-Zellen des Patienten wurde in verschiedenen Krankheitsbereichen therapeutisch genutzt und hat sich als sicher und klinisch wirksam erwiesen. Die Entwicklung von weniger patientenindividuellen Zellquellen für die adoptive T-Zell-Therapie, z.B. durch gentechnische Veränderung der Expression tumorspezifischer T-Zell-Rezeptoren (TCRs), stellt einen vielversprechenden Fortschritt in der Krebsimmuntherapie dar. Insbesondere T-Zellen, die Neo-Epitope erkennen, die aus frameshift (fs)-Mutationen von Tumorsuppressorgenen stammen, sind von außerordentlichem Interesse, da die Antigenexpression ausschließlich im Tumor stattfindet und die On-Target/Off-Tumor-Toxizität minimiert würde. Eine Quelle für die Identifizierung von Neo-Epitop-spezifischen TCRs kann das naive Repertoire gesunder Spender sein, das aufgrund seiner natürlichen Vielfalt, alle Arten von Spezifitäten umfassen sollte. Darüber hinaus weisen die natürlichen, peripheren TCR-Repertoires, dadurch dass sie die zentrale Toleranz überwunden haben, ein hohes Sicherheitsprofil für die therapeutische Anwendung auf. Naive Neo-Antigen-spezifische T-Zellen mit hoher Funktionalität sind jedoch in ihrer Häufigkeit äußerst gering und daher schwer zu isolieren.

Hier konzentrieren wir uns auf Neo-Epitope, die vom Ringfingerprotein 43 (RNF43) abgeleitet sind, einem Tumorsuppressorgen, welches bei Funktionsverlust das Tumorwachstum fördert und bei duktalen Adenokarzinomen des Pankreas (PDAC) und anderen gastrointestinalen Krebsarten häufig fs-mutiert ist. PDAC ist eine Krebsart mit sehr schlechter Prognose und begrenzten Behandlungsmöglichkeiten für die Patienten. Daher werden neue PDAC-Therapien dringend benötigt und bieten die Möglichkeit neue Strategien zu erforschen. Wir haben eine Plattform für die Isolierung extrem seltener epitopspezifischer naiver $CD8^+$ T-Zellen aus dem peripheren Blut gesunder Spender entwickelt, die mittels Einzelzellsortierung auf kombinatorischen Peptid-Multimeren des Haupthistokompatibilitätskomplexes (pMHC) basiert. Die Sequenzierung der sortierten epitopspezifischen T-Zellen ergab die TCR-Sequenz zur Reexpression und funktionellen Charakterisierung. Wir nutzten den kürzlich von unserer Gruppe entwickelten CRISPR/-Cas9-vermittelten orthotopen TCR-Austausch zum Knockout des endogenen TCRs und Knockin eines transgenen TCRs in den endogenen TCR-Lokus zur physiologischen Reexpression in Spender-T-Zellen. In anschließenden *in vitro*-Funktionstests haben wir die TCR-Spezifität über pMHC-Multimere und die T-Zell-Funktionalität durch Messungen der TCR-Strukturavidität (k_{off}-rate), der Peptidsensitivität und der Zytotoxizität bestimmt.

Wir haben hochfunktionelle TCRs erfolgreich isoliert, die für HLA-A*02:01 und HLA-B*07:02 beschränkte RNF43-Neoepitope spezifisch sind und bereits als Kandidaten für

die klinische Umsetzung dienen könnten. Der damit vorgestellte und validierte Arbeitsablauf kann im weiteren Sinne auf jedes Tumorantigen und jede Tumorerkrankung angewandt werden und wir geben einen Ausblick auf Technologieentwicklungen für Hochdurchsatzidentifizierung von hochfunktionalen TCRs.

Vor dem Hintergrund der COVID-19 Pandemie haben wir die Methodik und das Fachwissen zur Identifizierung und Charakterisierung antigenreaktiver T-Zellen auch auf den Bereich der Virusinfektion übertragen. Mit diesem interdisziplinären Ansatz identifizierten wir Transkriptionssignaturen von SARS-CoV-2-reaktiven T-Zellen und identifizierten immunogene Epitope. Darüber hinaus beschreiben wir eine langanhaltende, polyklonale und hochfunktionale $CD8^+$ T-Zell-Antwort bei genesenen Patienten mit mildem Krankheitsverlauf.

Contents

List of Figures

List of Tables

Abbreviations

β2m	β2-microglobulin
aa	amino acid
ACT	adoptive T cell therapy
aHSCT	allogeneic hematopoietic stem cell transplantation
APC	antigen-presenting cell
APL	altered peptide ligand
BFP	blue fluorescent protein
bp	base pair
C	constant
CAR	chimeric antigen receptor
Cas9	CRISPR-associated protein 9
CD	cluster of differentiation
CDR	complementarity determining region
CEA	carcinoembryonic antigen
CMV	cytomegalovirus
COVID-19	Coronavirus Disease 2019
CRISPR	clustered regularly interspaced short palindromic repeats
crRNA	CRISPR RNA
D	diversity
DMEM	Dulbecco's modified eagle medium
DMSO	dimethyl sulfoxide
DNA	deoxyribonucleic acid
dsDNA	double-stranded DNA
e.g.	exempli gratia
EMA	ethidium monoazide
FACS	Fluorescence activated cell sorting
FCS	fetal calf serum
fs	frameshift
GFP	green fluorescent protein

GI	gastro-intestinal
GMP	good manufacturing practice
gRNA	guide RNA
Gy	Gray
HDR	homology-directed repair
HLA	human leukocyte antigen
ICCS	intracellular cytokine staining
IFN-γ	Interferon-γ
IFNG	Interferon-γ (gene)
IL-15	Interleukin-15
IL-2	Interleukin-2
IL-7	Interleukin-7
Iono	ionomycin
J	joining
J-TPR	Jurkat triple parameter reporter
KI	knockin
KO	knockout
LC-MS	liquid chromatography mass spectrometry
mAB	monoclonal antibody
MAGE	melanoma antigen
MHC	major histocompatibility class
MSLN	mesothelin
mTRBC	murine T cell receptor *beta* chain
NGS	next generation sequencing
NHEJ	non-homologous end joining
O/N	over night
ORF	open reading frame
OTR	orthotopic TCR replacement
PBMC	Peripheral mononuclear blood cell
PBS	phosphate-buffered saline
PCR	polymerase chain reaction
PD-1	programmed cell death 1
PDAC	pancreatic ductal adenocarcinoma
PDX	patient derived xenografts
PHA	phytohaemagglutinin

PI	Propidium iodide
PMA	phorbol myristate acetate
pMHC	peptide major histocompatibility complex
RNA	ribonucleic acid
RNF43	Ring Finger Protein 43
RNP	ribonucleoprotein
RPMI	Roswell Park Memorial Institute medium
RT	room temperature
SARS-CoV-2	severe acute respiratory syndrome corona virus 2
scRNAseq	single cell RNA sequencing
SE	'speed enrichment'
T:E	target to effector
TAA	tumor-associated antigen
TAP	antigen peptide-transporter
TCR	T cell receptor
TIL	tumor infiltrating lymphocyte
TLA	targeted locus amplification
TME	tumor microenvironment
TNFα	tumor necrosis factor *alpha*
TRAC	T cell receptor *alpha* chain
tracrRNA	trans-activating crRNA
TRBC	T cell receptor *beta* chain
TRX	Triton X-100
ue	unedited
UV	ultraviolet
V	variable
WES	whole exome sequencing
WHO	World Health Organization
wt	wild type

1 Introduction

The human immune system is a highly complex network of cellular and humoral effector mechanisms. Its key function is to distinguish between self and non-self: be tolerant to self while consistently surveying the environment and eventually elicit an immune response upon encounter with a pathogen or aberrant cell structure. The immune system consists of two functional, highly integrative components: the innate and the adaptive immune system. The innate immune system is, on an evolutionary scale, more ancient. With its various physical, biochemical and cellular barriers, it constitutes the primary defence against an invading pathogen. The innate immune response is immediate upon pathogenic encounter but is rather unspecific. Indeed, cells of the innate system recognize invading pathogens via their repetitive structures called pathogen-associated molecular patterns. In contrast, the adaptive immune system is highly specific for the invading pathogen and has the capacity to generate memory, which provides long-term protection against secondary encounter with the same pathogen. Cells of the adaptive immune system are T and B lymphocytes. B cells can recognize very diverse antigens with their B cell receptor and mediate the antibody dependent immune response. Upon antigen recognition, antibodies are secreted and circulate through the blood stream to specifically recognize and bind foreign antigens for removal of pathogens by phagocytic cells. On the contrary, T cells build the cell-mediated immune response of the adaptive immune system. T cells recognize peptides (small chains of amino acid (aa)) that are bound to major histocompatibility class (MHC) (also named human leukocyte antigen (HLA)) and when eliciting an immune response are designated as 'epitopes'. T cells are strongly involved in the active killing of virus infected or otherwise aberrant host cells, but also in the activation and homeostatic regulation of other cell-mediated immune activities. Here, we focus on cytotoxic T cells recognizing viral targets or tumor-associated antigens (TAAs) and emphasize the transferability of T cells in therapeutic application in cancer adoptive T cell therapy (ACT).

1.1 T cells mediate highly specific and potent immune responses

1.1.1 Early T cell development and generation of the naive repertoire

T cells only recognize cognate epitopes displayed on antigen-presenting cells (APCs) via a membrane-bound protein complex - the T cell receptor (TCR). The ability of the TCR repertoire to recognize virtually any foreign antigen is rooted in the early T cell development. The TCR is encoded by a wide set of discrete gene segments that are joined by somatic recombination to individual chains during T cell development. In this

way, a large range of repertoire diversity with specificity to theoretically any antigen is encoded in a limited genomic space. In detail, the TCR is a heterodimeric protein that consists of an *alpha* and a *beta* chain (Fig. 1.1 A). Each chain is characterized by a variable (V) and constant (C) region. In the V region of each TCR chain, there are three hypervariable, or complementarity determining regions (CDRs), each corresponding to a loop in the V domain. The CDR3 is the most variable region determining antigen specificity [1]. For proper antigen recognition, both chains are required. TCRs recognize antigens, but for further signal transmission to initiate cellular activity, co-receptors such as CD8 and CD4 are needed.

T cells originate from the bone marrow stem cells and migrate as pre-cursor cells to the thymus for further development and maturation. At first, the progenitor cells are devoid of any co-receptors and are considered double-negative ($CD4^-CD8^-$). At this stage, cells undergo extensive somatic gene rearrangements of the TCR encoding genes segments (Fig. 1.1 B). First, the *beta* chain is produced by random combinations of the V, diversity (D) and joining (J) segments. Small nucleotide changes of insertions and deletions further increase junctional diversity and increase the ability of the different variations in the antigen-recognizing CDR3 region. Productive VDJ recombination of the *beta* chain leads to allelic exclusion and silencing of rearrangement of the other allele. In case of a non-functional chain due to out-of-frame or incomplete rearrangement, recombination will occur in the second inherited locus. Once a TCR *beta* chain protein is synthesized, it is expressed on the surface in association with an invariant pre-T*alpha*, to form the pre-TCR complex of pre-T cells. At this stage, progenitor cells become double positive in expression of CD3/CD4 and CD8 co-receptors. The pre-TCR complex then initiates VJ segment recombination for the *alpha* chain. Similarly to the *beta* chain, rearranged segments for the *alpha* chain are joined with high diversity. However, genotypic allelic exclusion, which ensures single *beta* chain expression, does not apply for the TCR *alpha* chain. In almost all mature T cells, both *alpha* loci were found to be fully rearranged with two fully productive *alpha* chains identified in 25 % of T cells [2]. Further, the diversity is increased by the ability of different TCR *alpha* and *beta* chains to pair. However, in the presence of two *alpha* chains, usually only one *alpha beta* chain pair will be eventually expressed on the surface [3]. Progenitor cells that fail to produce functional chain expression are eliminated from further development and undergo cell death. In the following step of lymphocyte maturation, the vast diversity of rearranged TCRs needs to be selected for functionality and safety in subsequent maturation steps. In the process of central tolerance, TCR expressing T cell progenitors are tested for MHC recognition. A self MHC molecule displaying a self-peptide is presented to the developing T cell. Cells with low to moderate binding strength to the MHC are positively selected. In this process, T cells become single positive with either CD4 or CD8 expression depending on the recognition of either MHC Class II or Class I molecules. T cells that do not recognize a MHC molecule in the thymus die by apoptosis. Strong recognition of the self-antigen/MHC will result in negative selection and such TCRs are eliminated from the evolving repertoire. This is an important mechanism to exclude autoreactive T cells from further maturation. Finally, only 3-5 % of thymocytes mature with successful TCR chain rearrangement and are released into the periphery as naive, antigen-inexperienced

T cells to migrate through the secondary lymphoid organs for antigen exposure and T cell priming [4].

Estimations of TCR diversity have calculated a theoretical receptor repertoire of 10^{20}-10^{61} uniquely re-arranged chains [5,6]. However, this number is much larger than what is eventually observed in the peripheral TCR repertoire. Biological features of skewed recombination events, preferential chain pairing and finally thymic selection reduces the overall repertoire diversity to an estimated number of approximately 10^6 to 10^8 unique TCRs for a human individual [5,7].

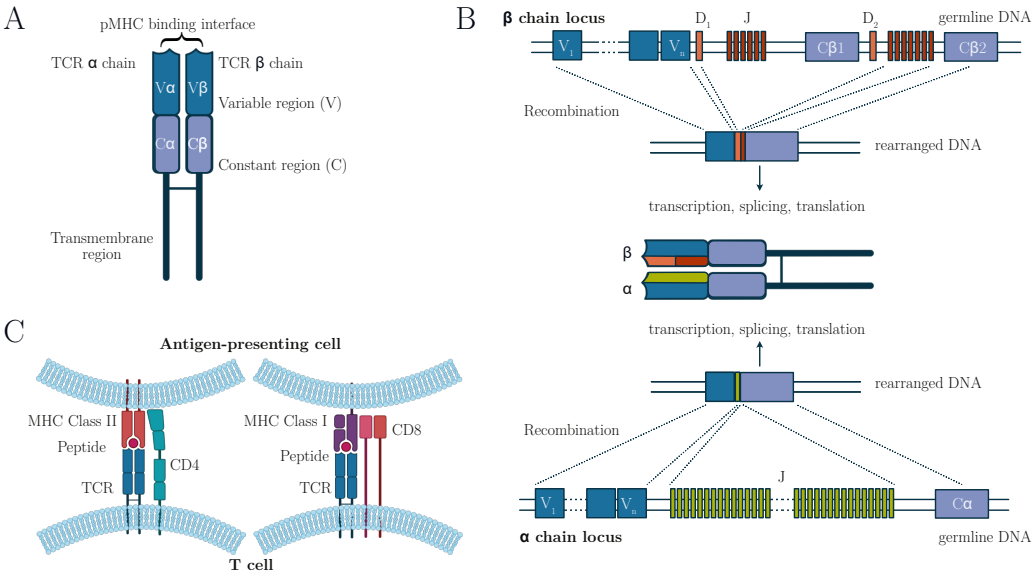

Figure 1.1: TCR structure, germline rearrangement and pMHC interaction. A) Schematic depiction of a heterodimer TCR with an *alpha* and a *beta* chain consisting of a variable and a constant region. The variable region accommodates the CDR3 region which mediates highly specific pMHC recognition. A disulfide bond connects the two chains and the transmembrane domain anchors the receptor in the cell membrane. B) Somatic recombination creates high receptor diversity by combining variable (V), joining (J) and constant regions (C) to constitute the TCR *alpha* chain. For the TCR *beta* chain an additional diversity (D) region is joined with V, J and C-regions. C) Schematic depiction of the interaction of a TCR with peptide major histocompatibility complex (pMHC) molecules. The TCR of a $CD4^+$ or a $CD8^+$ T cell recognizes MHC Class II or MHC Class I bound peptide respectively.

1.1.2 T cell target recognition and effector response

According to the surface expression of their co-receptors, T cells are subdivided into $CD4^+$ and $CD8^+$ T cells (Fig. 1.1 C). $CD4^+$ T cells recognize their target epitope on MHC Class II complex. Only professional APCs, such as B cells, macrophages and dendritic cells express MHC Class II and present mostly extracellular peptides that

entered a cell via receptor-mediated endocytosis or phagocytosis. $CD4^+$ T cells primarily function in cytokine release and play a key role in ensuring optimal immune response by other lymphocytes. Besides their function in tissue immune homeostasis as regulatory T cells, their 'helper' function promotes B cell activity and strengthens the generation of cytotoxic $CD8^+$ and memory T cell populations. On the contrary, $CD8^+$ T cells recognize peptides presented on the MHC Class I complex. This molecule is expressed not only on APCs, but also on all other nucleated cells. The MHC Class I complex specifically presents cytosolic peptides. Beside self-peptides that can bind to the MHC Class I, intracellular processed non-self-peptides, often originating from tumor mutation-derived proteins or viral infection, are presented at the cell surface for immune recognition.

Initially, $CD8^+$ T cells need to be primed for antigen-recognition and this usually happens distant from the site of infection/tumor tissue. APCs, such as dendritic cells, sense the infection and move to the nearest lymph node for peptide presentation to naive T cells. This process of cross-presentation of exogenous antigens and cross-priming of naive $CD8^+$ T cells is crucial for effective immune response triggered by viral infections and tumor cells. The structural binding of TCR to pMHC is of rather low avidity and has been selected in the thymus for low binding strength to self-peptides. Non-self-peptides however are recognized with higher avidity and are sufficient to prime T cell activation. Once activated, $CD8^+$ T cells move to the periphery, undergo clonal expansion and develop into short-lived effector T cells with heterogeneous phenotypes and functionality. Upon direct target cell contact and positive recognition of non-self-peptides, activated $CD8^+$ T cells release cytokines (such as Interferon-γ (IFN-γ), Interleukin-2 (IL-2) and tumor necrosis factor *alpha* (TNFα)) and other pro-apoptotic molecules that initiate cell death of the target expressing cell. Once the viral infection or tumor target is cleared, only a small percentage of effector T cells with a more stemness phenotype survive and persist as long-lived memory cells in the tissue or circulating through the lymphoid system. The contraction of effector cell populations is important to avoid overgrowing, large clonal populations at the expense of smaller ones. Still, the small proportion of memory cells surviving remains higher than the frequency of naive T cells and can induce an immediate response upon secondary antigen-encounter [8].

1.2 Adoptive T cell therapy

The immune system can raise highly potent and target-specific T cell-mediated immune responses to potentially any non-self-antigen and subsequently establish memory to protect against re-infection. The transfer of acquired T cell immunity via ACT has been used therapeutically over the last decades, and was first explored in immunocompromised patients upon allogeneic hematopoietic stem cell transplantation (aHSCT) often suffering from viral infections. In detail, virus-specific T cells were isolated from a virus-seropositive stem cell donor and transferred into a patient to restore viral immunity and protect against reactivation of cytomegalovirus (CMV) after aHSCT [9]. The discovery of tumoricidal T cells within tumor infiltrating lymphocytes (TILs) and deeper insights into the tight interplay of a tumor cell with the immune system have paved the way of

cancer immunotherapy. The often highly immunosuppressive tumor microenvironment (TME) can for example be targeted by so-called 'checkpoint inhibitors'. These are therapeutic antibodies targeting immune inhibitory molecules such a as programmed cell death 1 (PD-1) or PD-L1 and CTLA-4, thereby blocking the interaction with the immune system to release the breaks from the immune system to become active in killing the tumor target cell. In this way, the already existing endogenous, polyclonal repertoire of a patient becomes activated. Further, cancer vaccines are being developed to immunize for recognition of cancer targets and build up natural immunity [10]. However, these approaches rely on the existence of highly functional T cells that can be reactivated in the patient. Although for many tumors initial therapeutic effects with checkpoint inhibitors have been described, durable responses are still rare and limited to certain tumor entities. Therefore, an alternative and promising approach is the adoptive transfer of tumor-specific engineered T cells.

1.2.1 Tumor infiltrating lymphocytes

Elevated levels of cytotoxic $CD8^+$ T cells in the TME are correlated with improved anti-tumor effects and prognosis in various types of cancer [11–16], indicating a crucial role in tumor recognition and control. Especially, melanoma turned out to be a highly immunogenic cancer type and was pioneering in the development of cancer immunotherapies.

In the 1980s, the first studies by Rosenberg and colleagues reported the isolation and re-transfer of TILs with clinical success in patients with metastatic melanoma [17–19]. These observations paved the way for therapeutic applications of TILs (Fig. 1.2). In short, excisional tumor biopsies are cultured *in vitro* with IL-2 supplementation for TIL proliferation. After a few weeks, TILs are analyzed for T cell phenotype and reactivity to autologous tumor cells. Highly responsive cells are further expanded on a rapid feeder-cell-based expansion protocol and re-infused into the patient. TIL cultures can be successfully generated from 60-90 % of melanoma tumor samples and induced cancer remission in up to 72 % of patients [20–23]. Interestingly, it has been shown that only a restricted set of TCRs with high tumor specificity and functionality can mediate potent therapeutic effects [24, 25].

Despite many clinical trials and applications in different cancer types, this therapeutic approach comes with major obstacles for broader applicability. First, tumor tissue is, other than in melanoma, not always easily accessible and resection of the malignant mass is limited. In addition, *ex vivo* expansion of TILs is more difficult for certain tumor types and can also fail for a significant fraction of patients [26, 27]. The manufacturing process requires several weeks before re-infusion into the patient and remains a highly tumor-specific and personalized treatment for individual patients. Another important limitation is that the quality of the expanded product remains variable and poorly characterized in terms of functionality and target specificity. This aspect is relevant as TILs are often functionally impaired due to immune inhibitory signals of the TME and have often been described as exhausted, anergic and senescent [28]. Further, T cell functionality is often not maintained after extensive *in vitro* culture. Only a small fraction

(10 %) of intratumoral T cells demonstrated the capacity to recognize autologous cancer cells and the intratumoral TCR repertoire is often found with insufficient anti-tumor efficacy [29]. However, a precise definition of specificity and functionality of TIL-derived cell products remains challenging [30–32]. Approaches for rapid identification of T cells with high tumor specificity and functionality are currently being developed to achieve cell products with predictable and robust therapeutic efficacy. However, other limitations intrinsic to the use of naturally occurring tumor-specific T cells, namely limited functionality and already exhausted phenotypes, will be difficult to overcome. An alternative to that is represented by the genetic engineering of T cells with tumor-specific receptors.

1.2.2 CAR T cell therapy

T cells genetically engineered to express a chimeric antigen receptor (CAR) have proven groundbreaking success in the field of ACT. Briefly, a CAR is a recombinant, synthetic receptor derived from the single-chain variable fragment of an antibody that is connected to an extracellular hinge region, a transmembrane domain and an intracellular signaling domain for T cell activation (Fig. 1.2) [33]. Various generations of CAR design also including co-stimulatory receptors have enhanced T cell potency, specificity, and safety. Today, a wide range of surface expressed tumor antigens are targeted by CARs. Without any doubt, the anti-CD19 CAR, up to now, represents the biggest story of clinical success. Early studies of CAR-engineered T cells recognizing CD19 B cell lineage marker, have shown therapeutic benefit of specific B cell eradication in patients with advanced leukemia [34–36]. In 2011, anti-CD19-CAR T cells were first approved by the US Food and Drug Administration (FDA) and have by now been declared as standard of care for relapsed B cell malignancies.

The potency of autologous anti-CD19 CAR-engineered T cells is often associated with strong adverse events of cytokine release syndrome and neurotoxicity [37, 38]. Relapse events are often connected to poor persistence of the cellular infusion product. Induction of T cell signaling through target recognition of a synthetic receptor can result in unphysiologically strong T cell activation. High immunoreceptor affinity has been connected to adverse events in T cell responses [39, 40]. A recent study showed that T cells engineered with a low-affinity CD19-CAR demonstrated an increased proliferation and cytotoxicity *in vitro* and had enhanced proliferative and *in vivo* anti-tumor activity compared to T cells expressing a high-affinity receptor [41].

The enthusiasm about the clinical success of anti-CD19 CAR-engineered T cells moved the field to exploring this approach in many other cancer types, in particular solid tumors. CARs can only recognize surface expressed antigens and tumor cells often do not express a uniform, highly tumor-specific marker. Further, the chemokine-mediated migration to the tumor site is impaired and the immune suppressive TME inhibits T cell infiltration, functionality and survival in the tumor site [42]. Hence, approaches of T cell co-engineering, to induce expression of chemokine receptors for better trafficking to the tumor site, have been explored [43]. Despite immense efforts, target identification and therapeutic success in solid tumors remain challenging.

Innovative approaches in T cell engineering attempted to improve a wide CAR T cell applicability with high functionality and safety [44]. CARs are commonly virally transduced into donor T cells, with random integration of the transgene into the genome and unphysiological induced expression. Attempts of directing CAR expression via targeted knockin (KI) of the transgene into T cell receptor *alpha* chain (TRAC) locus have shown uniform CAR expression with physiological regulation of expression after antigen-stimulation. Thus, sophisticated methods of T cell engineering can outperform conventionally generated CAR T cells [45].

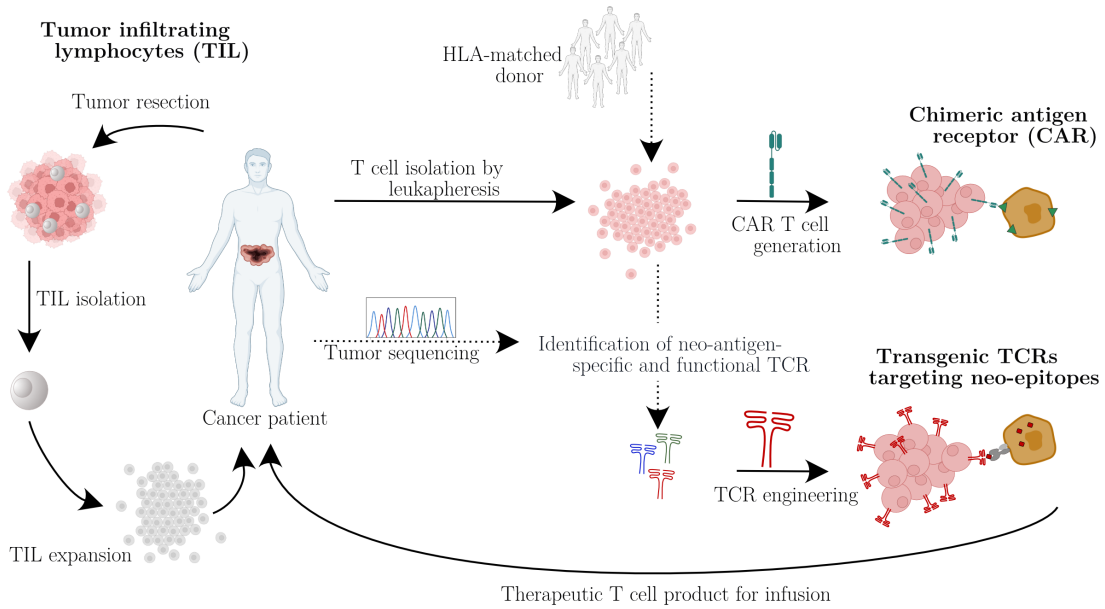

Figure 1.2: Approaches in adoptive T cell therapy. Schematic depiction of application of T cells in adoptive T cell therapy. TILs can be isolated from resected tumor tissue and expanded product is re-infused into the patient. Alternatively, genetically engineered T cells to specifically recognize cancer cells can be infused into the patient. Here, autologous T cells of the patient can be engineered for expression of a CAR to target surface expressed antigens. Tumor sequencing determines the mutational landscape and identifies the presence of tumor specific neo-antigens in a patient. TCRs can specifically recognize intracellular neo-antigens via the pMHC complex and can be identified from the patient or an HLA-matched healthy donor.

1.2.3 TCR-engineered T cell therapy

Naturally, T cells recognize their targets via the TCR and physiologically regulate T cell activation and effector functions. In contrast to CAR T cells, that recognize surface expressed antigens only, TCRs have the great advantage of recognizing pathogen-derived or tumor mutation-specific peptides that are intracellularly processed and presented via the MHC on the surface of a target cell (Fig. 1.2). Further, TCRs were found to be 10 to

100-fold more sensitive than CARs, presumably, due to less efficient signaling kinetics of the artificial receptor [46]. Hence, TCRs offer high sensitivity and specificity to a large target range.

In the recent years, various clinical studies have focused on the transfer of autologous T cells that were virally transduced for the expression of a TCR specifically recognizing TAAs [47]. Examples are MART-1 and gp100 melanoma/melanocyte differentiation antigens, the NY-ESO-1 cancer-testis antigen that is present on many common epithelial cancers, but also an epitope from the p53 molecule, which is expressed on approximately 50 % of cancers of common epithelial origin [48–50]. However, first studies suggesting therapeutic potential of TCR-engineered T cells remained with limited clinical response rates. Moreover, severe toxicities were observed in some circumstances. In one study, therapeutic transfer of T cells specific for the melanoma antigen (MAGE) A3 showed major neurological toxicities in treated patients. The TCRs were found to cross-recognize epitopes derived from MAGE-A3/A9/A12 that, combined with previously unrecognized expression of MAGE-A12 in the brain, resulted in T cell-mediated inflammation and neuronal cell destruction [51]. Moreover, a study targeting human carcinoembryonic antigen (CEA) needed to be terminated due to severe inflammatory colitis, further emphasizing on the destructive power of small numbers of high avidity T cells [52]. Taken together, the limited therapeutic efficacy and occurrence of related toxicities is linked to the currently limited choice of identified tumor target structures. It emphasizes the need for a broader repertoire of highly tumor-specific antigens and with this more functional TCRs for T cell-engineered products.

1.3 Cancer neo-antigens as therapeutic targets

T cells with specific recognition of TAAs mediate direct killing of aberrant cells and are considered major drivers of anti-tumor immunity. Various studies identified TAAs and conclusively demonstrated that tumor tissue can be discriminated from healthy cells according to them. Generally, TAAs can be classified in three major groups: 1) antigens that are present on healthy tissue, but strongly overexpressed in rapidly growing cancer cells (exempli gratia (e.g.) MART-I, MAGE, gp100, p53). 2) Cancer germline antigens, that are normally exclusively expressed on germ line cells (e.g. CEA, NY-ESO-1). 3) Cancer neo-antigens resulting from somatic mutations on cancer cells (e.g. KRAS ^{G12D}, BRAF^{V600E}). Previous studies with TCR-engineered T cells targeting TAAs of the first and second group have reported on-target/off-tumor side effects [51,52]. TAAs with high occurrence in cancer tissue and expression solely in germline cells or during embryonic development, are often not entirely absent in healthy tissue. Thus, tumor mutation-derived neo-antigens represent the most suitable targets for TCR-engineered ACT. Any peptide resulting from a somatically acquired change in the tumor cells, including structural variant, single nucleotide exchanges or insertion-deletion-derived frameshift (fs) mutations, represent a potential neo-antigen. Among them, fs-derived neo-epitopes are believed to be the most tumor-specific, as they are highly distinct from self-antigens.

Consequently, reduced on-tumor/off-target toxicities are also likely to be found. Interestingly, transferred T cells targeting tumor neo-antigens have shown improved safety profile with high T cell functionality resulting in durable tumor regression [24, 53, 54].

Ideally, a therapeutic TCR targeting a specific TAA is shared among a group of patients. However, somatic mutations in cancer are highly diverse and appear as a stochastic event. Large scale sequencing data sets report mutations in the range of 0.001 to 400 per megabase of coding genome across individuals and cancer types [55, 56]. Of these, there are only a few shared tumor-driving oncogenes such as $BRAF^{V600E}$ and $KRAS^{G12D/V/R}$ that are frequently found in certain cancer types and confer a certain selective advantage of the outgrowing tumor cells [57]. Still, most mutations do not appear in driving genes, but in passenger genes that do not contribute to a survival advantage of the tumor cell and represent a highly heterogenous spectrum. Another challenge is represented by the complexity of TCR target recognition of peptides presented by the HLA, as epitope presentation is highly dependent on the HLA-haplotype of the patient. HLAs are highly polymorphic and each individual only expresses six out of hundreds of variants. Due to different binding properties of a peptide to the diverse range of HLAs, not every epitope can be presented meaning that each patient has a specific epitope repertoire according to the HLA constellation. Thus, HLA-restriction of TCR target recognition further limits the number of patients who could potentially benefit from the same TCR-engineered T cell product. Neo-epitopes derived from fs-mutations however, bear the potential to be shared among HLA-matched patients. Although fs-mutations appear in patient-individual positions, the shift in neo-open reading frame (ORF), and thus the resulting neo-peptide, can be identical. This again highlights the relevance of such neo-epitopes for applicability in a larger patient cohort that shares overlapping neo-ORFs.

1.3.1 Neo-antigen identification

As mentioned already above, only a minor fraction of tumor-specific mutations are immunogenic, and thereby capable of inducing neo-antigen-reactive T cell responses. Therefore, technological approaches that facilitate the identification of this set of epitope targets are highly needed. Patient tumor samples can be analyzed for their mutational landscape by whole exome sequencing (WES), and RNA sequencing data may provide further information about the expression of a mutant gene [58]. Although WES is a fast and high-throughput technology, the method does not provide information on presentation and immunogenicity of a putative epitope. Furthermore, candidate neo-antigens can be evaluated in (1) downstream *in silico* computational predictions or experimental characterization by (2) *in vitro* assays, (3) mass spectrometry or (4) T cell-based assays [58].

In silico prediction tools are fast and easily accessible. Various computational tools focus on the different steps of the antigen processing pathways such as protein degradation, transport and binding to the endoplasmatic reticulum or binding to the MHC Class I or II molecules. Especially, high binding affinity of a peptide to its cognate MHC

molecule and thus high pMHC stability have been directly associated with immunogenicity [59, 60]. Thus, neuronal network tools for *in silico* predictions of MHC Class I binding affinity have been predominantly developed [61]. The limitation of these tools is that the level of accuracy depends on the size and quality of the training data set for a given allele. Thereby, predictions of peptide-MHC binding affinity can be modeled with a moderate to high level of accuracy for common HLAs, but predictions for rare HLA-types often lack accuracy. *In vitro* re-folding of soluble HLA chains that form stable pMHC complexes in the presence of peptide, can further confirm predicted high-binding affinity. Predictions in antigen processing can further be corroborated by *in vitro* assays of proteasomal processing. Here, N-terminally extended precursor peptides of the antigen of interest are degraded by purified 20S proteasome protein and analyzed by liquid chromatography mass spectrometry (LC-MS) [62]. The digested peptides of different sequence lengths have shown to reflect *in vivo* proteasome-mediated antigen processing [63, 64].

In stark contrast to *in silico* epitope prediction tools, that require *in vitro* and *in vivo* validation, mass spectrometry analysis of HLA-ligandome can identify thousands of actually MHC-presented peptides on cell lines or patient material [65]. Although it has been demonstrated that clinically relevant neo-antigens can be identified by massspectrometry from minimally 0.1 g tumor material, this technology requires sophisticated expertise [66]. Despite great improvements in instrumentation speed, chromatographic resolution, and proteogenomic database search strategies, this technology still remains with rather low sensitivity for the detection of true, often low abundant epitopes.

To further evaluate MHC binding and presentation of a candidate neo-antigen, T cells from the healthy or diseased repertoire can be stimulated in co-culture with candidate peptide-presenting target cells. Readouts of IFN-γ cytokine production or upregulation of activation markers indicate peptide reactivity. A natural TCR reacting to physiologically processed and expressed neo-antigen on a target cell provides ultimate proof for neo-epitope presentation. Such *in vitro* methods of T cell reactivity to neo-antigens can further optimize computational strategies for epitope prediction analysis by integrating experimental data into algorithms of immune predictions.

Even though the role of neo-antigens for clinical activity in cancer immunotherapy is widely accepted and immense efforts have been undertaken to identify potent immunogenic peptides, the question regarding the quality and spatial expression distribution across tumors, remains unanswered.

1.3.2 Identification of neo-antigen-reactive T cells

Apart from the difficulty of finding immunologically relevant, tumor-specific antigens, the identification and isolation of tumor-specific TCRs presents a particularly laborious process. In order to identify TAA-specific TCRs for potential clinical application, many studies have worked with immunized human HLA transgenic mice and identified highly potent TCRs [52, 67]. Briefly, mice expressing human HLA (e.g. HLA-A*02:01) are immunized with peptides of the immunogenic epitopes and spleens are harvested

12 days later. Splenocytes are then cultured with APCs expressing the matching HLA and pulsed with the target peptide. Reactive T cells are isolated for TCR sequencing and re-expression of the TCR of interest [68]. With this approach, highly potent T cell responses can be stimulated in the mice and TCRs with high avidity and functionality can be isolated. Still, murine TCR co-receptors only minimally interact with the *alpha* chain of human HLA [67]. Thus, identified functionally potent TCRs often act co-receptor-independent. Clinical use of murine TCRs targeting neo-antigens has so far been reported with high immunogenicity inducing e.g. severe inflammatory side effects [68]. Recently, the "VeliciT" mouse model has been described as an advanced method for discovery of therapeutic TCRs. In this humanized KI mouse model, variable TCR-*alpha*/*beta* regions as well as murine CD4 and CD8 co-receptors were replaced with the corresponding human genes and upon peptide immunization, highly functional human TCRs can be isolated [69].

Here, we focus on methods for TCR identification from the human immune repertoire. Various technologies have been developed to discover neo-antigen-specific TCRs [70]. A conventional approach of *in vitro* stimulation-based enrichment combines immunogenic antigen-identification with simultaneous TCR identification. In short, donor-derived T cells are *in vitro* cultured on peptide stimulus or tandem minigene expressing APCs. Antigen-reactive T cells expand and express activation markers (e.g. 41BB/OX40). Selection of reactive T cells and antigen deconvolution in peptide-reactivity matrices can identify tumor-antigen-reactive TCRs and their cognate target, as was successfully shown for T cells targeting neo-epitopes of mutated KRAS or p53 [71, 72]. Similarly, TILs expressing co-stimulatory markers have been sorted and expanded in a limiting-dilution approach to test for mutant peptide reactivity. Functional TCRs were identified from expanded peptide-reactive oligoclonal T cell populations [73].

The most common approach uses pMHC multimers to identify antigen-specific T cells by flow cytometry [74, 75]. pMHCs are *in vitro* refolded MHC Class I molecules loaded with the peptide of interest and carrying a functional tag to be multimerized on a fluorochrome-conjugated backbone [76]. Our group was one of the first providing proof-of-principle that pMHC multimers can serve as a tool to isolate functional TCRs for immunotherapy [77]. The main advantage of pMHC multimer technology is the direct *ex vivo* detection of defined antigen-specific T cells with simultaneous analysis of the cellular phenotype. pMHC multimer technologies have dramatically evolved over the last years, reaching high-throughput applications for identification of therapeutically valuable TCRs. Still, a precise target peptide needs to be pre-defined and the production of pMHCs for a large library is a laborious process.

The described technologies for identification of immunogenic epitopes and the isolation of antigen-specific TCRs find their application not only in cancer but also in infectious diseases and transplantation medicine. pMHC multimers specific for viral epitopes have effectively been used to isolate virus-specific T cells from seropositive donors. The adoptive transfer of this polyclonal virus-specific population to immunocompromised patients could protect against CMV re-activation after stem cell transplantation [78]. With the recent emergence of the novel severe acute respiratory syndrome corona virus 2 (SARS-CoV-2), established technologies quickly transferred to study immune re-

sponses to infections with the new virus. Peptide expansion protocols for isolation of virus-reactive T cells from covalescent donors have been established and clinical studies proposed the transfer of such T cells for treatment of severely diseased patients as well as immunocompromised patients with transplantation or hematological malignancies [79]. Such multifaceted application of technologies in different research fields will also be highlighted in this thesis.

1.3.3 Source of neo-antigen-reactive T cells

Technologies for efficient tumor-specific TCR identification and isolation often use patient material as a source. It was shown that therapeutically valuable TCRs could be retrieved from TILs as well as from peripheral blood memory T cells in various different cancer entities [71–73, 80, 81]. Peripheral patient blood presents a source of T cells with less limitations on accessibility and possible sample size. Although it is not fully understood to what extend neo-antigen-specific T cells from peripheral blood reflect the T cell repertoire in the tumor, first studies have identified PD-1 as a marker of tumor-reactive T cells within the TME as well as in the periphery [82, 83]. In a high-throughput personalized screening approach, neo-antigen-specific T cells were enriched from peripheral blood lymphocytes by PD-1 expression [83, 84]. Moreover, TCRs exhibiting patient-derived neo-antigen reactivity were previously identified in tumor and, although at lower frequency, also in memory T cell compartment of matched blood samples [71]. Still, T cell isolation is particularly challenging especially for poorly immunogenic tumors and for those in which the T cell infiltrate is scant. Not all tumor neo-antigens may lead to sufficient antigen cross-presentation for T cell priming by the immunosuppressive TME. Recent investigations revealed that, in different cancers, tumor-reactive TILs represent only a minimal fraction of the total T cell population infiltrating the tumor [29]. Indeed, a tumor strongly shapes the immune repertoire of a patient. The immunosuppressive TME can trigger apoptosis of (presumably highly functional) tumor-specific T cells [85]. Additionally, patients are often heavily treated with broadband cancer chemoradiation leading to a lymphopenic and immunocompromised condition that further limits sample accessibility [86].

In stark contrast to the TCR repertoire of a patient, the TCR repertoire of a healthy donor is not skewed by the tumor pressure. In support of that, T cells identified from the naive repertoire responded to epitopes, that were neglected by patient autologous TILs and efficiently recognized target-expressing cancer cells of the patient [87]. Despite the limitation of HLA-matching between patient and the donor repertoire, the unexperienced naive repertoire provides an easily accessible and almost unlimited source of highly functional tumor neo-antigen-specific TCRs. Although often of low functionality, naive T cells have not been deleted by central tolerance in early T cell development and guarantee a certain safety profile. The naive repertoire holds an extremely high TCR diversity, which is balanced by the small size of the majority of antigen-specific T cell clones [88, 89]. Indeed, in depth sequencing studies identified most TCR sequences only once, consistent with the low frequencies. Depended on the epitope, frequencies of

antigen-specific T cells are estimated around 1x10^{-6} of CD8^{+} T cells [90].

1.3.4 Detection of low-frequency naive antigen-specific T cells

In contrast to the memory T cell repertoire, the naive repertoire consist of low-frequency, small size clones of antigen-specific T cells. Selection of antigen-reactive T cells by expression of activation markers (e.g. PD-1), as discussed above, is only valid for patient material but cannot be translated to biosamples from unexposed healthy donors. A laborious step of *in vitro* expansion on autologous APCs can enrich rare naive antigen-reactive T cells to successfully isolate functional TCRs targeting various cancer antigens [87]. Although an expanded T cell clone can be evaluated by functional readouts, this approach of TCR identification is extremely tedious and relevant T cell clones can also be lost upon *in vitro* culture.

pMHC multimers build the state-of-the-art technology for direct *ex vivo* detection and isolation of antigen-specific T cells. Fluorescence activated cell sorting (FACS) cannot only detect pMHC multimer positive T cells with high specificity, but also analyze cellular phenotypes simultaneously. However, pMHCs multimers have a detection limit of approximately 5×10^{-5} and sorting on antigen-specific T cells with extremely low precursor frequency requires a step of pre-enrichment [90]. A multimer-reactive TCR is then subsequently sequenced and can be re-expressed in donor cells for further functional characterization.

1.4 Methods of T cell engineering

ACT using TILs often entails a physiological variable cell product with often undefined specificity and remains a laborious, highly personalized approach with unpredictable success. Genetic engineering of patient cells to carry a tumor-specific TCR or CAR induces immune reactivity toward defined antigens, broadens applicability of the therapy and enables a faster manufacturing process.

Conventionally, T cells are engineered for transgenic receptor expression via retroviral transduction [91]. Although being highly effective in the induction of stable transgene expression and integration, this engineering approach entails several challenges. Viral transduction randomly integrates the transgene at variable copy number into a host cell genome and could potentially disrupt loci of gene expression important for T cell function and fitness. Furthermore, the endogenous dimeric TCR is often still co-expressed, thereby competing with the transgenic TCR for surface expression; in addition putative mispaired TCR variants propose a major safety concern in terms of unpredictable self-reactivities [92,93]. Attempts to prevent mispairing include methods of TCR framework engineering, TCR-specific disulfide bonds or murinization of the TCR constant region [94–96]. Lastly, extrinsic gene promoters are necessary for transgene expression, thus neglecting physiological expression and regulation. Endogenous TCRs respond highly sensitive to antigen recognition with downregulation of the TCR [97, 98]. In

contrast, virally transduced TCRs are constitutively active and hardly exhibit negative feedback mechanisms for constraining T cell effector function [99, 100].

Recent development in precise, locus-targeted genetic engineering using clustered regularly interspaced short palindromic repeats (CRISPR)/CRISPR-associated protein 9 (Cas9) has revolutionized the field of T cell engineering for ACT. The possibility to specifically re-express a TCR (but also CAR) in the endogenous TCR locus with physiological expression motifs without the requirement of viral vectors addresses many of the above mentioned concerns of therapeutic, engineered T cells [45, 100, 101]. In detail, the endogenous TCR is specifically targeted by guiding sequences of the CRISPR/Cas9 ribonucleoprotein (RNP) complex, and a double-strand break is induced at the designated locus. Repair attempts via the non-homologous end joining (NHEJ) pathway results most frequently in shift of the reading frame, which eventually leads to gene knockout (KO). A provided homology-directed repair (HDR) template encoding the transgene TCR can guide the gene KI into the targeted locus. The targeted KO of the endogenous TCR combined with simultaneous KI of a transgenic receptor into the endogenous locus of the TRAC has been termed in the field as orthotopic TCR replacement (OTR) (Fig. 1.3). Our group has done pioneering work in CRISPR/Cas9-mediated TCR transgene insertion into the TCR gene locus and described a more homogeneous TCR expression in engineered T cells, similar to physiological T cells [102]. OTR-engineered TCRs or CARs lead to a highly dynamic, physiological downregulation of the receptor upon antigen stimulation [45, 100]. In contrast to conventional T cell engineering methods, OTR generates a more predictable therapeutic cell product that bears the potential for decreased exhaustion and long-term maintenance even in the setting of strong antigen exposure of viral infections or cancer.

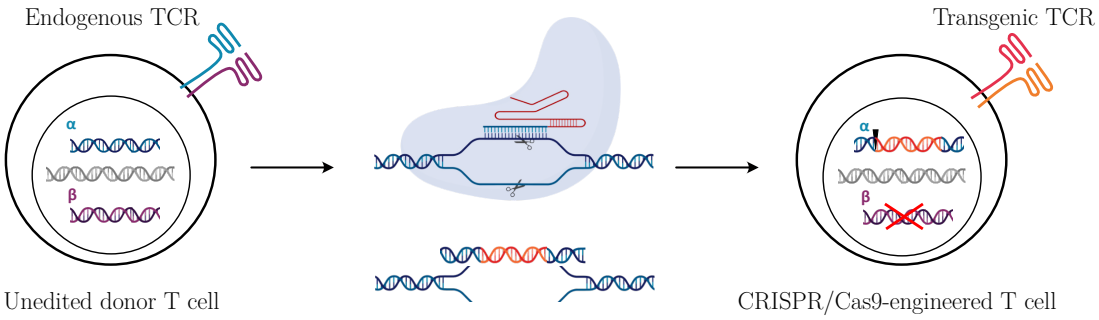

Figure 1.3: Advanced T cell engineering through orthotopic TCR replacement. Schematic depiction of CRISPR/Cas9-mediated KO of the endogenous TCR *alpha* and *beta* chain of a donor T cell. Targeted TCR KI via HDR into the endogenous TCR *alpha* chain locus enables physiological transcription of the transgene.

1.5 TCR characterization

pMHC multimers can detect and guide the isolation of antigen-specific T cells of low frequency in the naive repertoire of a healthy donor. Despite high specificity, the pMHC

multimer technology, as well as other available approaches for T cell isolation, lacks an absolute determination of functionality. Antigen-specific, naive T cell populations are mainly composed of TCRs with low functional avidities [103]. Thus, a cost and time consuming process of careful TCR characterization is required to select appropriate candidates for clinical application.

The structural avidity of a TCR to its cognate antigen peptide presented on a pMHC is a key parameter for cell-mediated immunity. Biophysical assays, such as surface plasmon resonance can accurately define the affinity (or interaction strength) between a receptor and its ligand [104]. However, this method requires tedious production of recombinant pMHCs and TCRs. Furthermore, the effect of CD4/CD8 co-receptors, as well as the synergistic effect of multiple binding of adjacent TCRs, are neglected. In our laboratory, we have developed a flow-cytometry-based assay to measure monomeric TCR:pMHC dissociation rates of living T cells [105]. The measured TCR:pMHC k_{off}-rate is a major determinant of the overall TCR structural avidity (TCR affinity in presence of a co-receptor). Importantly, we showed that this parameter can reliably identify functional TCRs.

In addition to measurements of structural avidity, common *in vitro* assays for T cell functionality evaluate cytokine release, upregulation of activation markers and cytotoxicity upon co-culture with target cells. Optimally, patient-derived tumor cells can serve as target cells; however, whenever this is not possible, artificial APCs have been established as an efficient alternative tool. The human erythroleukemic cell line K562 is largely used for this purpose due to its demonstrated ability in antigen-processing and presentation. Furthermore, the cell line lacks natural surface expression of MHC I and MHC II alleles but does express β2-microglobulin (β2m) [106], thus offering a flexible basis for engineering with the desired transgenic MHC chain of interest. Upon genetic engineering for MHC-expression, cells acquire antigen-processing and presenting properties and serve as an ideal cell line to test TCR functionality [107, 108].

Functional characterization of tumor-specific TCRs in *in vivo* models is facing many obstacles. TCR functionality is restricted to the MHC efficiently presenting the target peptide, and differences between humans and mice in the processing and presentation of antigens are imperative. A number of HLA class I transgenic mouse lines have been used in pre-clinical trials [109, 110]. However, available humanized mouse models are often limited to a selected HLA-epitope set and do not reflect the vast range of potentially interesting neo-antigen targets and HLA restrictions. Moreover, immunodeficient mice can be engrafted with human tumor cell lines to evaluate the potency of infused T cell products. However, such xenograft models lack physiological tumor mutational load and the patient specificity of tumor neo-antigens is often not represented in cell line models. Yet, patient derived xenografts (PDX), although being highly patient-individual, elegantly recapitulate primary tumor behavior and can reflect the effect of targeted therapy more closely [111]. Indeed, PDXs have demonstrated conservation of the patient's mutational profile in the model and a potent autologous anti-tumor T cell response [112]. Still, technical challenges and biological limitations of immunodeficient mice restrict their application in wide immunotherapeutic studies. To overcome the limitation of an absent effective immune system in these mice, $CD34^+$ human hematopoietic stem cells can be

transplanted into immunodeficient mice to reconstruct human hematopoietic lineages for a functional immune system [113]. Nonetheless, such a cumbersome approach depends on the availability of bone marrow or cord blood of an HLA-matched donor.

Alternatively, technological progress in culturing three-dimensional patient-derived organoids, has greatly advanced *in vitro* disease modeling, toxicology studies, and drug discovery. Nevertheless, the complexity, diversity and physical structure of the TME can often not be kept in a cell culture dish model. Recent studies report on the preservation of the TME through primary tumor epithelial and stroma cells and suggest a promising model in personalized immunotherapy testing [114].

1.6 Targeting pancreatic cancer

1.6.1 Adoptive T cell therapy in pancreatic cancer

Patients diagnosed with pancreatic cancer show the lowest survival rate with approximately 10 % of patients surviving longer than 5 years [115]. Despite significant advances in treatment and therapeutic options in other cancer entities, treatment success of pancreatic cancer remains low. Estimates predict pancreatic cancer to become the second most common cause of cancer-related deaths by the year 2040 [116]. Pancreatic cancer is often diagnosed late, at advanced stage of the disease after metastatic spread. Therefore, the only curable treatment by radical surgical resection is usually out of scope. Systemic treatment with chemo- and radiation therapy remains as major treatment option, but exhibits severe side effects and has shown limited success [117]. Therefore, there is a high clinical need for efficient treatment options to improve prognosis of pancreatic ductal adenocarcinoma (PDAC) patients and a window of opportunity for novel experimental therapies in compassionate use.

Besides surgery, chemotherapy and radiation, cancer immunotherapy represents the fourth pillar of cancer treatment and it has proven remarkable success in other cancer entities. Although PDAC was previously considered an immunologically silent disease, the presence of TILs in patient's tumor lesions was identified as a good indicator of outcome after surgical resection and infiltrates of $CD8^+$ T cells as well as a high neo-antigen quality expressed in the pancreatic tumor tissue have been linked to prolonged patient survival [15, 118]. These observations imply a potential use of immunotherapies with checkpoint inhibitors in PDAC. However, the checkpoint inhibition studies conducted in patients with microsatellite instability so far have not improved the overall survival [119]. Presumably, the strong immunosuppressive TME with a high stromal barrier of cellular and molecular suppressive components hinders the efficacy of immunotherapy [120].

Further, studies on cancer vaccines that aim to initiate a tumor-specific immune response have generated promising results, but failed to demonstrate improved patient survival [121].

The adoptive transfer of PDAC-specific therapeutic T cells could provide a solid alternative to restore the compromised immunity in PDAC patients. Studies showed successful expansion of TILs from patient material, but clinical applications remain scarce [122]. Multiple studies report on the therapeutic application of CAR-engineered T cells recog-

nizing surface expressed TAAs such as mesothelin (MSLN), CEA, MUC1, PSCA, CD133, or HER2 [123]. Generally, CAR T cells have only shown limited success in solid tumors and especially in PDAC struggle to overcome the highly immunosuppressive TME. First studies on T cells engineered with an affinity-enhanced MSLN-specific TCR reported on the stromal remodeling and the induction of tumor cell death, however infiltrating T cells became progressively dysfunctional [124]. In summary, PDAC presents a tumor disease with an urgent need for novel therapeutic strategies. Recent advances in cancer immunotherapy and ACT have shown promising effects and highlight the interest in T cell-mediated therapies. Further, comprehensive studies on genomic profiles of PDAC patients postulate that nearly all PDAC samples harbor neo-antigens that broaden the potential targets for T cell therapy [125].

1.6.2 RNF43 as a potential target for T cell therapy in pancreatic cancer

Sequencing studies of whole genome sequencing and copy number variation have revealed a highly complex mutational landscape in PDAC. Structural variants and deleterious point mutations leading to gene disruption were frequently found in KRAS (90 %), TP53 (74 %), and SMAD4 (31 %) [126]. However, a closer look at the mutational distribution reveals, especially for KRAS, a dominant occurrence of single-point missense mutations. This reduces the probability for occurrence of highly immunogenic neo-antigens, as misssense mutation-derived neo-epitopes are still close to identical with self-antigens. As discussed above, fs mutations create novel ORFs that generate a large quantity of neo-antigenic peptides that are highly distinct from self, and can also potentially be shared among different patients. With this, fs-derived neo-epitopes build a promising target for TCR-engineered ACT. Remarkably, the Ring Finger Protein 43 (RNF43) gene is also frequently mutated in pancreatic cancer (14 %), as well as in other gastro-intestinal (GI) cancer diseases, but, different from other mutated genes, it exhibits a relatively high occurrence of fs-mutations (Fig. 1.4) [127]. Interestingly, certain fs-mutations, such as G659fs mutation, are recurrent in a significant proportion of patients [128].

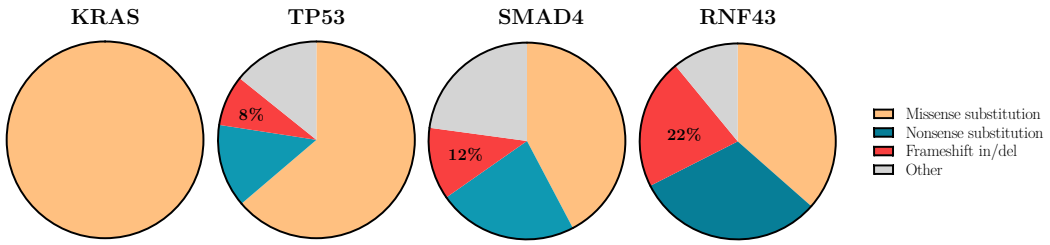

Figure 1.4: Mutational distribution of genes frequently mutated in PDAC. Frequency of mutations identified in commonly mutated genes in PDAC. Source: Catalogue Of Somatic Mutations In Cancer (3/2022)

RNF43 is a tumor suppressor gene encoding an E3 ubiquitin ligase that acts as a negative regulator on the Wnt signaling pathway. Wnt is a key signaling cascade in

development and stemness. Oncogenic mutations downstream the pathway activate and induce aberrant signaling, leading to carcinogenesis [129]. RNF43 acts downstream of pathway activation by either impairing the Frizzled receptor turnover at the cellular membrane, or by direct inhibition of TCF4 transcriptional activity in the nucleus to downregulate TCF4 target genes [130, 131]. Studies on loss of function of RNF43 have shown to enhance tumor cell line proliferation and invasive capacity in *in vitro* and *in vivo* models of gastric and colorectal cancer, which further corroborates its role in tumor suppression [132]. The impact of RNF43 mutations in PDAC are characterized to lesser extent. However, recent studies support its function as a tumor suppressor gene also in the pancreas. In a genetically engineered mouse model of PDAC expressing oncogenic KRAS it was shown that loss of RNF43 leads to a decreased survival of the mice. Nevertheless, loss of RNF43 was also found to mediate a unique immune microenvironment with increased lymphocyte infiltration. These findings are in line with the observed increased survival of PDAC patients upon presence of RNF43 tumor mutations [133].

In summary, we propose RNF43 fs-derived mutations as a promising immunogenic target for T cell therapy.

2 Material and methods

2.1 Material

2.1.1 Commodities

Item	Supplier
0.22µm sterile filter	Millipore, Eschborn, Germany
0.45µm sterile filter	Millipore, Eschborn, Germany
1.0 mL Sub-Q	BD Biosciences, Franklin Lakes, USA
1.0 mL, 1.5 mL 2.0 mL reagent tubes	Zefa Laborservice, Grasbrunn, Germany
1.5 mL LoBind-DNA reaction tube	Eppendorf, Hamburg, Germany
15 mL, 50mL Falcon Cell Star	Greiner bio-one, Heidelberg, Germany
2.0 mL Cryo-vial	Alpha Laboratories, Eastleigh, UK
384-well plates medium binding	Greiner bio-one, Heidelberg, Germany
5 mL Polypropylen round-bottom tube	Greiner Corning, Durham, USA
5 mL Polystyrene round-bottom tube	Greiner Corning, Durham, USA
C-Slide cell counting chamber slide	NanoEnTek, Seoul, South Korea
Culture flask 25 cm^2, 75 cm^2, 150 cm^2	VWR. Radnor, USA
E-Plate 96	OLS, Bremen, Germany
Parafilm	Merck, Darmstadt, Germany
PCR reaction tubes	Brand, Werthelm, Germany
PCR reaction 96-well plate	Azenta Life Siences, Chelmsford, USA
PCR plate seals	Azenta Life Siences, Chelmsford, USA
Pipette filter tips (1µl, 10/20µl, 200µl, 1 mL)	STARLAB, Hamburg, Germany
Pipette tips multi-step	Eppendorf, Hamburg, Germany
Serological pipettes (5 mL, 10 mL, 25 mL)	Greiner bio-one, Heidelberg, Germany

Syringe (1 mL, 3 mL, 5 mL, 50 mL)	Braun, Melsungen, Germany
Tissue culture treated plates (6-, 12-, 24-, 96-Well)	Greiner Corning, Durham, USA

2.1.2 Chemicals and reagents

Compound	**Supplier**
2-Propanol	Roth, Karlsruhe, Germany
β-Mercaptoethanol	Roth, Karlsruhe, Germany
aCD3/aCD28 Expamer	Juno Therapeutics/BMS, München, Germany
ADVABLUE 0.1 % PCR dye	Beckman Coulter, Brea CA, USA
Affinity Script Reverse transcriptase	Agilent, Santa Clara, USA
Agarose	Roth, Karlsruhe, Germany
Alt-R® Cas9 Electroporation Enhancer	IDT DNA, Coralville, USA
Alt-R® S.p. HiFi Cas9 Nuclease V3	IDT DNA, Coralville, USA
Ampicillin	Roth, Karlsruhe, Germany
Bicoll Separating Solution	Merck, Darmstadt, Germany
Bovine Serum Albumin	Sigma, Taufkirchen, Germany
$CaCl_2$	Merck, Darmstadt, Germany
CRISPR/Cas9 tracrRNA	IDT DNA, Coralville, USA
DBCO-PEG4-Atto488	Jena Bioscience, Jena, Germany
DBCO-PEG4-Biotin	Jena Bioscience, Jena, Germany
D-Biotin	Merck, Darmstadt, Germany
dGTP PCR grade	Merck, Darmstadt, Germany
DMEM	Thermo Fisher Scientific, Ulm, Germany
DMSO	Merck, Darmstadt, Germany
dNTPs	Roche, Penzberg, Germany
DTT	Merck, Darmstadt, Germany

Dulbeccos Phosphate Buffered Saline	Merck, Darmstadt, Germany
Ethanol	Roth, Karlsruhe, Germany
Ethidium Monoazide	Molecular Probes, Leiden, Netherlands
Exonuclease	Thermo Fisher Scientific, Ulm, Germany
Fetal Calf Serum	GE Healthcare, Chalfont St. Giles, UK
Formamid	Merck, Darmstadt, Germany
Gentamicin	Thermo Fisher Scientific, Ulm, Germany
Golgi-Plug	BD Biosciences, Franklin Lakes, USA
HCl	Roth, Karlsruhe, Germany
HEPES	Roth, Karlsruhe, Germany
Human serum	in-house production
Interleukin-2	Peprotech, Hamburg, Germany
Interleukin-2 Proleukin S (Single cell expansion)	Novartis, Basel, Switzerland
Interleukin-7	Peprotech, Hamburg, Germany
Interleukin-15	Peprotech, Hamburg, Germany
Ionomycin	Merck, Darmstadt, Germany
Kanamycin	Merck, Darmstadt, Germany
LB agar	in-house
LB medium	in-house
L-Glutamine	Merck, Darmstadt, Germany
MgCl2	Merck, Darmstadt, Germany
Nonident P40 (IGEPAL)	Merck, Darmstadt, Germany
Penicillin/Streptomycin	Thermo Fisher Scientific, Ulm, Germany
Phorbol myristate acetate	Merck, Darmstadt, Germany
Phytohaemagglutinin	Thermo Fisher Scientific, Ulm, Germany
Propidium Iodide	Merck, Darmstadt, Germany
Retronectin	Takara Bio, Shiga, Japan
RNasin Plus Ribonuclease Inhibitor	Promega, Madison, USA

Rotisafe Gel Stain	Roth, Karlsruhe, Germany
RPMI 1640	Thermo Fisher Scientific, Ulm, Germany
Terminal Deoxynucleotidyl Transferase (TdT)	Promega, Madison, USA
Tris pH 8.5	in-house
Tris-HCl	Roth, Karlsruhe, Germany
Triton-X 100	Roth, Karlsruhe, Germany
tRNA	in-house
Trypan blue	Roth, Karlsruhe, Germany
Trypsin-EDTA (0.25 %)	Thermo Fisher Scientific, Ulm, Germany

2.1.3 Buffers and media

Solution	**Composition**
Antibiotics supplement (add 5 %)	20 mL Gentamicin
	200 mL Penicilin/Streptomycin
Complete freezing medium	1x FCS
	10 % (v/v) DMSO
FACS buffer	1x PBS
	0.5 % (w/v) BSA
	pH 7.45
Complete RPMI	500 mL RPMI 1640
	50 mL FCS
	25 mL SC^{+}
RPMI SC^{-}	500 mL RPMI 1640
	50 mL FCS
	25 mL SC^{-}
Complete DMEM	500 mL DMEM
	50 mL FCS
	25 mL SC^{-}
LB-Ampicillin/Kanamycin	1 L LB-medium
	100 mg/L Ampicillin/Kanamycin

SC^+ (supplement complete, in 1 L medium)	1 mL β-mercaptoethanol
	20 mL Gentamicin
	23.83 g HEPES
	4 g L-Glutamine
	200 mL Penicilin/Streptomycin
SC^- (supplement complete, in 1 L medium)	1 mL β-mercaptoethanol
	23.83 g HEPES
	4 g L-Glutamine
Trypan blue solution	1x PBS
	0.15 % (v/v) trypan blue

2.1.4 Peptides

Peptide	**Sequence**	**HLA haplotype**	**Supplier**
RNF43_1	VPSVWRSSL	B*07:02	peptides & elephants, Potsdam, Germany
RNF43_2	SLLPTCWAL	A*02:01	peptides & elephants, Potsdam, Germany
RNF43_4	TQLARFFPI	A*02:01	peptides & elephants, Potsdam, Germany
A2-pp65	NLVPMVATV	A*02:01	peptides & elephants, Potsdam, Germany
B7-pp65	TPRVTGGGAM	B*07:02	peptides & elephants, Potsdam, Germany

2.1.5 Antibodies

Human Antigen	**Fluorophore**	**Clone**	**Supplier***
APC	purified	APC003	BioLegend
CD154	PE	24-31	BioLegend
CD19	ECD	J3-119	Beckman Coulter

CD28	purified	L293	BD Biosciences
CD3	purified	OKT3	BioLegend
CD3	APC	UCHT1	Life Technologies
CD3	APC-Cyanine7	UCHT1	BioLegend
CD3	BV421	SK7	BD Biosciences
CD3	BV650	OKT3	BioLegend
CD3	Pacific Blue	UCHT1	BD Biosciences
CD3	PE	UCHT1	Beckman Coulter
CD3	PC7	UCHT1	Beckman Coulter
CD45	APC-eFlour 780	HI30	eBioscience
CD45	ECD	J33	Beckman Coulter
CD45	eF450	2D1	eBioscience
CD45	PB	PB986	DAKO/Agilent, Santa Clara, USA
CD45	PE-Cyanine7	2D1	eBioscience
CD45	PO	HI30	Exbio, Prague, Czech Republic
CD45RA	APC-eFlour 780	HI100	eBioscience
CD69	PE	FN50	eBioscience
CD69	PE-Cyanine7	FN50	BioLegend
CD62L	FITC	DREG-56	BioLegend
CD62L	PE	DREG-56	BioLegend
CD8	FITC	B9.11	Beckman Coulter
CD8	PE	3B5	eBioscience
CD8α	APC	RPA-T8	BioLegend
CD8α	APC-eFlour 780	OKT8	eBioscience
CD8α	eFlour 450	OKT8	eBioscience
CD8α	PE	OKT8	eBioscience
CD8α	PE-Cyanine7	OKT8	eBioscience
HLA-A2	APC	BB7.2	BD Biosciences
HLA-A2	FITC	BB7.2	BD Biosciences
HLA-A2	PE	BB7.2	BioLegend
HLA-B7	APC	BB7.1	BioLegend

HLA-B7	PE	BB7.1	BioLegend
hTCR	FITC	IP26	BioLegend
hTCR	PE	IP26	BioLegend
IFNγ	FITC	25723.11	BD Biosciences
IL-2	APC	5.344.111	BD Biosciences
murine TRBC	APC	H57-597	BioLegend
murine TRBC	APCFire750	H57-597	BioLegend
murine TRBC	PE	h57-597	BioLegend
PD1	APC	eBioJ105	eBioscience

*BD Biosciences, Franklin Lakes, USA
Beckman Coulter, Beckman Coulter, Brea, USA
Biolegend, San Diego, USA
eBioscience now Thermo Fisher Scientific, Ulm, Germany

2.1.6 Fluorescently labeled pMHC backbones

Backbone	**Fluorophore**	**Supplier**
StrepTactin	APC	IBA Lifesciences, Göttingen, Germany
StrepTactin	PE	IBA Lifesciences, Göttingen, Germany
Streptavidin	APC	Thermo Fisher Scientific, Ulm, Germany
Streptavidin	BV421	Biolegend, San Diego, USA
Streptavidin	PE	Thermo Fisher Scientific, Ulm, Germany

2.1.7 CRISPR guides

Name	**Target**	**Sequence**	**Supplier**
TRAC guide6 antisense	1st exon TRAC	AGAGTCTCTCAGCTGGTACA	IDT DNA, Coralville, USA
TRBC guide3 sense	1st exon TRBC	GGAGAATGACGAGTGGACCC	IDT DNA, Coralville, USA

2.1.8 PCR primers

Primer	Sequence	Supplier
hTRAC HDR genomic fwd	CTGCCTTTACTCTGCCAGAG	Merck, Darmstadt, Germany
hTRAC HDR genomic rev	CATCATTGACCAGAGCTCTG	
Single clone PCR		
	Reverse Transcription	
hTCRAC1 rev	CTTTCAGGAGGAGGATTC	
hTCRAC2 rev	AAGTTT GGTTCGTATCTG	
hTCRAC3 rev	ATAATGCTGTTGTTGAAGG	
hTCRBC1 rev	TAGAACTGGACTTGACAG	
hTCRBC2 rev	GTATCTGGAGTCATTGAGG	
hTCRBC3 rev	CACCTCCTTCCCATTCAC	
	Adaptor PCR	
hTCRalpha_RT rev	ACACATCAGAATCCTTACTTTG	
hTCRbeta_RT rev	CACGTGGTCGGGGAAGAAGC	
dC-adaptorPTO fwd	ACAGCAGGTCAGTCAAGCAGTA-GCAGCAGTTCGATAAGCGGCCG-CCATGGACCCCCCCCCCCCV-PTO-N	
	Nest I	
hTCRalpha_1 rev	GGTGAATAGGCAGACAGACTT	
hTCRbeta_1 rev	GTGGCCAGGCACACCAGTGT	
Adaptor Primer 1 fwd	ACAGCAGGTCAGTCAAGCAGTA	
	Nest II for NGS	
NGS_Adap_hTCRalpha fwd	TCGTCGGCAGCGTCAGATGTGTATAAG-AGACAGGCTGGTACACGGCAGGGTC	
NGS_Adap_hTCRbeta fwd	TCGTCGGCAGCGTCAGATGTGTATAAG-AGACAGCTGCTTCTGATGGCTCAAAC	
NGS_Adap_Adaptor 2 rev	GTCTCGTGGGCTCGGAGATGTGTATAAG-AGACAGAGCAGTAGCAGCAGTTCGATAA	

2.1.9 Molecular kits and standards

Kit / Standard	Supplier
BD Cytofix/Cytoperm	BD Biosciences, Franklin Lakes, USA
DNeasy Blood & Tissue Kit	QIAGEN, Venlo, Netherlands
Agencout AMPure XP	Beckman Coulter, Brea, USA
GeneRuler 1 kb DNA ladder	Thermo Fisher Scientific, Ulm, Germany
GoTaq® G2 Flexi DNA Polymerase	Promega, Madison, USA
Herculase II Fusion Enzyme with dNTPs Combo	Agilent, Santa Clara, USA
Plasmid MaxiPrep Kit	Thermo Fisher Scientific, Ulm, Germany
MiSeq Reagent Kit v2 (500 cycles)	Illumina, San Diego, USA
P3 Primary Cell Nucleofector™ Kit	Lonza, Basel, Switzerland
SV Wizard® Gel and PCR Clean-Up System	Promega, Madison, USA
Wizard® Genomic DNA Purification Kit	Promega, Madison, USA
123count eBeads® Counting Beads	Thermo Fisher Scientific, Ulm, Germany

2.1.10 Vectors and organisms

Vector/ Organism	Purpose	Supplier
MP72	retroviral vector	custom design
K562 A*02:01$^+$	target cells	in-house
K562 B*07:02$^+$	target cells	in-house
K562 A*02:01$^+$ RNF43A269fs-eGFP $^+$	target cells	in-house
K562 B*07:02$^+$ RNF43A269fs-eGFP $^+$	target cells	in-house
Capan-2	target cells	in-house
Capan-2 A*02:01$^+$	target cells	in-house
Panc28	target cells	in-house
RD114	Packaging cell line	in-house
Stbl3	bacteria for plasmid amplification	Thermo Fisher Scientific, Ulm, Germany
T3M4 A*02:01$^+$	target cells	in-house

2.1.11 Equipment

Equipment	Model	Supplier
Automated Cell Counter	EVE™PLUS	NanoEnTek, Seoul, South Korea
Balance	ACS/ ACJ 320-4M	Kern & Sohn, Balingen, Germany
	EG 2200-2NM	Kern & Sohn, Balingen, Germany
Centrifuges	Biofuge fresco	Heraeus, Hanau, Germany
	Biofuge stratos	Heraeus, Hanau, Germany
	Multifuge 3 S-R	Heraeus, Hanau, Germany
	Sorvall RC6+	Thermo scientific, Ulm, Germany
	Varifuge 3.0RS	Heraeus, Hanau, Germany
Electrophoresis chamber	PerfectBlue™ Gel System Mini L	Peqlab, Erlangen, Germany
Electrophoresis power supply	EPS 600	Pharmacia Biotech, Uppsala, Sweden

EVOS cell imaging	FL Auto 2	Thermo scientific, Ulm, Germany
Flow Cytometer	Cytoflex	Beckman Coulter, Brea, USA
	Cytoflex S	Beckman Coulter, Brea, USA
	Cytoflex LX	Beckman Coulter, Brea, USA
	MoFlo XDP Cell Sorter	Beckman Coulter, Brea, USA
	MoFlo Astrios EQ	Beckman Coulter, Brea, USA
	BD FACSAria™ III Cell Sorter	BD Biosciences, Franklin Lakes, USA
Gel imaging system	Molecular Imager® Gel Doc™ XR+	BioRad, München, Germany
Heat block	Thermomixer compact	Eppendorf, Hamburg, Germany
Ice maker	ZBE 30-10	Ziegra Eismaschinen, Isernhagen, Germany
Incubator	HERAcell 240	Heraeus, Hanau, Germany
Laminar flow hood	HERAsafe	Heraeus, Hanau, Germany
Magnet stand	DynaMag™-2	Thermo scientific, Ulm, Germany
Microscope	Axiovert S100	Carl Zeiss, Jena, Germany
Nanodrop device	ND-1000	Kisker, Steinfurt, Germany
NGS sequencing	MiSeq	Illumina, San Diego, USA
Neubauer chamber	Neubauer improved	Schubert, München, Germany
PCR Cycler	T3000 Thermocycler	Biometra, Göttingen, Germany
Protein purification	ÄKTApure	GE Healthcare, Chalfont St. Giles, UK
RTCA System	xCELLigence® RTCA MP	ACEA Bio, San Diego, USA
Transfection device	4D-Nucleofector™ Core Unit	Lonza, Basel, Switzerland
	4D-Nucleofector™ X-Unit	Lonza, Basel, Switzerland
	96-well Shuttle™ Add-on	Lonza, Basel, Switzerland
Water bath	Type 1002	GFL, Burgwedel, Germany

2.1.12 Software

Software	Version	Supplier
Affinity Designer	1.8.2	Serif
BioRender	2022	Biorender
Excel 2016		Microsoft
FlowJo 10	10.6.1	Becton Dickinson & Company (BD)
Prism Software	9.2.0	GraphPad Software
RTCA Software Pro (ACEA)		Agilent
Summit	v62	Beckman Coulter

2.2 Methodology

2.2.1 Cell culture

2.2.1.1 Cell culture of primary T cells and cell lines

Primary human T cells, K562 leukemic cells as well as Capan-2, T3M4 and Panc28 pancreatic cancer cell lines were cultured in Roswell Park Memorial Institute medium (RPMI) supplemented with 10 % fetal calf serum (FCS) and 5 % SC^+ (hereafter named complete RPMI) and regularly split with medium change to appropriate cell density. Medium of primary human T cells was additionally supplemented with 180 IU/mL IL-2 every 3-4 days. For resting and functional assays, IL-2 supplementation was reduced to 50 IU/mL.

RD114 cells for production of viral particles were cultured in Dulbecco's modified eagle medium (DMEM) supplemented with 10 % FCS and 5 % SC^+ (hereafter named complete DMEM). For splitting of adherent cell lines, cells grown to 90 % confluency were rinsed with phosphate-buffered saline (PBS) once to remove dead, floating cells. Next, cells were incubated with Trypsin-EDTA for 5-10 min at 37 °C. Trypsinization was stopped by adding complete medium. Cell suspension was washed twice in PBS and finally resuspended in complete medium for seeding (split 1:10 or 1:20).

All cells were cultured in a humidified incubator at 37 °C and 5 % CO_2 unless indicated otherwise. All cultured cells were frequently checked for mycoplasma contamination via PCR of cell culture supernatant.

2.2.1.2 Isolation of PBMCs

Peripheral mononuclear blood cells (PBMCs) were isolated from either fresh blood or buffy coats of healthy donors by gradient density centrifugation according to manufacturer's instructions (Bicoll Separating Solution, Merck). Fresh whole blood was diluted 1:0.5 and buffy coats 1:2 with sterile PBS and carefully layered on 15 mL of Bicoll in a 50 mL Falcon tube. For gradient density separation, the tube was centrifuged for 15 min at 1000 x g at room temperature (RT). The forming ring of PBMCs was harvested and washed twice with sterile PBS via centrifugation for 10 min at 1500 rpm at RT. Cells were counted with a Neubauer improved cell counting chamber or an automated cell counting device using Trypan blue solution for live/dead discrimination, and finally seeded in complete RPMI at $0.5 - 1 \times 10^6$cells/ mL.

Written informed consent of the donors was obtained and usage of the corresponding biosamples was approved according to national law by the Institutional Review Board (Ethikkomission der Medizinischen Fakultät der Technischen Universität München).

2.2.1.3 Apheresis processing

$CD8^+$ purified apheresis was kindly provided by Juno Therapeutics, a Bristol Myers Squibb Company. After column purification of the $CD8^+$ fraction, cells were washed in sterile PBS twice and cryopreserved at 20×10^6cells/ mL in FCS + 10 % dimethyl

sulfoxide (DMSO). Vials were frozen down to -80 °C at a rate of -1 K/min by using a Mr.Frosty™ cryo container filled with isopropyl alcohol. Frozen samples were stored at -80 °C or liquid nitrogen. An aliquot of the cell suspension was stained for phenotypic markers and HLA class I molecules via monoclonal antibodies (mABs) (panel: CD3-PC7, CD8-eF450, CD62L-FITC, CD45RA-APCeF780 and HLA-A2-PE or HLA-B7-PE) and analyzed via flow cytometry.

For thawing of apheresis material, cryo-vials were quickly thawed in a 37 °C water bath, rapidly transferred into pre-warmed complete RPMI and finally washed twice in order to eliminate DMSO residuals. Before flow cytometry-based cell sorting, cells were rested over night (O/N) at a cell density of 5×10^6cells/ mL in complete RPMI containing 50 IU/mL IL-2.

2.2.1.4 Feeder-free single cell expansion

For feeder-free single cell expansion, a 384-well plate was coated O/N at 4 °C with 10 µg/mL CD3/CD28 antibodies diluted in PBS. The following day, the coated wells were blocked with FCS for at least 1 h at 37 °C. FCS was then removed by firm inversion and all wells were filled with 20 µl RPMI containing 5 % SC^+ and 10 % human serum. Medium was further supplemented with 100 IU/mL Proleukin IL-2, 25 ng/µl Interleukin-7 (IL-7) and 25 ng/µl Interleukin-15 (IL-15). After single cell sort, plates were spun down to force cells to the bottom of the plate and eventually sealed with parafilm. After 7 to 12 days of culture, successful clone growth was monitored under the microscope, and clones with suitable size were processed for pMHC re-staining and/or TCR sequencing.

2.2.1.5 Feeder-cell-based T cell expansion

Allogeneic PBMCs (feeder cells) were mitotically inactivated by irradiation with 35 Gy and subsequently washed twice with complete RPMI. Feeder cells were added to sorted $CD8^+$ T cells expressing transgenic TCRs to reach 100.000 total cells in 100 µl per 96-well-U-bottom plate. Complete RPMI medium was supplemented with 180 IU/mL IL-2 and 1 µg/mL phytohaemagglutinin (PHA). After seven days, 100 µl fresh medium including supplements and 100.000 freshly irradiated allogeneic feeder cells (identical donor) were added to 96-well. If needed, expanding cell population was transferred to a larger culture plate to reach a cell density of 1×10^6cells/ mL. After 14 days only IL-2 was continuously supplemented and cultured as described above for primary human T cells.

2.2.2 Transformation and plasmid purification

Stbl3 chemo competent *E.coli* were transformed with plasmid deoxyribonucleic acid (DNA) via 42 °C heat shock, plated on LB-agar plates containing appropriate antibiotic selection (100 µg/mL Ampicillin) and incubated O/N at 37 °C. 4 mL of antibiotic containing LB medium were inoculated with a single colony forming unit and incubated O/N at 37 °C. Plasmid preparation was performed with the PureYield Plasmid Miniprep System following manufacturer's protocol using 3 mL of bacterial culture. For high-yield

plasmid purification, 300 mL bacterial culture were purified via Plasmid MaxiPrep Kit. DNA was eluted with H_2O and concentration was measured via Nanodrop.

2.2.3 Neo-epitope prediction

All neo-ORFs of the RNF43 were simulated and peptide-MHC Class I binding affinities were predicted for the most common HLA class I molecules in the European Caucasian population (HLA-A*01:01, HLA-A*02:01, HLA-A*03:01, HLA-B*07:02, HLA-B*08:01, HLA-B*44:02, HLA-C*04:01, HLA-C*05:01, HLA-C*07:01, HLA-C*07:02) using NetMHC 4.0 (`https://services.healthtech.dtu.dk/service.php?NetMHC-4.0`). The prediction revealed all possible 8mers, 9mers, 10mers and 11mers with a wide range of affinities.

In vitro proteasomal processing was performed by the group of Prof. Dr. Peter Kloetzel (Institute for Biochemistry, Charité Berlin, Germany) and followed a published protocol [62]. Briefly, pre-cursor peptides containing the epitope sequence of interest have been *in vitro* digested (80 µM peptide and 5 µg proteasome in 100 µl TEAD buffer) for 24 h at 37 °C. Polypeptide digestion products were analyzed by LC-MS.

2.2.4 pMHC multimers

2.2.4.1 pMHC Class I monomer production

All pMHC monomers were produced in-house as previously described [76, 134]. Briefly, recombinant expressed and purified human HLA-A*02:01 and HLA-B*07:02 heavy chain and β2m were denatured in urea and subsequently refolded into heterodimeric pMHC complexes in the presence of an access of respective synthetic peptide. Re-folded pMHC monomers were purified using size exclusion chromatography on the ÄKTApure. The pMHC containing fraction of the second peak was collected, pooled, concentrated and stored at -80 °C. Click functionalization of azido-FLEXamers with either 400 µM DBCO-PEG4-Biotin or 400 µM DBCO-PEG4-Atto488 were performed as described in Effenberger et al. [76].

2.2.4.2 pMHC multimer staining

For non-reversible pMHC multimer staining, 0.4 µg biotinylated pMHC was multimerized on 0.1 µg fluorophore-conjugated Streptavidin backbone in a final volume of 50 µl for 30 min on ice, protected from light.

For reversible pMHC StrepTamer staining, 1 µg ATTO488-dye conjugated pMHC monomers was multimerized on 1 µl fluorophore-conjugated StrepTactin-backbone in a total volume of 50 µl FACS buffer (PBS + 0.5 % BSA, pH 7.0) for 30 min on ice, protected from light.

For staining, up to 5×10^6 cells were incubated with 50 µl fluorescent-labeled multimers/StrepTamers for 45 min on ice, protected from light. Surface mAB staining was added after 25 min and incubated for remaining 20 min.

2.2.5 TCR isolation

2.2.5.1 Double multimer-guided single cell sort for TCR isolation

HLA-matched $CD8^+$ purified apheresis material was thawed and rested O/N for 18 h. Cells were then washed twice in cold FACS buffer. Biotinylated pMHCs were multimerized either on a Streptavidin-BV421 or on a Streptavidin-APC backbone according to cell sample size (0.4 µg pMHC + 0.1 µg Streptavidin in 50 µl FACS buffer for up to 5×10^6 cells). Cells were incubated with BV421-conjugated multimer for 30 min on ice and protected from light, washed with FACS buffer, rinsed through nylon filter and processed for 'speed enrichment' (SE) on BV421 signal. Here, a fluorescent trigger was set on the BV421 channel and low frequency positive events were rapidly sorted with a loss in single cell resolution. Enriched cell fraction was counted and stained with APC-conjugated pMHC multimers of the same specificity for 45 min. After 25 min of multimer incubation, surface mABs for staining of phenotypic markers (panel: CD8-PC7, CD62L-PE and CD45RA-APCeF780) were added for additionally 20 min. Stained cell samples were washed twice with FACS buffer. Propidium iodide (PI) (1:100) was added for live/dead discrimination shortly before the single cell sorting of double multimer positive $CD8^+$ $CD62L^+$ $CD45RA^+$ cells.

2.2.5.2 pMHC multimer clone re-staining

After 12 days of feeder-free cell expansion in 384-well plate, growing clones were moved into a 96-well plate and cultured in complete RPMI supplemented with 180 IU/mL IL-2. Cells were taken off the T cell specific CD3/CD28 stimulus and maintained under the cytokine stimulus. Four to six days later, each clone was evaluated for pMHC re-staining. Cells were washed twice with cold FACS buffer and stained with CD45 mABs conjugated to different fluorophores (CD45-PO, CD45-PB, CD45-APCeF780 and/or CD45-PE-Cyanine7) for 20 min. Cells were washed twice with cold FACS buffer and individual samples were pooled according to a CD45-color code matrix. Biotinylated pMHC monomers were multimerized on Streptavidin-APC and Streptavidin-PE for double multimer staining of the multiplexed cell samples. Both multimers were stained consecutively for 20 min with a washing step in between. Bulk PBMCs stained with the same color code but as an individual sample, served as a negative control for fluorochrome artefacts, whereas PBMCs added within a pooled sample controlled for unspecific multimer recognition.

2.2.5.3 Single clone TCR PCR for NGS

A single cell derived clone population consisting of only a few cells up to larger clone sizes covering the bottom of a 384-well plate was of sufficient size for TCR sequence retrieval via single clone TCR polymerase chain reaction (PCR). The following protocol was adapted from a protocol published on "TCR SCAN" for specific amplification of the TCR *alpha* and *beta* chain sequence on single cells [77]. A scheme of the single clone

TCR PCR is depicted in figure 2.1 and further details of the individual reactions are listed in table 2.1 and the Materials section above.

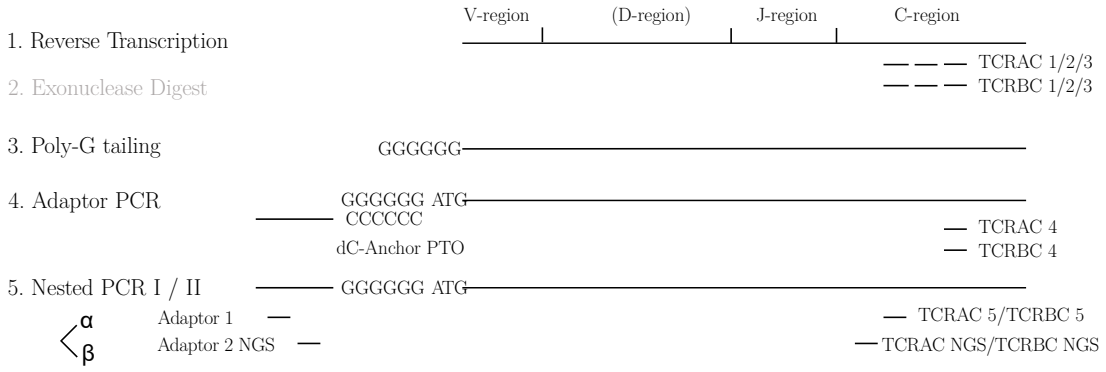

Figure 2.1: Single clone TCR PCR scheme. Single cell derived clones were processed in succeeding steps of PCR to specifically amplify the TCR *alpha* and *beta* chain fragments for next generation sequencing (NGS).

In detail, clones growing in a 384-well plate were spun down for cells to collect at the bottom of the plate. Next, cell culture supernatant was carefully removed, cells were resuspended in 2 µl reverse transcription reaction mix and transferred into a 96-well PCR plate. Efficient transfer of the cells was observed under the microscope. The PCR plate was sealed with an adherent foil and 10 µl of PCR-grade mineral oil overlaying each sample prevented evaporation of the small reaction volume. The first PCR step of reverse transcription for cDNA synthesis was followed by a step of exonuclease digest. Effective addition of 0.51 µl exonuclease reaction mix to each sample could be seen by the blue color of ADVABLUE PCR dye. In the next step of poly-guanine tailing, 7 µl of Terminal Deoxynucleotidyl Transferase and guanine nucleotide containing reaction mix was added and induced mononucleotide tailing to the 5' end of the amplicon. Subsequently, 40 µl of reaction mix containing the dC-Anchor forward primer was added for the next step of Adaptor PCR. For the first round of Nested PCR, 1 µl of Adaptor PCR product was added to 19 µl of reaction mix. In the second and final step of Nested PCR, 1 µl of Nested PCR I was added to 19 µl of reaction mix containing primers with NGS compatible indices. All PCR pipetting steps were performed in a DNAase/RNAase cleaned ultraviolet (UV)-irradiated UV box. PCR product of Nested PCR II was further processed for sequencing of TCR chain fragments on Illumnia MiSeq.

Table 2.1: PCR reactions for single clone TCR PCR..

PCR Step	Reverse Transcription		Exonuclease		Adaptor		Nest I/Nest II	
Master mix for 10 samples Volume in µl	Buffer	3.33	Buffer	3.48	Buffer	108.00	Buffer	43.20
	dNTP	5.33	Exonuclease I	1.74	dNTP	10.80	dNTP	4.32
	DTT	3.33	Adva Blue	0.63	Formamid	81.00	Formamid	32.40
	BSA	3.33			Herculase	10.80	Herculase	
	tRNA	3.33			Anchor Mix	8.18	Adaptor Mix 1/2	2.16
	Nonident P40	0.83			H_2O	213.22	H_2O	
	RNAsin	0.67						
	Reverse Transcriptase	1.67						
	RT Primer Mix	1.96						
	H_2O	2.87						
Vol Master mix per sample		2 µl		0.51		7 µl		19 µl for 1 µl DNAsample
Thermocycler settings								
	51 °C	30 min	37 °C	30 min	94 °C	3 min	94 °C	3 min
					24 cycles		24 cycles	
	70 °C	20 min	70 °C	20 min		30 s		30 s
					94 °C		94 °C	
	4 °C	pause	4 °C	pause	60 °C	30 s	62°C Nest I 62 °C Nest II	30 s
					72 °C	45 s	72 °C	45 s
					72 °C	5 min	72 °C	5 min
					4 °C	pause	4 °C	pause

2.2.6 Genome engineering via CRISPR/Cas9

Genome engineering via CRISPR/Cas9 gene KO and TCR KI has been described in previous publications [100, 135], and it is here described specifically to the experiments published in this thesis.

2.2.6.1 Generation of dsDNA HDR template

The double-stranded DNA (dsDNA) templates for CRISPR/Cas9-mediated HDR at TRAC locus were designed *in silico* with the following structure of the expression cassette: 5'homology arm (396 base pair (bp)), P2A, TCR-β, T2A, TCR-α (short C-region to merge with homology targeted TRAC locus), bGHpA tail, 3'homology arm (332 bp). Likewise, TCRs could be designed *in silico* with a murinized TCR constant region. The dsDNA templates were designed as following: 5'homology arm (396 bp), P2A, TCR-β (including mTRBC with additional cysteine bridge [95]), T2A, TCR-α (including mTRAC with additional cysteine bridge [95]), bGHpA tail, 3'homology arm (332 bp). All HDR DNA template sequences were synthesized by Twist and cloned into a vector with Ampicillin resistance for bacterial amplification.

dsDNA HDR templates were generated via PCR using the Herculase II Fusion Enzyme. PCR reaction mix for one TCR template amplification of 8×100 µl and thermocycler settings are listed in table 2.2. A sample of the PCR reaction was run on a 1 % agarose gel in an electrophoresis chamber for 40 min at 115 V to confirm template amplification and correct band size (1,5 kb for fully humanized TCR constructs and 2,1 kb for murinized TCR constructs).

PCR products were purified via Ampure XP bead purification following the manufacturer's protocol instructions. In short, 8×100 µl PCR reactions for one TCR template were pooled and mixed at a 1:1 volume ratio with Ampure XP beads in a LoBind-DNA Eppendorf tube. DNA-bound beads were washed twice with fresh 70 % ethanol. After all ethanol residuals were removed from the pellet on the magnet stand, DNA was eluted from the beads in 20µl 10mM Tris buffer pH 8.5. Concentration of dsDNA was measured via Nanodrop and set to 1 µg/µl.

Table 2.2: PCR reaction for generation of dsDNA HDR template.

Mastermix composition (800 µl)	**Thermocycler settings**	
8 µl DNA template	95 °C 3 min	
32 µl 10 mM forward primer	95 °C 30 s	×34
32 µl 10 mM reverse primer	62 °C 30 s	
8 µl Herculase II	72 °C 3 min	
8 µl 100 mM dNTPs	72 °C 3 min	
160 µl 5 × Herculase buffer	pause at 4 °C	
552 µl PCR grade H_2O		

2.2.6.2 RNP production

To assemble the guide RNA (gRNA) for targeted locus CRISPR/Cas9-engineering, 80 µM crRNA (see 2.1.7 for guide sequences) and 80 µM trans-activating crRNA (tracrRNA) were mixed in a 1:1 ratio, incubated at 95 °C for 5 min, and cooled to RT. HiFi-Cas9 was diluted in PBS to 6 µM (20 µl electroporation volume) or 20 µM (100 µl electroporation volume). 20 µM electroporation enhancer was added to gRNA. Diluted HiFi-Cas9 was added in 1:1 volume ratio to assembled gRNA and incubated at RT for 15 min. Generated RNPs were immediately applied to cells for CRISPR/Cas9-mediated KO and KI of T cells.

2.2.6.3 CRISPR/Cas9-mediated KO and KI of TCRs

Isolated PBMCs from whole blood were activated two days prior to electroporation using 2 µg CD3/CD28 Expamer, 300 IU IL-2, 5 ng/mL IL-7 and 5 ng/mL IL-15 in complete RPMI for 1×10^6 cells in 1 mL. Shortly before electroporation with RNPs, expamer stimulus was removed by incubating cells in PBS supplemented with 1 mM D-Biotin for 20 min at RT and then washing twice in PBS. Up to 1×10^6 cells were electroporated in 96-well nucleofection cuvettes (20 µl electroporation volume), whereas 5-20$\times10^6$ cells were electroporated in large nucleofection cuvettes (100 µl electroporation volume). Immediately before cell electroporation, hTRAC6/hTRBC3 RNPs (3 µl for 1×10^6 cells, 1 µl for $> 5\times10^6$ cells) and HDR template (1 µg/µ1$\times10^6$ cells) were incubated at RT for at least 30 s. For final electroporation step, cell samples with desired cell number were centrifuged and resuspended in appropriate volume of supplemented P3 buffer (20 µl for

1×10^6 cells in 20 µl cuvette, or depending on cell number up to 80 µl in 100 µl cuvette). Then, resuspended cell samples were thoroughly mixed with the prepared RNPs and HDR template mix and eventually transferred into the nucleofection cuvette. For electroporation, Lonza Nucleofector 4D X-unit or 96-well Shuttle Add-on was used with the pulse code EH-100 for primary human T cells. After electroporation, cells were cultured in RPMI SC^- supplemented with 180 IU/mL IL-2. After 12 h, 5 % antibiotics supplement was added to the culture.

Efficient editing was monitored 4-5 days post-electroporation via surface mABs and pMHC multimer staining for flow cytometry.

2.2.7 Genome engineering via retroviral transduction

2.2.7.1 Generation of retrovirus

For production of retroviral particles, the RD114 packaging cell line was seeded 24 h prior to transfection at 0.5×10^6 cells in 3 mL in a 6-well culture plate, to obtain optimal confluency (70 %) and proliferative state. Transfection of RD114 cells was achieved by calcium phosphate precipitation. Here, 18 µg of plasmid DNA were diluted in H_2O to a total volume of 135 µl. 15 µl of $CaCl_2$ solution (1,8375 g $CaCl_2$ in 5 mL H_2O, filtered through a 0.22 µm filter) was added to DNA and mixed with 150 µl transfection buffer under vortexing. Precipitate forming solution was incubated for 30 min at RT and subsequently added dropwise to adherent RD114 cells. After 6 h, medium was carefully discarded and replaced with 3 mL fresh complete DMEM. Transfected RD114 were incubated for 48-72 h until harvest of retroviral particles. For collection of retrovirus, the cell-free supernatant was collected, filtered through 0.45 µm filter, and stored for up to four weeks at 4 °C.

2.2.7.2 Retroviral transduction

Capan-2 and K562 target cell lines were retrovirally transduced via spinoculation. A 24-well plate (non-tissue culture treated) was coated with 250 µl retronectin for 2 h at RT according to the manufacturer's protocol. Then, retronectin was removed from the well and harvested virus supernatant was plated onto the retronectin-coated wells by centrifugation at 32 °C, for 2 h at 3000 x g. Target cells were seeded at 100.000 cells/well and spinoculation was performed by centrifugation at 32 °C, for 10 min at 1000 x g. Plate was incubated at 37 °C and transduction efficacy was assessed four days post-transduction via mAB staining and flow cytometry.

K562 target cells transduced with a HLA Class I heavy chain encoding vector were co-transduced with blue fluorescent protein (BFP) vector to facilitate selection of transgene expressing cells and discrimination in functional assays. Successfully transduced cells were purity sorted for transgene expression.

2.3 Functional assays

2.3.1 k-off rate measurements

For TCR:pMHC k_{off}-rate measurements with 20 min acquisition time, samples of >8000 $CD8^+$ TCR^+ cells were washed twice in cold FACS buffer and stained with CD45 color code mABs for 20 min on ice. After washing, samples were pooled according to color code and stained with 50 µl reversible APC-conjugated pMHC StrepTamer for 45 min on ice, in dark (for up to 5×10^6 total cells). After 25 min, surface mABs (CD8-APCeF780 and hTCR-PE or mTRBC-PE) were added and incubated for remaining 20 min of multimer staining. Bulk samples of fully humanized TCR-engineered T cells were washed twice with FACS buffer and then additionally stained for 20 min with 50 µl of anti-APC antibody. Subsequently, stained cells were washed twice with FACS buffer, resuspended in 1 mL FACS buffer and filtered into a polypropylene tube for acquisition at 4 °C. Shortly before acquisition, PI was added (1:100). After 30 s of acquisition, 1 mL of cold D-Biotin solution (2 mM) was added to the tube to initiate the dissociation of the pMHC backbone. Dissociation kinetics was measured for 20 min, or up to 30 min (increase cell sample size accordingly). For analysis of TCR:pMHC k_{off}-rate data, fluorescence data was exported from FlowJo to PRISM (GraphPad Software). The t1/2 was determined by fitting a one phase exponential decay curve.

2.3.2 Intracellular cytokine staining

To study *in vitro* responses of candidate TCRs to cognate peptide stimulation, cytokine release was measured upon co-incubation with peptide-presenting target cells. One day prior to co-culture, K562 target cells (retrovirally transduced with HLA-A*02:01 or HLA-B*07:02 and BFP) were irradiated at 80 Gy, washed twice, and resuspended in complete RPMI at a density of 3×10^6 /mL. Crude peptide diluted in DMSO was added to seeded K562 cells in a dilution series (10^{-4}M, 10^{-5}M, 10^{-6}M, 10^{-7}M, 10^{-8}M, 10^{-9}M, 10^{-10}M, 10^{-11}M, 10^{-12}M) and incubated O/N at 37 °C. TCR-engineered T cells were rested O/N in complete RPMI without supplementation of IL-2.

On the day of co-culture, peptide-pulsed K562 target cells were collected, washed three times in complete RPMI, and seeded into 96-well-U-bottom plate at 50.000 cells per well. Effector $CD8^+$ transgenic-TCR^+ T cells were seeded at 1:1 target to effector (T:E) ratio. Effector T cells and peptide-pulsed K562 target cells were co-cultured in complete RPMI supplemented with 1 µl/mL GolgiPlug for 4 h at 37 °C in a total volume of 200 µl. As positive control, 50,000 $CD8^+$ transgenic-TCR^+ T cells were incubated without target cells and stimulated with 1 µl/mL Brefeldin A containing protein transport inhibitor (GolgiPlug), 25 ng/mL phorbol myristate acetate (PMA) and 25 ng/mL ionomycin (Iono). As negative control, 50,000 $CD8^+$ transgenic-TCR^+ T cells were co-incubated with peptide-unpulsed K562 target cells or with medium only. All conditions were performed in technical duplicates.

After 4 h of co-culture, cells were transferred into 96-well-V-bottom plate for intracellular cytokine staining (ICCS). Cells were washed in FACS buffer and stained with 2 µg/mL ethidium monoazide (EMA) for 15 min on ice with direct light exposure for

live/dead discrimination. Next, cells were washed twice and incubated for 20 min with a mAB mix for surface markers (CD3-BV421, CD8-APCeF780 and hTCR-PE or mTRBC-PE). After washing in cold FACS buffer, cells were resuspended in 100 µl Cytofix/Cytoperm solution and incubated for 30 min in the dark on ice for permeabilization and fixation. Samples were washed twice in cold Permwash buffer. From now on cells were pelleted using 1700 rpm instead of 1500 rpm. For intracellular staining, mABs for cytokines (IL-2-APC and IFNγ-FITC) were diluted in Permwash buffer and applied to cells for 40 min. Samples were washed twice in cold Permwash buffer and finally resuspended in cold FACS buffer, filtered through nylon mesh, and processed for sample acquisition on a flow cytometer Cytoflex S Cell analyzer.

2.3.3 xCELLigence killing assay

Real-time T cell cytotoxicity assays were performed using the xCELLigence RTCA System. Adherent target cells were collected and washed twice in complete RPMI. For peptide pulsing, adherent target cancer cell lines were incubated for 2 h under gentle agitation in complete RPMI with 10^{-5} M crude peptide at 2×10^6 cells/mL. Then, peptide-pulsed target cells were washed twice in complete RPMI to remove excess of peptide.

96-well E-plates were filled with 100 µl complete RPMI and placed in the craddle of xCELLigence® RTCA System for plate set-up and background measurement. 1×10^4 target cells were then seeded in 100 µl per well. Growth of target cells was measured via impedance signal for at least 24 h before effector T cell addition. Growth of target cells was titrated for each cell line to find optimal initial seeding number. Target cells should have initiated growth curves up to a minimum of a cell index of 0.5.

$CD8^+$ transgenic-TCR^+ T cells were rested O/N, washed in complete RPMI before cell seeding. Prior to addition of effector T cells, 100 µl medium were carefully removed from each sample well. Effector T cells were added in 100 µl complete RPMI supplemented with 100 IU/mL IL-2 with variable cell numbers according to different T:E ratios (1:1, 1:3, 1:5, 1:10, and 1:20). Real-time cytotoxicity was measured in 15 min sweeps for at least 48 h. As positive control of target cell line growth, 100 µl complete RPMI without effector T cells were added (medium control wells). As positive control of target cell lysis, 100 µl of complete RPMI containing 2 % Triton X-100 (TRX) were added.

xCELLigence RTCA Software Pro (ACEA) and Prism8 (GraphPad) were used to analyze the data.

E-plates were re-used up to five times. For plate regeneration, all cell containing wells were trypsinized O/N, and thoroughly washed twice with PBS and finally with H_2O. Washed plates were dried with open lid under the sterile bench.

3 Results

3.1 Isolation and characterization of RNF43 neo-epitope-specific TCRs

3.1.1 Identification of candidate neo-epitopes by *in silico* predictions

The tumor suppressor gene RNF43 is frequently mutated in pancreatic cancer and other GI cancers. Due to the high occurrence of fs-mutations (Fig. 1.4), RNF43 bears the potential for highly immunogenic neo-epitopes that can serve as targets in ACT. In order to predict putative RNF43 neo-epitopes via *in silico* prediction tools in an unbiased manner, we simulated all possible neo-ORFs derived from a deletion of one or two DNA nucleotides (Fig. 3.1). Using NetMHC4.0, we predicted the peptide-MHC class I binding affinity for all peptides between 8 and 11 aa length to the most common HLA class I molecules present in the European Causcasian population. The *in silico* prediction revealed 1200 possible 8mers, 1167 possible 9mers, 1136 possible 10mers and 1105 possible 11mers with a range of affinities from 4.4 nM to 48,000 nM. High binding affinity of <500 nM, but preferably <50 nM, is routinely used as a threshold for peptide selection, as it ensures the capacity of a peptide epitope to elicit an immunogenic response [136]. Further studies showed that the binding of a peptide to the cognate MHC correlates with tumor eradication, and affinities of at least 10 nM are required for relapse-free cancer regression [137]. According to this evidence, we set a cut-off of 20 nM binding affinity to reduce the number of potential candidates (35 peptides) that were further evaluated by Prof. Dr. Peter Kloetzel (Institute for Biochemistry, Charité Berlin, Germany). For seven selected neo-epitope candidates, longer pre-cursor-peptides (18 to 27aa length) were synthesized and tested for proteasomal processing using an *in vitro* proteasome digestion assay followed by mass spectrometry analysis (Fig. 3.1). *In vitro* proteasomal processing revealed only three peptides to be processed from precursor peptides in their exact epitope sequence (Table 3.1). Other candidate peptides were processed in slightly longer peptide variants (up to 14mers), which no longer showed high predicted MHC Class I binding affinity.

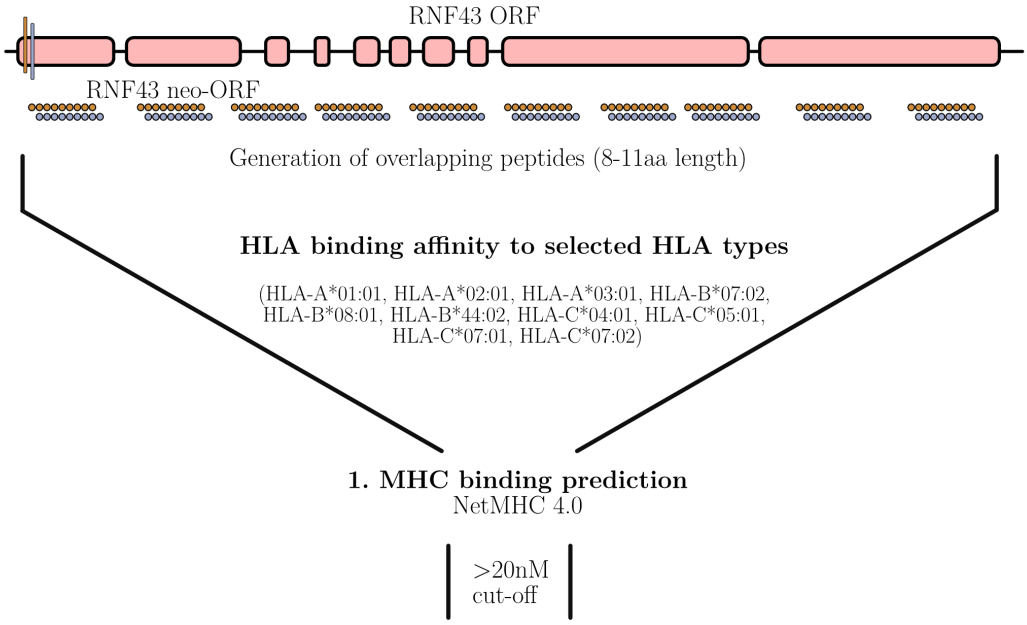

Figure 3.1: RNF43 neo-epitope prediction from neo-ORFs. Schematic depiction of RNF43 neo-epitope prediction and selection of candidate peptides. All fs-derived neo-ORFs have been simulated and binding affinities to common HLA Class I molecules were *in silico* predicted for all neo-peptides of 8-11aa length. Candidates below the binding affinity cut-off were further evaluated for proteasomal processing.

We decided to first focus on two neo-epitopes - SLLPTCWAL specific for HLA-A*02:01 and VPSVWRSSL specific for HLA-B*07:02. The selected HLAs are relatively abundant in the European Caucasian population, with the HLA-A*02:01 being the most common haplotype (25 % HLA-A*02:01 and 9 % HLA-B*07:02, Source: `http://allelefrequencies.net/`). Surprisingly, many predicted epitopes showed high binding affinity to HLA-B*07:02. Notably, a substantial number of fs-mutations reported in PDAC patients lead to the translation of the selected neo-peptides (Table 3.1), emphasizing the degree of sharedness among individual patients and indicating a high relevance of the target for clinical application.

Furthermore, we included a second HLA-A*02:01-restricted specific neo-epitope that results from the G659fs mutation. This mutation is most frequently occurring in patients with GI cancers, including PDAC [128, 138]. This epitope showed a predicted peptide-MHC class I binding affinity of 50 nM that was exceeding the set cut-off of >20 nM. However, as the predicted binding affinity was still within the range of expected immunogenic epitopes, it was included as a third epitope candidate in the screen for neo-epitope-specific TCRs.

Altogether, we set the focus on three distinct RNF43 fs-derived neo-epitopes: A2-RNF43_SLLPTCWAL, B7-RNF43_VPWVWRSLL and A2-RNF43_TQLARFFPI.

Table 3.1: RNF43 neo-epitope selection.

Peptide	HLA haplotype	Predicted affinity (Kd, nM)	Mutations in patients leading to neo-epitope	Precursor peptide for *in vitro* processing	*In vitro* processed
SLLPTCWAL	HLA-A*02:01	6.8	R27fs, K145fs, R40fs, S41fs, E43fs, L65fs, A115fs, C119fs, P192fs, P195fs, R225fs, Q254fs, S264fs, A269fs, C275fs, E318fs, C309fs	SFASIPAMPTTT SLLPTCWALPGVQW	epitope
HPRSQAWAL	HLA-B*07:02	5	R27fs, K145fs, R40fs, S41fs, E43fs, L65fs, A115fs, R117fs, C119fs, P192fs, R225fs, Q254fs, S264fs, C275fs, A269fs, E318fs, C309fs	LVPSCHPRSQAWALGITAS	11mer 12mer 14mer
VPSVWRSSL	HLA-B*07:02	6	R27fs, K145fs, R40fs, S41fs, E43fs, L65fs, A115fs, C119fs, P192fs, P195fs, R225fs, Q254fs, S264fs, A269fs	AQPLCVPSVWRSSLRGRSY	epitope 10mer 11mer
IPAMPTTTSL	HLA-B*07:02	6.5	R27fs, K145fs, R40fs, S41fs, E43fs, L65fs, A115fs, R117fs, C119fs, P192fs, P195fs, R225fs, Q254fs, S264fs, A269fs, C275fs, E318fs, C309fs	SFASIPAMPTTT SLLPTCWALPGVQW	13mer 14mer
RPAAGRPGV	HLA-B*07:02	13.2	R27fs, K145fs, R40fs, S41fs, E43fs, L65fs, A115fs, R117fs, C119fs, P195fs, R225fs,	PPGGT RPAAGRPGVSGQTQG	12mer 14mer
APGRSPAPL	HLA-B*07:02	15	A33fs, K54fs, L88fs, R117fs, R119fs, L311fs, R363fs, K45fs, L61fs, F69fs, P195fs,	SRAAAPGRSPAPLCTRL	epitope
HPRSQAWAL	HLA-B*08:01	17.7	See above	LVPSCHPRSQAWALGITAS	See above
TQLARFFPI	HLA-A*02:01	50	G659fs	N/A	N/A

3.1.2 Candidate neo-epitopes can be stably refolded in pMHC complexes

After having identified a pool of candidate neo-epitopes, we generated pMHC multimer reagents for the isolation of neo-epitope-specific TCRs. For this purpose, recombinant human HLA class I heavy chains (HLA-A*02:01 or HLA-B*07:02) and β2m were *in vitro* refolded with peptides of interest to form stable pMHC monomers. Purification via size exclusion chromatography indicated stable refolding into trimeric pMHC monomers for all three neo-peptides (Fig. 3.2, middle peak).

Considering that the HLA binding affinity of the selected RNF43 fs-derived neo-epitopes has only been predicted using *in silico* tools, successful pMHC refolding was a first indicator of strong peptide-MHC binding affinity, thus validating the initial *in silico* prediction.

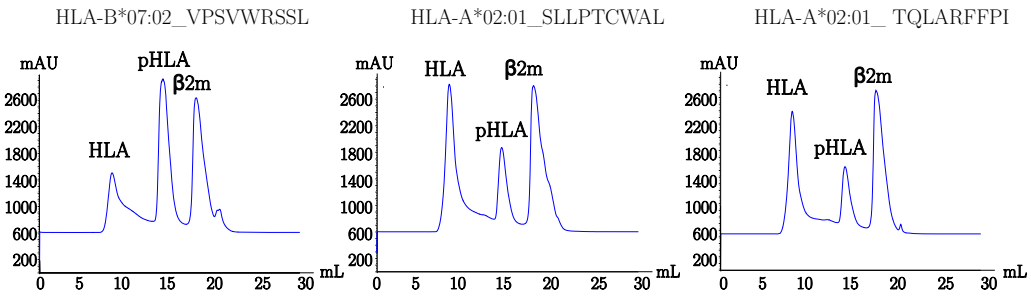

Figure 3.2: RNF43 neo-epitopes form stable pMHC monomers. Exemplary ÄKTA profiles for selected RNF43 neo-epitope candidates show stable pMHC monomer refolding in presence of MHC heavy chain and β2m. Distinct second size exclusion chromatography peak represents stably refolded pMHC protein.

3.1.3 TCR isolation platform

pMHC multimers represent a versatile tool to specifically detect and isolate antigen-reactive T cells. However, neo-epitope-specific TCRs are only found in extremely low frequencies in the naive repertoire of healthy donors. To tackle this challenge, we have established a platform for efficient identification and isolation of rare antigen-specific T cells using a combination of target cell pre-enrichment (SE) followed by sensitive single cell sorting based on double multimer pMHC staining. Consecutively, we introduced a workflow for TCR sequencing, re-expression and functional characterization to identify highly functional TCRs suitable for ACT (Fig. 3.3). The TCR isolation routine presented in this thesis was applied to isolate and characterize TCRs targeting the three selected RNF43 fs-derived neo-epitopes. Each epitope will be discussed in a separate results section. To give an overview of the general procedure, we briefly introduce into the major steps of the platform.

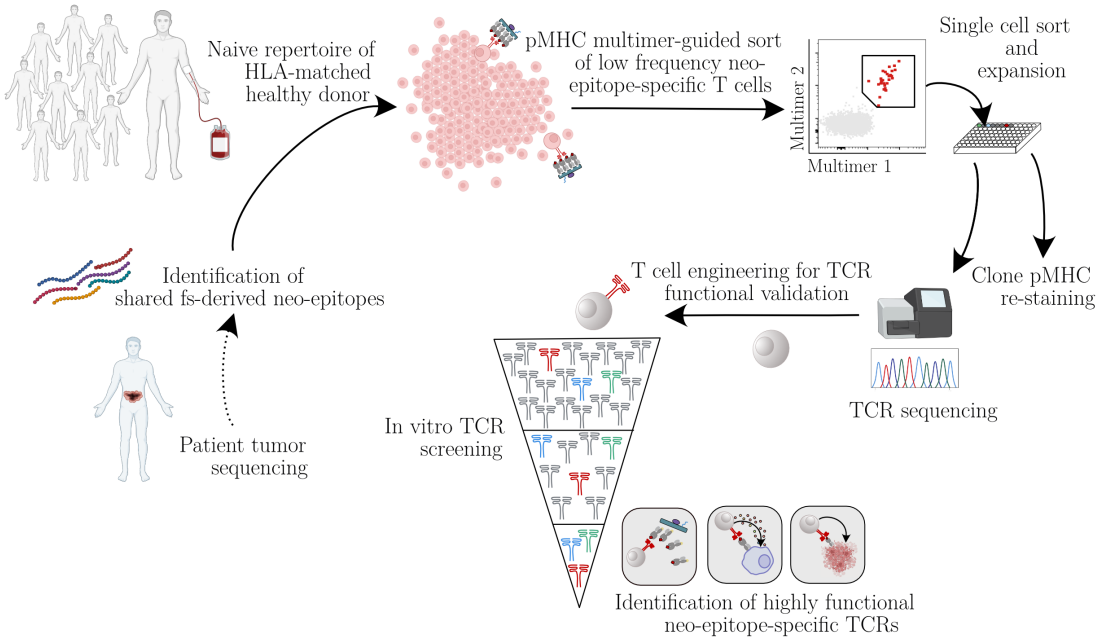

Figure 3.3: TCR isolation platform and workflow for functional characterization. Schematic depiction of neo-epitope identification and isolation of low-frequency neo-epitope-specific TCRs from the naive repertoire of HLA-matched healthy donors. $CD8^+$ apheresis material is initially processed for SE on pMHC multimer specificity and subsequently single cell sorted for double pMHC multimer positive, naive $CD8^+$ T cells. Expanded clones were re-stained with pMHC multimers and processed in single clone TCR PCR for sequencing of the TCR *alpha* and *beta* chain via NGS. Identified TCRs were re-expressed via CRISPR/Cas9-guided OTR for functional characterization. Indicated *in vitro* assays identify highly functional TCRs. Patient tumor sequencing information comes from database searches and is not included in this thesis, but shown for the sake of completeness (dotted arrow).

To overcome the indisputable low frequency of neo-epitope-specific naive CD8$^+$ T cells, firstly we increased the total number of donor cells. Instead of conventional whole blood supply, we used CD8$^+$ T cell-enriched apheresis as a starting material for the TCR isolation process. Initially, CD8$^+$ purified apheresis material was stained for assessing purity and frequencies of naive CD8$^+$ T cells. The HLA-type was also determined via mAB staining (Fig. 3.4).

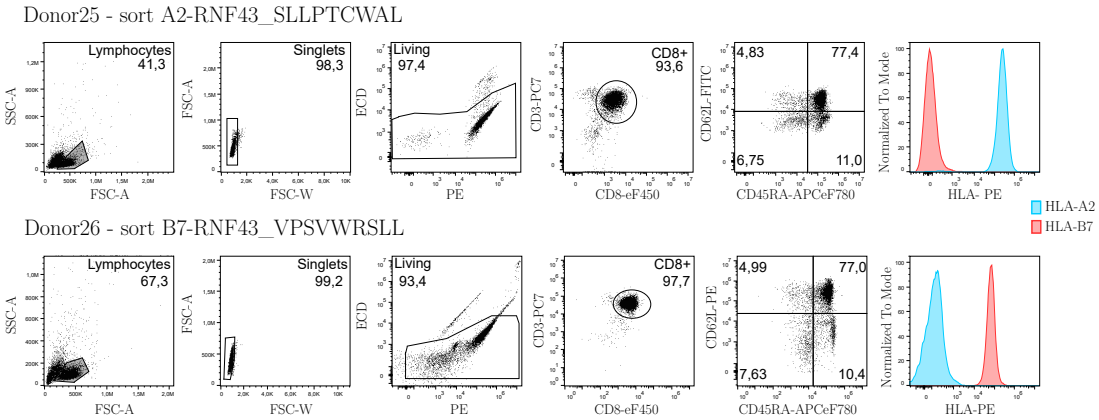

Figure 3.4: Staining of CD8$^+$ purified apheresis. Exemplary flow cytometry plots of CD8$^+$ apheresis stained for purity. Staining with mABs identified HLA-type of the donor and frequency of naive (CD62L$^+$/CD45RA$^+$) CD3$^+$ CD8$^+$ T cells.

CD8$^+$ T cell-enriched apheresis material comprised between 3-6$\times10^8$ cells, a number exceeding feasible sorting procedure and pMHC consumption. Thus, we took advantage of a flow cytometric method called 'fluorescent triggering' or SE, for a quick enrichment of minor subpopulations [139]. In detail, a fluorescent trigger is set on one channel, thereby limiting the complexity of the analysis of the detected events to one parameter. A threshold is set to a definable value, and all events within the pulse width are selected. Despite a loss of single cell resolution, this method of SE enables the enrichment of low frequency events from large sample sizes in a short time, thanks to the application of a high flow-rate with low electronic hardware resources.

Applied to our purpose, CD8$^+$ purified apheresis material was first stained with one neo-epitope-specific pMHC multimer conjugated to a BV421-fluorochrome, and enriched according to this fluorochrome signal (Fig. 3.5). The step of SE usually reduced the total number of cells in the donor material to 1-5$\times10^6$. Enriched cells were subsequently stained with a second pMHC multimer of the same specificity but conjugated to a different fluorochrome. Double multimer staining significantly enhances specificity of the staining, thus minimizing the selection of false positive neo-epitope-specific TCRs. Additionally, a staining panel of mABs for phenotypic surface markers was established to identify specifically the naive cell population. All double multimer positive, CD8$^+$ naive (CD62L$^+$ CD45RA$^+$) T cells were single cell index sorted and monoclonally expanded in a feeder-cell-free system. The lack of feeder cells and solely plate-bound CD3/CD28

T cell stimulation for single cell expansion, is crucial for sensitivity and specificity of the subsequent single clone TCR PCR.

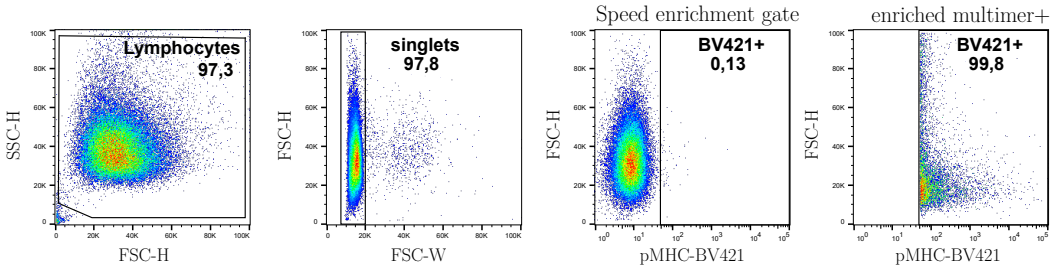

Figure 3.5: Speed enrichment of neo-epitope-specific T cells from CD8$^+$ purified apheresis through single multimer staining. Flow cytometry plots indicate gating strategy for size and granularity for detection of lymphocytes and singlets. Fluorescent trigger and threshold value is set on BV421-fluorochrome conjugated pMHC multimer.

After 10-12 days, clones have grown to a considerable size to analyze a cell sample for multimer recognition. The pMHC multimer re-staining builds a first step in the evaluation for neo-epitope specificity, as it facilitates the exclusion of false neo-epitope-specific TCRs from the downstream steps of TCR characterization. Importantly, the remaining cells were processed in a reverse transcription reaction and several steps of TCR PCR for retrieval of the cDNA sequence of the TCR *alpha* and *beta* chains (Fig. 2.1). PCR fragments were sequenced via NGS. With the identified TCR sequence of the sorted and expanded clones, TCRs were *in silico* assembled for gene synthesis and subsequent genetic engineering into donor T cells for TCR re-expression and further functional characterization (Fig. 3.3).

3.1.4 TCR re-expression via OTR for functional characterization

To re-express and characterize the isolated TCRs, we applied advanced genetic engineering using CRISPR/Cas9-mediated editing of donor primary T cells as previously established by our group [100]. We simultaneously KO the TCR *alpha* and *beta* chains, and introduce the transgenic TCR into the endogenous TCR *alpha* locus via HDR of a linear DNA template encoding the new TCR sequence. This method of OTR is a non-viral approach for targeted T cell engineering, leading to physiological and homogeneous expression of the transgenic TCR [100, 102].

HDR templates for TCR KI were designed to encode the homology arms for targeted integration into the TRAC locus of exon 1 (Fig. 3.6). The inserted transgene is expressed from the locus in its physiological way and no extrinsic promoters are needed. Self-cleaving peptides (P2A and T2A) ensure separate expression of the two chains (*beta* chain followed by *alpha* chain). Here, we used two different approaches of TCR *in silico* design. TCR sequences can be either left fully humanized in the constant region or edited for its murine counterpart, which included an additional cysteine bridge (mTRBC-Cys,

mTRAC-Cys) [95]. This modification enables improved surface expression of the TCR and facilitates identification of re-expressed transgenic TCR via surface mAB staining of the murine T cell receptor *beta* chain (mTRBC). In short-term *in vitro* assays, OTR-engineered TCRs with a murine constant region did not show any functional differences to TCRs with a human TCR constant region [100]. Detailed protocols and description of template design are publicly available [135].

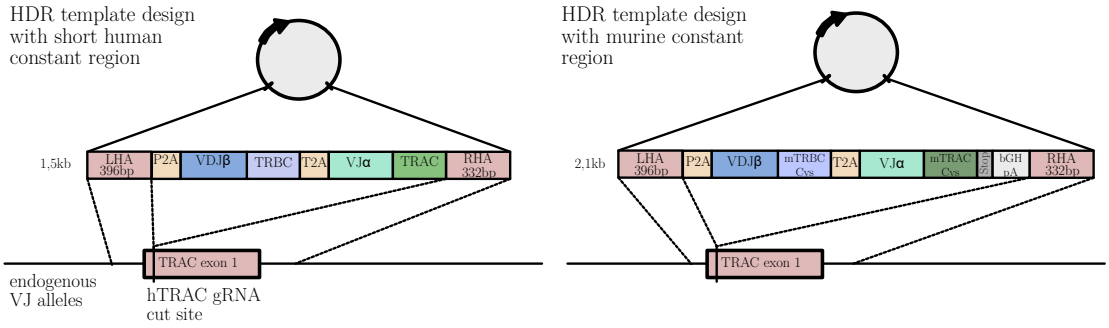

Figure 3.6: HDR template design for OTR. The construct is synthesized and expressed on a simple plasmid for bacterial amplification. The HDR dsDNA fragment is generated via PCR with primers binding in the flanking left and right homology arms (LHA, RHA). Homology arms facilitate integration via HDR into the TRAC locus of exon 1. The LHA is followed by the self-cleaving peptide P2A, which allows the separation of the following VDJ *beta* chain segments from the LHA. A following self-cleaving peptide (T2A) promotes separate expression of the VJ *alpha* chain segments. The *TCR* chains are either kept fully humanized in the constant region (left) or are edited for a murine constant region (right). For humanized constructs, the transgenic hTRAC region only encompasses the part that lies upstream of the editing site (TRAC exon 1) and then seamlessly continues into the RHA. For murinized constructs, the *alpha* chain concludes with a stop codon (TGA). The following bovine growth hormone polyA signal (bGHpA) facilitates stability of the mRNA transcript.

In the following, re-expressed candidate TCRs were deeply characterized for *in vitro* functionality. Various assays including pMHC-multimer re-staining, peptide stimulation, TCR structural avidity measurements and cytotoxicity assays classified highly specific and potent TCRs. Identified highly functional TCRs can then be transferred into *in vivo* models and potential clinical application.

3.1.5 Characterization of TCRs targeting A2-RNF43_SLLPTCWAL neo-epitope

3.1.5.1 Identification of TCRs specific for A2-RNF43_SLLPTCWAL neo-epitope

In silico predictions of neo-epitopes derived from fs-mutations of the tumor suppressor gene RNF43 predicted high binding affinity of the peptide SLLPTCWAL to the HLA-A*02:01. Furthermore, the peptide was successfully processed from precursor peptides in its exact epitope sequence in an assay of *in vitro* proteasomal processing (Table 3.1). Together with the fact that HLA-A*02:01 is the most common HLA class I molecule in the European Caucasian population, we prioritized this epitope as a first target to isolate RNF43 neo-epitope-specific TCRs from the naive repertoire of a healthy donor.

$CD8^+$ enriched apheresis of a HLA-A*02 positive donor was used as starting material and source for TCR identification (Fig. 3.4, top). The cell material was processed as described above (chapter 3.1.3). Briefly, neo-epitope-specific T cells were first enriched according to a single A2-RNF43_SLLPTCWAL pMHC multimer staining, and then sorted according to double multimer staining and phenotypic naive markers. In total, 22 naive $CD8^+$ T cells with a noticeable double multimer staining were single cell index sorted from this donor (Fig. 3.7).

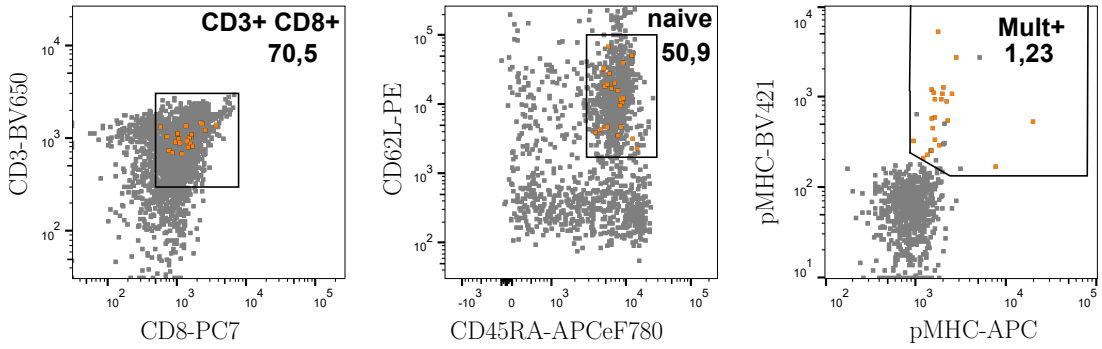

Figure 3.7: Isolation of A2-RNF43_SLLPTCWAL neo-epitope-specific T cells. 247×10^8 $CD8^+$ apheresis cells were stained with A2-RNF43_SLLPTCWAL-specific pMHCs multimerized on a BV421-fluorochrome labeled Streptavidin backbone, and multimer positive cells were enriched through speed enrichment. Subsequently, 0.5×10^6 enriched cells were stained with a second A2-RNF43_SLLPTCWAL pMHCs multimerized on an APC-fluorochrome labeled backbone for higher specificity of the staining. Further, surface mAB staining for phenotypic markers allowed distinct detection of $CD8^+$ naive ($CD62L^+$ $CD45RA^+$) T cells. Depicted is the gating strategy for accessing neo-epitope-specific naive $CD8^+$ T cells, where sorted double multimer positive cells are indicated in orange. Sorted cells clearly originated from $CD8^+$ naive T cell population. Pre-gated on lymphocytes, singlets, living.

Sorted cells were expanded in a feeder-cell-free system for 12 days and clone growth was scored under the microscope (Fig. 3.8 A). We observed a recovery rate of 50 %

(Fig. 3.8 B), as expected from the use of frozen material. All growing clones reaching a minimum score of II (<25 % of the well covered) were evaluated for pMHC multimer re-staining, besides TCR sequencing (Fig. 2.1). On the contrary, clones reaching a score of I were not split for pMHC re-staining and only processed in the single clone TCR PCR. However, clones with low expansion often showed poor sequencing results and no clear identification of the two TCR chains.

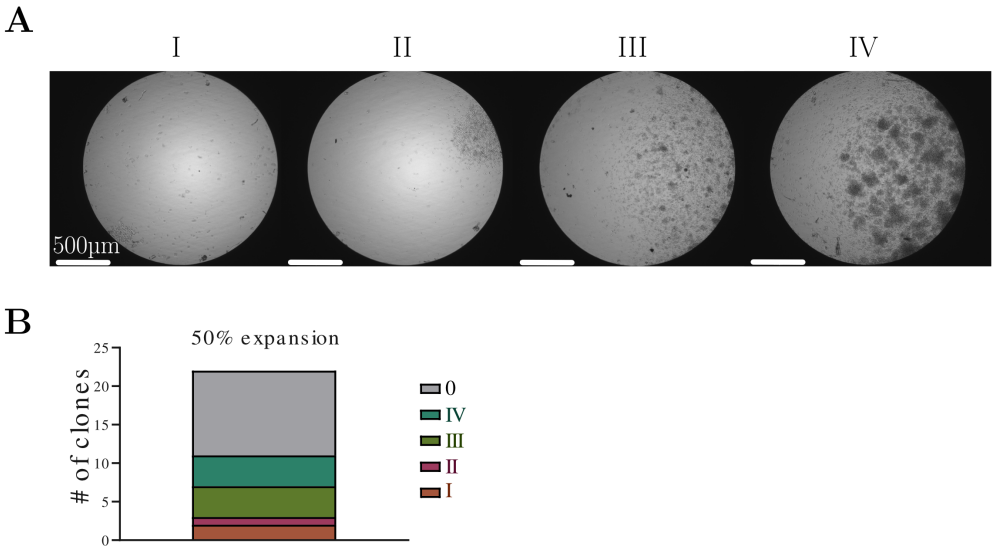

Figure 3.8: Expansion of A2-RNF43_SLLPTCWAL neo-epitope-specific sorted T cells. Evaluation of clone growth of putative neo-epitope-specific $CD8^+$ naive T cells sorted according to double multimer staining. A) Exemplary pictures of expanded clones evaluated for clonal expansion in 384-well plate under the microscope. Scoring system defines 0=not expanded, I=few cells growing, II≤25 %, III≤50 % and IV≥50 % of the well covered with expanded clone population. Microscopic pictures were taken at 4 x magnification. Scale bar indicates 500 µm. B) Scoring of A2-RNF43_SLLPTCWAL-specific sorted T cells, expanded in a feeder-free system for 12 days. Single cell-derived clones were processed for TCR sequence for identification and, whenever possible according to the clone size, stained with pMHC multimers to assess epitope specificity.

For pMHC re-staining, clones were color coded via different CD45 fluorochrome-coupled mABs and then pooled for double pMHC multimer re-staining. On the one hand, staining with pMHC multimers labeled with two different fluorochromes increases signal specificity. On the other hand, the clone multiplexing approach facilitates efficient processing and simultaneous analysis of many samples of small cell number. Additionally, samples receive homogeneous pMHC staining exposure for better comparability. Unrelated PBMCs spiked within the multiplexed sample controlled for unspecific multimer recognition.

In total, eight clones were evaluated for pMHC recognition (Fig. 3.9). Four clones (B5, B16, B19 and B21) showed a clear recognition of the A2-RNF43_SLLPTCWAL multimer,

which the cells were initially sorted with. A positive pMHC recognition validates the epitope specificity of the expanded clone and represents a first hint for a promising TCR candidate. Clone B11 and B12 showed an intermediate double multimer staining that still distinguished from the negative control but hinted at a weaker pMHC multimer recognition. Clone B2 and B10 showed no considerable pMHC recognition above the control cell population of unrelated PBMCs.

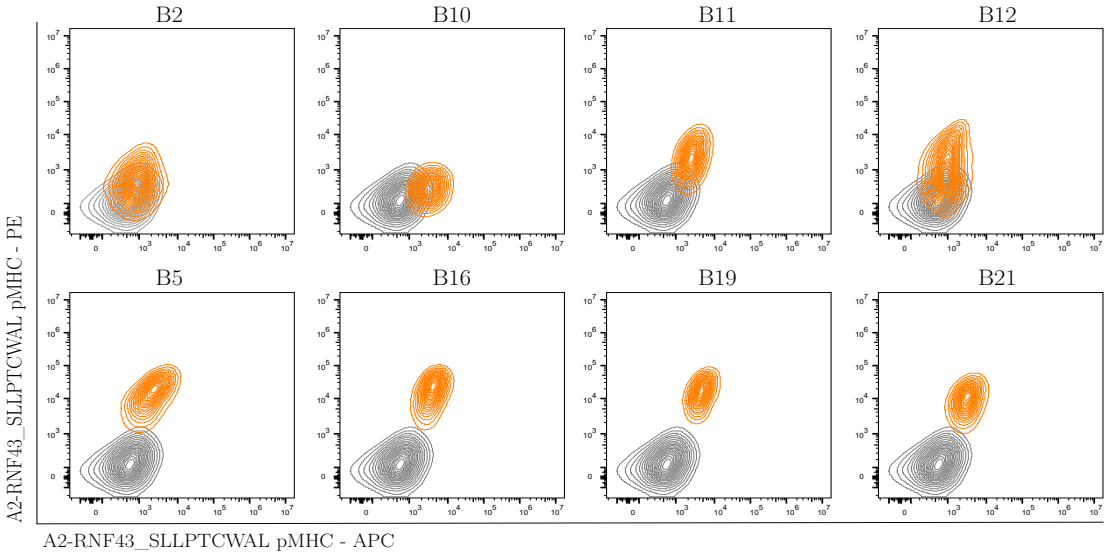

Figure 3.9: A2-RNF43_SLLPTCWAL pMHC multimer staining of expanded T cell clones. Clones derived from double multimer sort on putative neo-epitope-specific naive $CD8^+$ cells were split after 12 days of clonal expansion and stained as color-coded, multiplexed samples with PE- and APC-fluorochrome labeled A2-RNF43_SLLPTCWAL pMHC multimers. Labeling above the flow cytometry plots indicates the name given to each clone. Double multimer staining of expanded clones is shown in orange, whereas unrelated PBMCs used as negative control for multimer recognition are shown in grey. Pre-gated on lymphocytes, singlets, living, $CD8^+$, $CD45^+$ color code.

All 11 clones expanding after single cell sort were sequenced and 10 clones were identified with a clear result of TCR *alpha* and *beta* sequence (Table 3.2). Surprisingly, five clones showed identical variable chains and CDR3 regions for both the TCR *alpha* and *beta* chain. Backgating of the individual index sorted cells showed a clear naive phenotype, thus excluding any contamination from a clonal expanded TCR from the memory repertoire. Clone B11 was identified with two distinct *alpha* chains. For *in silico* assembly of TCR sequences for TCR re-expression, the chain with the higher clone count in the sequencing result was chosen. We identified a clear TCR sequence also for clone B9 and B22 and, despite pMHC re-staining data were not available due to limited sample size, we considered these TCRs as valuable candidates for TCR re-expression and functional characterization (Table 3.2).

We concluded with six identified A2-RNF43_SLLPTCWAL-specific candidate TCRs for further *in vitro* functional characterization, of which two showed promising pMHC multimer re-staining.

Table 3.2: TCR sequences of A2-RNF43_SLLPTCWAL sorted clones.

	all V Hits		aaSeqCDR3		Clone Count		MHC-staining*	
Clone name	**TRAV**	**TRBV**	**TRAV**	**TRBV**	**TRAV**	**TRBV**		**RNF43 TCR****
B5					197	4002	+	
B12					4390	3962	+/-	
B16	TRAV21	TRBV19	CAVRPDYNAGNMLTF	CASTLVPGDTIYF	482	2513	+	R11
B19					350	1747	+	
B21					1838	252	+	
B2	TRAV12-2	TRBV20-1	CAARDNNARLMF	CSARDINTGELFF	4902	7615	-	R12
B9	TRAV8-1	TRBV20-1	CAVNPGNTDKLIF	CSALSRVPETQYF	211	360	?	R13
B10	TRAV8-6	TRBV29-1	CAVSTRGYNKLIF	CSVEDLRLEGSNTEAFF	879	519	-	R14
B22	TRAV12-2	TRBV4-2	CAPFTNTGNQFYF	CASSPGTGIGEQYF	26267	7997	?	R15
B11	TRAV19	TRBV20-1	CALSGNNARLMF	CSAHQASAQETQYF	728	1845	+/-	R16
	TRAV22		CAVDISNFGNEKLTF		526			
B17	no NGS result						?	

* pMHC multimer re-staining is specified as positive (+), intermediate (+/-), negative (-) and not tested (?).

** Identifier of candidate A2-RNF43_SLLPTCWAL TCR for *in silico* assembly and re-expression is indicated.

3.1.5.2 pMHC multimer staining of TCR-engineered T cells for A2-RNF43_SLLPTCWAL-specificity

To start in depth *in vitro* functional characterization of the identified candidate TCRs, we generated HDR templates for CRISPR/Cas9-mediated OTR. All six TCRs (R11-R16) were synthesized in a fully humanized version with a shortened human constant region in the *alpha* chain that integrates into the physiological locus of the TRAC exon 1 (Fig. 3.6 left). OTR enables close to physiological expression of the candidate TCR in the endogenous locus under the regulation of the endogenous promoter.

All candidate TCRs were re-expressed via OTR in healthy donor PBMCs and, starting from five days post-editing, expression of the transgenic TCR was evaluated via flow cytometry. Effective KO of endogenous TCR expression can be assessed via surface mAB staining of the human TCR. In contrast to a TCR design including a murine constant region, the KI of a fully humanized transgenic TCR can only be detected via pMHC multimer staining, which was therefore used for evaluating transgenic TCR KI efficiency and specificity simultaneously.

We identified a clear recognition of the A2-RNF43_SLLPTCWAL multimer in $CD8^+$ T cells expressing TCR R11, R12, R13 and R15 (Fig. 3.10 A). Indeed, TCR R11 and R15 showed a strong A2-RNF43_SLLPTCWAL $multimer^+$ human TCR^+ population. Despite a convincing multimer recognition, TCR R13 was consistently found to be of minor cell viability post-editing. Finally, TCR R12 showed a weaker multimer staining but consistently separated from the remaining human TCR^+ population. Importantly, all four TCRs specifically recognized the A2-RNF43_SLLPTCWAL epitope, as indicated by the absence of signal when stained with a HLA-A*02:01 multimer specific for an irrelevant epitope (A2-pp65 CMV epitope) (Fig. 3.10). TCR KI efficacy in $CD8^+$ T

cells ranged between 2 and 10 % as estimated by the frequency of multimer positive events (Fig. 3.10 B). In contrast, we could not confirm epitope specificity for TCR R14 and R16, which only showed background noise comparable to the TCR KO only samples and mock (unedited cells) negative controls.

Altogether, we identified four TCRs specifically recognizing A2-RNF43_SLLPTCWAL pMHC multimers, but we also observed a scarce reliability of the pMHC multimer re-staining at the level of single cell-derived clones in predicting TCR specificity. Indeed, the initial pMHC recognition of clones expressing the TCR R11 could be confirmed after re-expression of the TCR. However, this was not the case for TCR R12 and R16 for which the initial data on pMHC re-staining were not validated in TCR-engineered T cells. Unfortunately, clone pMHC re-staining was not available for TCR R13 and R15.

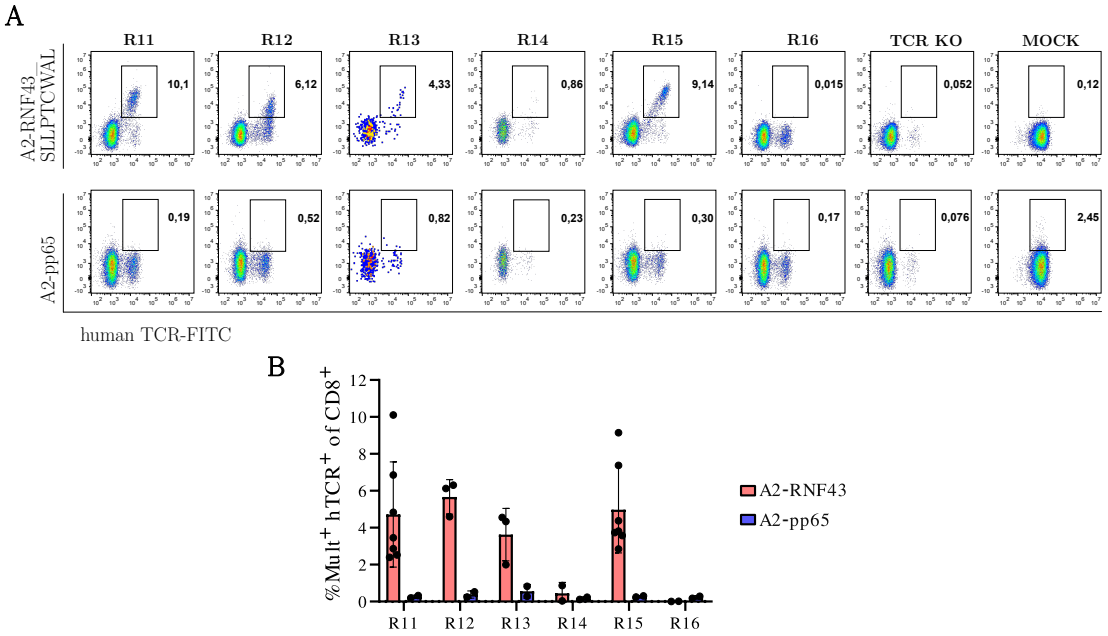

Figure 3.10: A2-RNF43_SLLPTCWAL-specific multimer recognition. A) Exemplary flow cytometric analysis of pMHC multimer reactivity and specificity of OTR-engineered PBMCs. Successful editing was determined by mAB staining for human TCR and pMHC multimer staining. pMHC-multimer reactivity and specificity was analyzed by staining with relevant (A2-RNF43_SLLPTCWAL) or irrelevant (A2-pp65) pMHC multimer. Unedited PBMCs (mock) served as negative control. Labeling above the flow cytometry plots indicates the name given to each TCR. B) Quantification of multimer staining with relevant A2-RNF43_SLLPTCWAL and irrelevant A2-pp65 pMHCs. Pre-gated on lymphocytes, singlets, living, $CD8^+$.

3.1.5.3 Measurement of A2-RNF43_SLLPTCWAL-specific TCR structural avidity

Initial pMHC multimer staining indicated TCR R11, R13 and R15 as TCRs with sole recognition of A2-RNF43_SLLPTCWAL pMHC multimers. A strong multimer stain-

ing is already a good indicator of TCR specificity. The measurement of the TCR structural avidity - binding strength of a TCR to its cognate antigen in presence of CD8/CD4 co-receptor - can further identify functionally potent TCR candidates [105]. In our laboratory, we have developed a flow cytometry-based assay for measuring the TCR:pMHC k_{off}-rate, which is a major determinant of the overall TCR structural avidity. In short, TCR-expressing $CD8^+$ T cells are stained with a reversible StrepTamer (pMHC-ATTO488 multimerized on a fluorochrome-conjugated StrepTactin backbone). Upon the addition of D-Biotin, the binding interaction between the pMHC-streptag and StrepTactin is disrupted and the multimer complex dissociates (Fig. 3.11 A). Monomeric TCR:pMHC interactions are of low avidity. Therefore, pMHCs start dissociating depending on the binding strength of the cognate TCR, and the kinetic of dissociation can be measured by the acquisition of the decay of pMHC-ATTO488 signal over time (Fig. 3.11 B-C). Even though a fully humanized TCR is the most physiological approach to express a candidate TCR, it remains challenging to track the TCR expressing cells in a bulk population upon signal loss of the pMHC multimer. Moreover, due to rather low CRISPR/Cas9-editing frequencies, achieving the necessary number of transgenic TCR-expressing cells would require excessive amount of starting material. Therefore, OTR-edited cells have been purity sorted for pMHC $multimer^+$ $CD8^+$ T cells and rapidly expanded on feeder cells for following experiments.

TCR:pMHC k_{off}-rates have been measured for the TCRs with strong pMHC multimer recognition only. Color coding of the samples via CD45-fluorochrome labeled mABs allowed multiplexing of samples for homogeneous StrepTamer exposure and identical D-Biotin mediated dissociation. Unfortunately, the measurement did not result in a reliable detection of pMHC monomer signal decay. Fitting one-phase exponential decay curves through the reduction of pMHC-ATTO488 fluorescence intensity over time, did not yield in defined half-life for the TCR:pMHC interaction (Fig. 3.11 C). Many measurements of low structural avidity TCRs stayed below the detection limit.

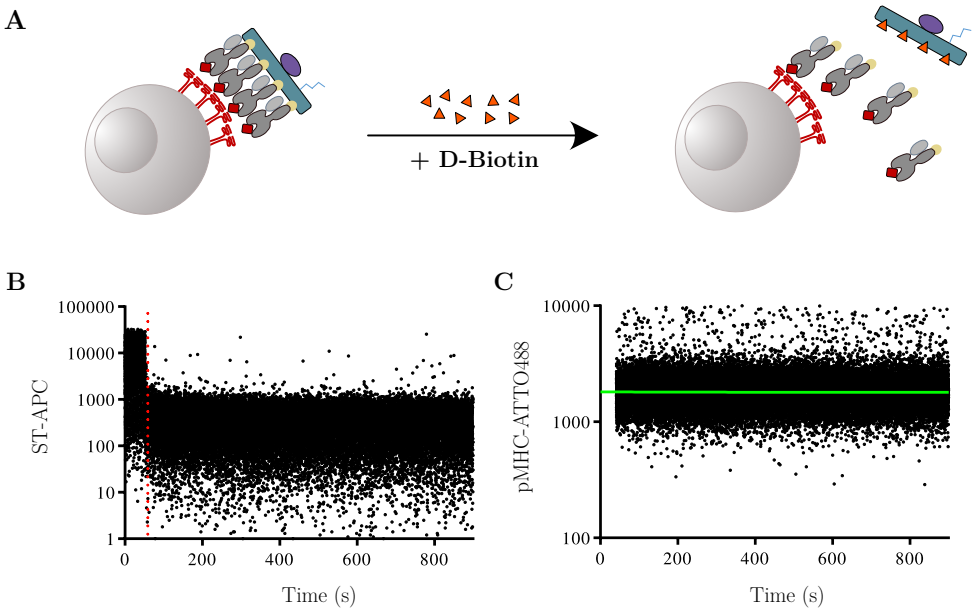

Figure 3.11: Structural avidity measurement of A2-RNF43_SLLPTCWAL pMHC multimer-reactive TCRs. A) Schematic depiction of TCR:pMHC k_{off}-rate measurements. B-C) Flow cytometry-based TCR:pMHC k_{off}-rate measurements with purity sorted A2-RNF43_SLLPTCWAL pMHC multimer$^+$ CD8$^+$ T cells. Representative plot indicates initial high signal for StrepTactin-APC (ST-APC) multimer and rapid signal loss over time upon D-Biotin addition. Red dotted line indicates time point of D-Biotin addition for backbone dissociation (B). Tracking of pMHC-ATTO488 fluorescence intensity over time. Green line attempts to fit a one-phase exponential decay curves through the reduction of pMHC-ATTO488 fluorescence intensity over time (C). Pre-gated on lymphocytes, singlets, living, CD8$^+$, color code CD45 resolution.

3.1.5.4 Evaluation of peptide sensitivity of A2-RNF43_SLLPTCWAL-specific TCRs.

Flow cytometry-based measurement of TCR structural avidity did in this case not reveal further indications of potentially functional TCR candidates. To further validate TCR functionality, we performed peptide stimulation assays and measured reactivity of OTR-engineered T cells by means of cytokine release and TCR downregulation. IFN-γ is a highly T cell-specific and assay sensitive cytokine that is commonly used to detect recent CD8$^+$ T cell activation and reactivity to peptide stimulation. Besides IFN-γ, we also stained for IL-2, a cytokine released upon recent antigen recognition. Further, T cells respond highly sensitive to antigen recognition with downregulation of the TCR [97]. Similarly to the TCR:pMHC k_{off}-rate assay, the low CRISPR/Cas9-editing efficacy remained an obstacle in the analysis of peptide sensitivity in a bulk TCR-engineered T cell population. Therefore, we purity sorted transgenic TCR-expressing CD8$^+$ T cells according to A2-RNF43_SLLPTCWAL multimer and rapidly expanded them on feeder cells to a feasible cell number for further functional assays. We used a K562 cell line,

retrovirally transduced to express the human HLA-A*02:01, as artificial APC line. K562 target cells were pulsed with different concentrations of SLLPTCWAL peptide and then co-cultured with TCR transgenic $CD8^+$ T cells. T cells cultured in medium only or co-incubated with unpulsed K562-HLA-$A2^+$ cells served as negative controls, whereas a strong TCR independent stimulus via PMA/Iono was used as a positive technical control for T cell stimulation and subsequent staining.

We measured peptide reactivity of all four TCR candidates showing positive multimer recognition. TCR R11, R13 and R15 showed IFN-γ release upon stimulation with high peptide concentrations (-4M and -5M) (Fig. 3.12 A-B), but only TCR R11 responded also to lower peptide concentrations (-8M), thereby exhibiting the most sensitive response. TCR R11 was also the only TCR with a stimulation dose-dependent release of IL-2. TCR R13 and R15 showed a minor profile of IL-2 release. In line with the cytokine responses, we found TCR R11 to strongly downregulate the surface expression of the TCR with increasing concentration of peptide stimulation, and TCR R13 and R15 reducing TCR expression only at high level of peptide stimulation (Fig. 3.12 B). Quantification of relative IFN-γ release and TCR downregulation uncovered a spectrum of peptide sensitivity. The peptide concentration mediating half-maximal effector function (EC_{50}) was lowest for TCR R11 (Fig. 3.12 C) followed by R15 and finally R13. TCR R12 did not show response to peptide stimulation in any of the three parameters measured for T cell reactivity, and a quantification in EC_{50} value was not measurable. Release of IL-2 did not display a sensitive readout for TCR reactivity to peptide stimulation and could not be further quantified in EC_{50} values.

Taken together, TCR R11 was highly sensitive to A2-RNF43_SLLPTCWAL peptide stimulation, responding in all evaluated parameters of TCR functionality. TCR R13 and R15 were identified as functional but less sensitive to peptide stimulation. TCR R12, which already showed a weak pMHC multimer recognition in previous assays, persisted with low target recognition and lack of functionality.

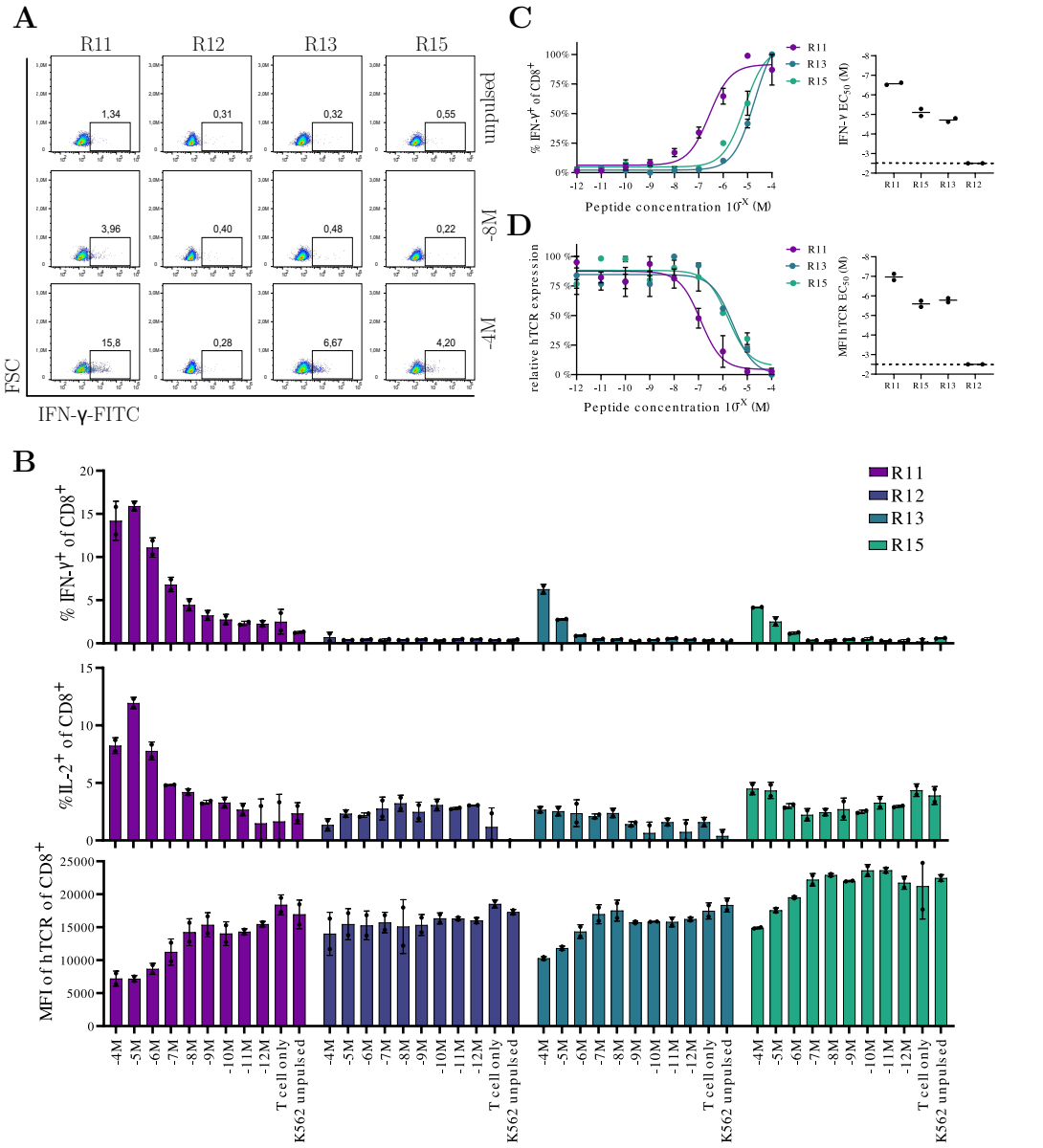

Figure 3.12: A2-RNF43_SLLPTCWAL-specific TCRs responded to peptide stimulation. OTR-engineered T cells were co-cultured with peptide-pulsed K562-HLA-A*02:01 target cells at equal T:E ratio (1:1) for 4 h of stimulation. Addition of a Brefeldin A containing protein transport inhibitor prevented cytokine release and enabled intracellular cytokine staining for detection via flow cytometry. A) Representative raw data plots of all A2-RNF43_SLLPTCWAL-specific TCRs for IFN-γ release upon stimulation with peptide-pulsed target cells. B) Dose-dependent response to peptide stimulation of TCR showing release of IFN-γ, IL-2 and TCR downregulation. T cell only and unpulsed target cells served as negative controls. C) Quantification and EC_{50} value of relative response of IFN-γ release. D) Quantification and EC_{50} value of relative response of TCR downregulation. Dotted line indicates non-measurable EC_{50} value due to lack of dose-dependent response. Flow cytometry analysis pre-gated on lymphocytes, living, singlets, $CD8^+$.

3.1.5.5 *In vitro* processing and presentation of A2-RNF43_SLLPTCWAL epitope in K562 cells

So far, we have proven a high MHC Class I binding affinity of RNF43 neo-epitope SLLPTCWAL to the HLA-A*02:01 via successful pMHC refolding and used this pMHC for the isolation of neo-epitope-specific TCRs. Importantly, A2-RNF43_SLLPTCWAL-specific TCRs responded to stimulation with peptide-pulsed target cells with high sensitivity.

Still, we have not demonstrated yet the processing and physiological presentation of the target epitope. The K562 cell line is an ideal platform for both exogenous and endogenous antigen presentation to human T cells, as previously described in various studies [140–142]. In addition, it is easy to genetically manipulate. Thus, we designed a vector for retroviral expression of the RNF43 A269fs-mutation (deletion of an A in position 804 of the coding sequence), which is one of the mutations leading to the expression of the SLLPTCWAL neo-epitope (Fig. 3.13 A). The K562 cell line, already retrovirally engineered for HLA-A*02:01 expression, was additionally transduced with viral particles for stable integration and expression of the RNF43 fs-mutated protein. Co-expression of a green fluorescent protein (GFP) facilitated the purification and tracking in functional assays of RNF43 A269fs-mutation expressing cells via flow cytometry (Fig. 3.13 B). The newly generated target cell line could then be used for stimulation assays with A2-RNF43_SLLPTCWAL-specific OTR-engineered T cells.

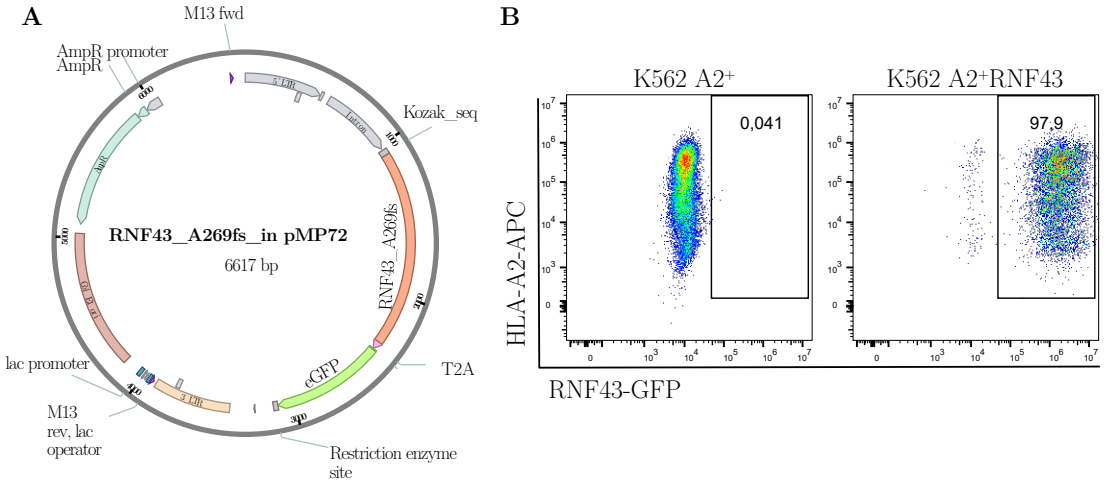

Figure 3.13: Engineering of K562 cells to model epitope processing. A) Schematic depiction of the design of the retroviral expression vector. Expression of RNF43 A269fs-mutation is separated from GFP expression via a T2A element for simultaneous but non-fused protein expression. The transfection of the plasmid into the RD114 retroviral packaging cell lines, lead to the generation of retroviral particles. B) HLA-A*02:01$^+$ K562 cells (left) were retrovirally transduced. Flow cytometry plots depicting successfully edited and purity sorted HLA-A*02:01$^+$ K562 cells (right). GFP expression indicates RNF43 A269fs-mutated protein expression.

Similarly to the previously described peptide stimulation assay with peptide-pulsed HLA-A*02:01$^+$ K562 cells (K562 A2$^+$) and cytokine release as an analytical readout, we performed a similar experiment with the newly generated K562 A2$^+$ target cell line expressing the RNF43 A269fs-mutation (K562 A2$^+$RNF43) (Fig. 3.14).

After purity sorting and expansion, TCR R11-engineered CD8$^+$ T cells have been co-cultured with K562 A2$^+$RNF43 target cells at increasing T:E ratio, reflecting an increasing stimulation strength due to higher target availability. SLLPTCWAL peptide-pulsed K562 A2$^+$ cells served as a positive control. As negative control, we used unpulsed K562 A2$^+$ cells, and K562 cells expressing an irrelevant HLA class I molecule either or not engineered for the additional expression of the mutated RNF43, namely K562 B7$^+$ and K562 B7$^+$RNF43. Furthermore, CD8$^+$ T cells expressing an irrelevant HLA-A*02:01-restricted TCR specific for a viral epitope (SCoV34) served as an additional negative control for unspecific reactivity towards RNF43 fs-expressing K562 cell lines.

Besides the stimulation with peptide-pulsed APCs, remarkably, we could detect a strong response of TCR R11 also after stimulation with K562 A2$^+$RNF43 cells. The response in IFN-γ release was titratable with increasing T:E ratio. Absence of cytokine release in all other negative controls validated the epitope specificity of this TCR. Overall, we concluded that the HLA-A*02:01-restricted RNF43 fs-derived neo-epitope is indeed intracellularly processed in K562 cells and presented via the MHC Class I complex at the cell surface.

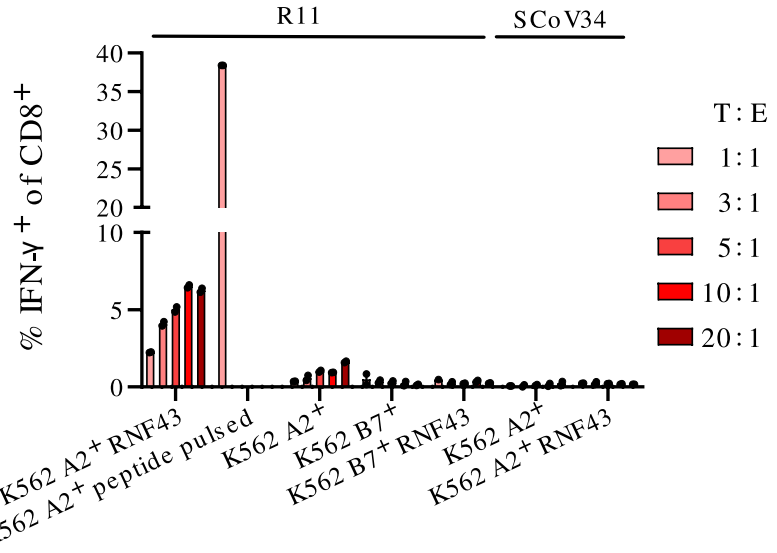

Figure 3.14: A2-RNF43_SLLPTCWAL TCRs target recognition upon physiological processing in K562 HLA-A2$^+$ transduced RNF43 fs-expressing cells. OTR-engineered T cells were co-cultured with indicated K562 target cells at specified T:E ratio for 4 h of stimulation. Inhibition of protein transport via Brefeldin A during co-culture time enabled intracellular mAB staining for IFN-γ and readout via flow cytometry. TCR R11-engineered T cells responding to SLLPTCWAL peptide pulsed (-5M) K562 A2$^+$ target cells at 1:1 T:E ratio served as positive control. Non-target expressing K562 cells and T cells expressing irrelevant SCoV34 TCR served as negative control. Flow cytometry analysis pre-gated on lymphocytes, living, singlets, CD8$^+$.

3.1.5.6 Neo-epitope expressing PDAC cell line is killed by TCR-engineered T cells

In the system of artificial antigen presentation in K562 cells, we have identified physiological processing and surface presentation of the A2-RNF43_SLLPTCWAL neo-epitope. Moreover, we confirmed the high specificity and functionality of the neo-epitope-specific TCR R11. Next, we sought to show physiological epitope presentation and T cell activity in a disease relevant system.

RNF43 is frequently fs-mutated in patients with GI cancers. By screening the literature and large biobanks of cancer cell lines for RNF43 fs-mutations, we have identified the Capan-2 PDAC cell line carrying the R330fs-mutation (Fig. 3.15 A) [143]. This mutation leads to a neo-ORF and the expression of the SLLPTCWAL neo-epitope. We determined the HLA-type via surface mAB staining and found this cell line to be negative for HLA-A*02:01 (Fig. 3.15B left). Therefore, we retrovirally transduced the Capan-2 cell lines for HLA-A*02:01 expression (Fig. 3.15B right).

A

	RNF43 mutational status (endogenous)		HLA type		
cell line	Position of mutation	Classification	HLA-A2	HLA-B7	engineering
Capan-2	R330fs	frameshift	negative	negative	transduce HLA- A*02:01

B

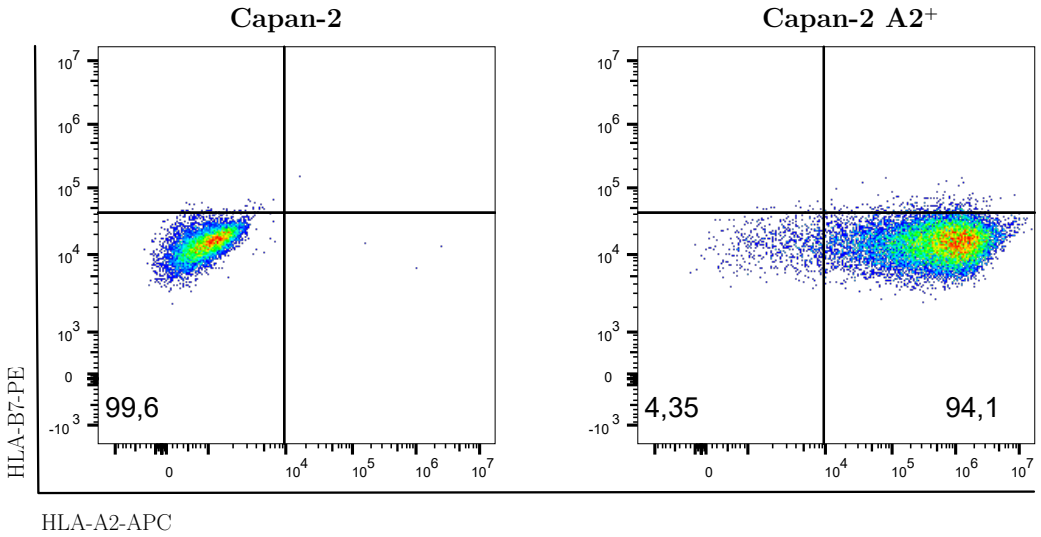

Figure 3.15: HLA-engineering of RNF43 fs-expressing Capan-2 PDAC cell line. A) Overview of Capan-2 mutational status for RNF43 fs-mutation. B) Capan-2 cells (left) were retrovirally transduced for expression of HLA-A*02:01. HLA-type was monitored via flow cytometry after staining with HLA-A*02 and HLA-B*07 mABs. Successfully engineered Capan-2 cells with stable HLA-A*02:01 surface expression were purity sorted and expanded into a newly generated Capan-2 A2$^+$ target cell line (right). Pre-gated on living cells.

The Capan-2 A2$^+$ represents a good target cell line for further cytotoxicity assays to evaluate the killing potential of candidate TCRs. We used the xCelligence technology for impedance-based real-time immune cell cytotoxicity assays. Adherent target cells are seeded in a plate with gold microelectrodes in the bottom of each well. For impedance measurements, a very low electric current is applied. Adherent cells act as electrical insulators and cell growth is reported as a dimensionless parameter called Cell Index (CI, CI= (impedance at time point n – impedance without cells)/nominal impedance value). Lysis of target cells initiated by for instance immune cell cytotoxicity results in loss of adherent properties of the growing target cell lines and a drop in impedance detection.

In order to determine the killing potency of A2-RNF43_SLLPTCWAL-specific TCRs, Capan-2 (HLA-A*02:01 negative) and Capan-2 A2$^+$ target cells were seeded and grown in the measurement well for 24 h. Next, A2-RNF43_SLLPTCWAL multimer sorted and expanded CD8$^+$ T cells were added at various T:E ratios to growing target cells, and cell growth was monitored via the impedance signal for additional 48 h. Target cells

growing in medium only (no T cell addition) served as positive control for undisturbed cell growth. The detergent TRX was added as a positive control for cell lysis.

We analyzed the cytotoxic potential of the three A2-RNF43_SLLPTCWAL-specific TCRs that showed reactivity in the peptide stimulation assay (Fig. 3.12). Previous assays for measurements of TCR structural avidity and *in vitro* functionality have identified TCR R11 as the most potent TCR, followed by TCR R15 and R13. Corroborating previous results, cytotoxicity assays showed a strong killing of the Capan-2 $A2^+$ cells by TCR R11 (Fig. 3.16 A top). Increasing number of effector cells continuously strengthened target cell lysis, and a T:E ratio of 1:20 killed Capan-2 $A2^+$ cells entirely. TCR R13 did not show an effect of Capan-2 $A2^+$ target cell lysis, regardless of the number of effector cells added. TCR R15 showed intermediate, but titratable cytotoxicity on Capan-2 $A2^+$ cells, but even the highest T:E ratio of 1:20 did not induce full killing but rather a strong inhibition of target cell growth. The impact of target cell growth inhibition of TCR R15 at a 1:5 ratio is comparable to the effect of TCR R11 at a 1:3 ratio, pointing out the increased potency of the latter. As a control for unspecific killing of target cells just by the pure addition of T cells to the measurement well, unedited $CD8^+$ T cells (mock) were added to seeded target cells. The addition of high numbers of unedited $CD8^+$ T cells (1:20) dampened target cell line growth and we conclude that high T:E ratios have a negative impact on the sensitivity of the assay due to unspecific cytotoxicity on the target cell line. Further, unedited T cells remain a TCR-heterogenous population with potential allogeneic reactivity. As a control for target-specific killing, TCR-engineered T cells were added to growing Capan-2 cells. In this system the fs-derived neo-epitope SLLPTCWAL, cannot be presented to the T cells due to the lack of HLA-A*02:01 expression. Expectably, there was no target cell lysis induced by any of the candidate TCRs (Fig. 3.16 A bottom). Further, we studied target-specific cell lysis of the TCR R11 on another PDAC cell line. T3M4 is a HLA-A*02:01^+ cancer cell line with RNF43 wild type (wt) expression. Transgenic TCR-engineered T cells did not induce lysis in this particular target cell line that lacks neo-epitope expression, thus supporting the neo-epitope dependency for specific target killing (Fig. 3.16 B). T3M4 showed an initial transient drop in the cell index upon addition of high number of effector cells. However, this was imputable to the pure addition of T cells as the same kinetic was observed after the addition of the identical number of unedited (ue) T cells (Fig. 3.16 B). To further control for specific killing of RNF43 fs-specific TCRs, we compared the full titration of TCR R11-engineered effector cells with the cytotoxic potential of effector cells engineered with a HLA-A*02:01-restricted TCR specific for a viral SARS-CoV-2 epitope (irrelevant TCR). SCoV34 TCR-engineered T cells showed no killing effect on Capan-2 $A2^+$ and Capan-2 target cell line growth (Fig. 3.16 C). Only high numbers of effector cells (T:E 1:20) dampened the growth curves minimally. TCR R11-engineered T cells continuously showed a titratable cytotoxic impact specifically on the Capan-2 $A2^+$ cells.

In summary, we concluded that TCR R11 is a highly potent TCR with strong killing potency on cells expressing the fs-derived SLLPTCWAL neo-epitope in the context of HLA-A*02:01 expression. TCR R11 did not recognize wt RNF43 HLA-A*02:01 target

cells. TCR R15 also recognized and killed target expressing cells, however at lower functionality.

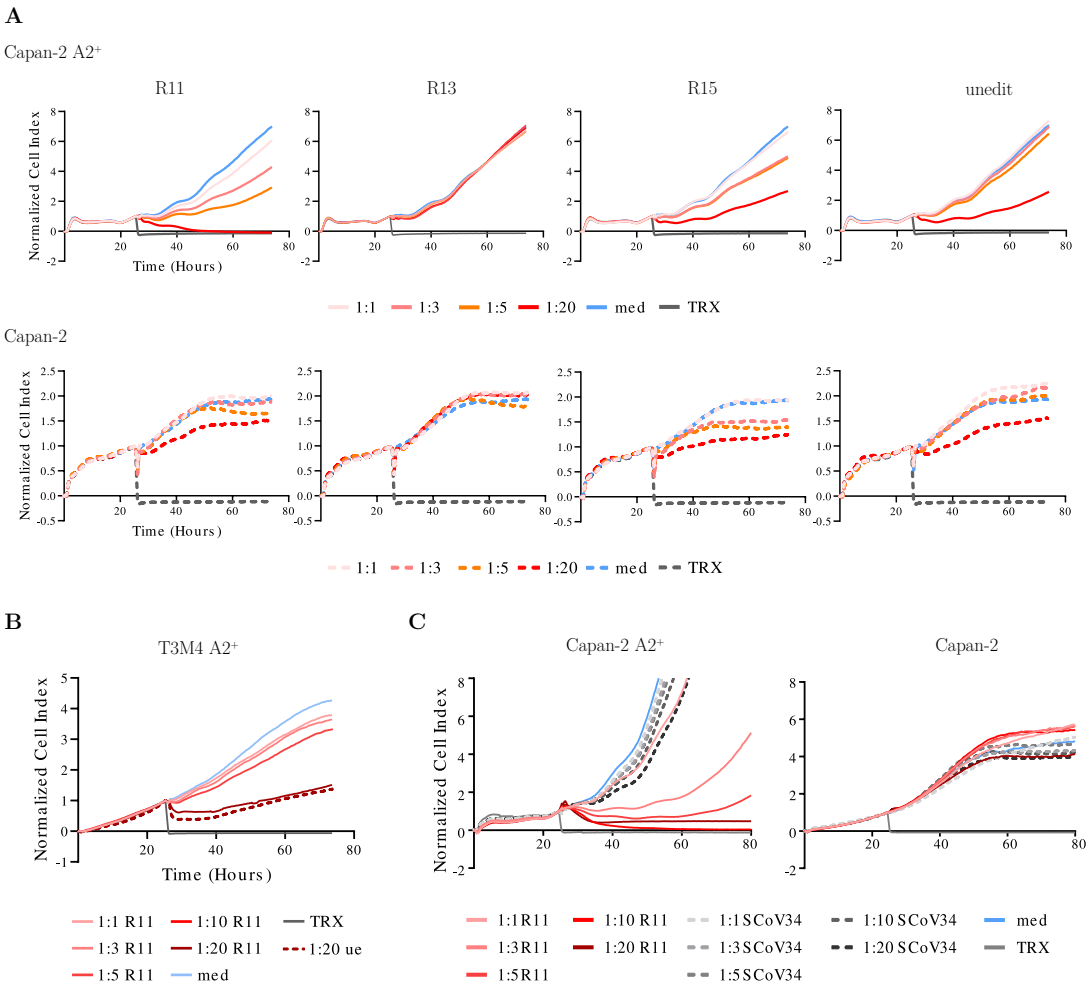

Figure 3.16: TCR R11 specifically kills RNF43 fs-mutated Capan-2 A2$^+$ PDAC cells. OTR-engineered T cells were co-cultured with target cells at specified T:E ratio in 96-well E-plate for time continuous impedance measurement. After 24 h of target cell growth, TCR-engineered CD8$^+$ T cells expressing A2-RNF43_SLLPTCWAL-specific TCRs were added at indicated T:E ratio. Medium was added as negative control for unimpaired target cell growth. TRX was added as positive control for immediate cell lysis. A) Capan-2 cells carry endogenous RNF43 fs-mutation and was engineered for expression of HLA-A*02:01. Unedit (ue) T cells control for unspecific target cell killing. B) HLA-A*02:01 positive T3M4 cell line expressed wt RNF43. C) T cells engineered with an irrelevant virus specific HLA-A*02:01 TCR (SCoV34) controlled for unspecific killing due to effector cell addition.

3.1.5.7 Evaluation of identification of A2-RNF43_SLLPTCWAL-specific TCRs

In the previous sections, we have shown that the identified TCR R11 is a highly functional TCR specifically recognizing the HLA-A*02:01 fs-derived RNF43 neo-epitope SLLPTCWAL. TCR R11 showed strong pMHC multimer recognition and responded sensitive to peptide stimulation. Further, TCR R11 specifically killed neo-epitope-expressing cancer cells in real-time cytotoxicity assays. Besides TCR R11, we have identified TCR R13 and TCR R15 as target-specific TCRs with intermediate functionality. The initially selected set of TCRs for in depth functional characterization also comprised TCR candidates that did not confirm multimer recognition after re-expression and were therefore considered as non-functional.

All selected TCR candidates were identified via flow cytometry sort as multimer-specific T cells. Backgating to the original sort gate concluded that all five identified cells with TCR R11 clustered at the tip of highly double multimer positive cells (Fig. 3.17 A). TCR R13 and R15 with intermediate functionality were located right below R11 in the multimer sort gate (Fig. 3.17 B). Interestingly, non-functional TCRs cluster at the bottom end of the multimer sorted population. TCR R16 located in the initial sort gate close to the functional TCRs R13 and R15, but did not show A2-RNF43_SLLPTCWAL multimer recognition, and was consequently considered as non-functional. Still, it needs to be mentioned that the initial clone of TCR R16 was identified with a fully expressed second *alpha* chain, that was neglected for re-expression with the TCR *beta* chain due to lower clone count (Table 3.2). It has not been tested, whether the TCR expression the other *alpha* chain would have led to a target-specific TCR.

Overall, we observed an enrichment in functional TCRs in cells showing high fluorescent intensities of pMHC multimers at the time of sorting. However, this observation was not consistent enough to suggest the use of multimer staining as a reliable predictor of TCR functionality.

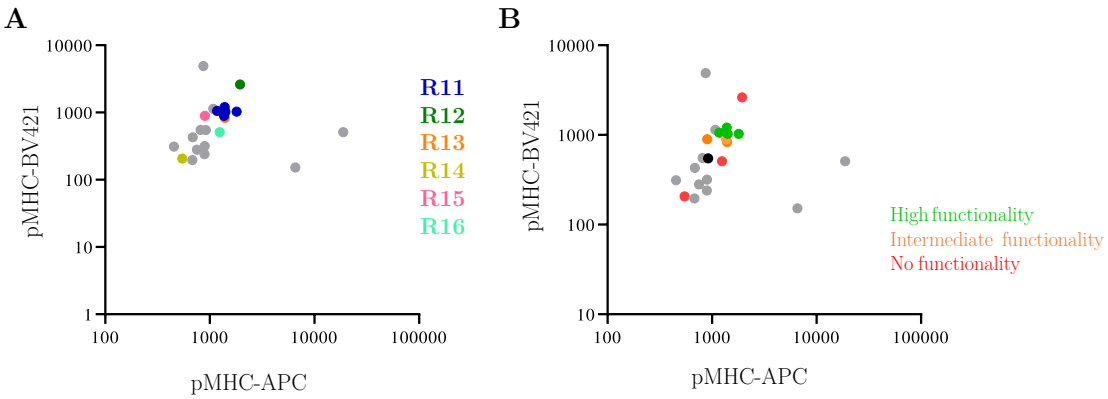

Figure 3.17: Evaluation of A2-RNF43_SLLPTCWAL TCR functionality. Initial double multimer sort gate with sorted cells indicated as individual dots. Displayed are the pMHC multimer fluorescence intensities at the time of sorting (index data). A) Colored dots represent location of identified TCRs in the sort gate. B) Color scale specifies identified functionality. Grey dots mark sorted cells that did not expand. Black dot indicates an expanded clone with lack of TCR sequence identification.

3.1.6 Characterization of TCRs targeting B7-RNF43_VPSVWRSLL neo-epitope

3.1.6.1 Identification of TCRs specific for B7-RNF43_VPSVWRSLL neo-epitope

In silico predictions of MHC Class I binding affinity of neo-epitopes derived from fs-mutations of RNF43 have predicted a surprisingly high number of HLA-B*07:02-restricted peptides (Table 3.1). HLA-B*07:02 is also one of the HLA-types frequently found in the European Caucasian population. Of the many different HLA-B*07:02-restricted peptides, only two were found to be processed *in vitro* by the proteasome in the exact epitope sequence. Here, we focused on the B7-RNF43_VPSVWRSLL neo-epitope for TCR isolation, as this epitope has the highest predicted MHC binding affinity. Strong binding affinity of the peptide to the HLA was confirmed by the successful refolding of stable pMHC (Fig. 3.2).

For the isolation of B7-RNF43_VPSVWRSLL-specific TCRs, we used $CD8^+$ purified apheresis material of a HLA-B*07:02 positive donor (Fig. 3.4 bottom), and we followed the above described sorting workflow for the identification of neo-epitope-specific T cells from the naive repertoire of a healthy donor. In short, the cell material was initially processed in a step of SE on single pMHC multimer staining, and subsequently stained for single cell sort according to double pMHC multimer and $CD8^+$ naive T cell markers ($CD62L^+$ $CD45RA^+$) (Fig. 3.18). In this way, we successfully identified 94 B7-RNF43_VPSVWRSLL pMHC-specific T cells that were single cell expanded in a feeder-cell-free system.

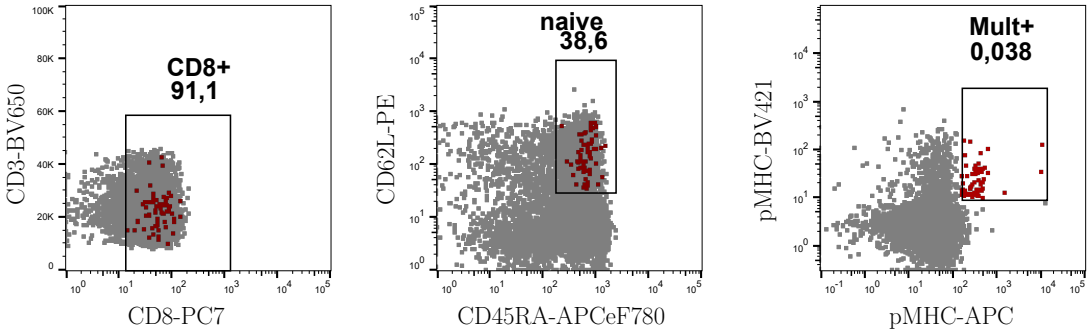

Figure 3.18: Isolation of B7-RNF43_VPSVWRSLL neo-epitope-specific T cells. 491×10^8 $CD8^+$ apheresis cells were stained with B7-RNF43_VPSVWRSLL-specific pMHCs multimerized on a BV421-fluorochrome labeled Streptavidin backbone, and multimer positive cells were enriched through speed enrichment. Subsequently, 1.9×10^6 enriched cells were stained with a second B7-RNF43_VPSVWRSLL-specific pMHCs multimerized on an APC-fluorochrome labeled backbone for higher specificity of the staining. Further, surface mAB staining for phenotypic markers allowed distinct detection of $CD8^+$ naive ($CD62L^+$ $CD45RA^+$) T cells. Depicted is the gating strategy for accessing neo-epitope-specific naive $CD8^+$ T cells, where sorted double multimer positive cells are indicated in red. Sorted cells clearly originated from $CD8^+$ naive T cell population. Pre-gated on lymphocytes, singlets, living.

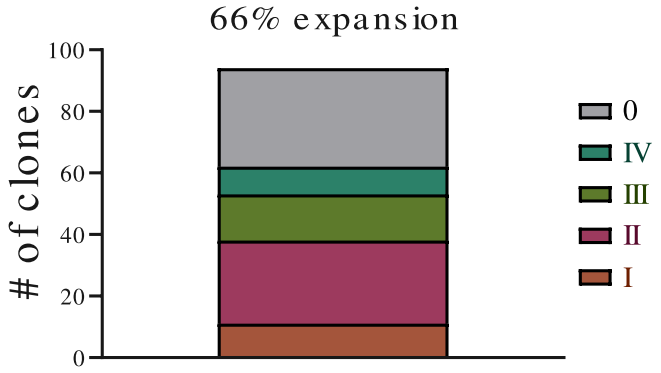

Figure 3.19: Expansion of B7-RNF43_VPSVWRSLL neo-epitope-specific sorted T cells. $CD8^+$ naive T cells sorted according to double pMHC multimer staining were expanded in a feeder-cell-free system. 10 days post-sort, expanded clones were evaluated for clonal expansion in 384-well plate under the microscope. Scoring system defines 0=not expanded, I=few cells growing, II$\leq$25 %, III$\leq$50 % and IV$\geq$50 % of the well covered with the expanded clone population. Single cell-derived clones were processed for TCR sequence identification and, whenever possible according to the clone size, stained with pMHC multimers to assess epitope specificity.

Over a time of 10 days, 66 % of single sorted cells expanded into a bigger clone (Fig. 3.19). All 66 growing clones were processed for TCR *alpha* and *beta* chain sequencing. 43 clones reached sufficient size for concomitant pMHC re-staining. For this, all clones were CD45 color barcoded and multiplexed for double pMHC re-staining and simultaneous analysis, as described above. Promisingly, many clones strongly recognized the B7-RNF43_VPSVWRSLL pMHC multimer with which the single cells were initially sorted (Fig. 3.20). A few clones showed an intermediate pMHC multimer re-staining and only a minority of clones showed insufficient pMHC signal. Unrelated PBMCs stained separately with the same color code served as a negative control for staining artefacts. Similarly unrelated PBMCs spiked within a multiplexed sample controlled for unspecific multimer recognition. For reasons of simplicity, we have depicted only pMHC re-staining plots of clones with a clear sequencing result of both TCR chains and subsequent selection as candidate TCR for further functional characterization.

Sequencing of all 66 growing clones resulted in a high number of paired *alpha-beta* TCR sequences (Table 3.3). To limit the set of TCRs for re-expression and further *in vitro* functional characterization, we prioritized candidate TCRs that showed reliable pMHC multimer clone re-staining and a clear identification of the TCR *alpha* and *beta* chain sequences. In total, 12 clones fulfilled these criteria and were defined as candidate TCR R17-R28. Furthermore, we selected five and two clones with a clear TCR sequencing result, but only, respectively, intermediate and insufficient pMHC multimer recognition of the growing clone. Finally, the set of candidate TCRs was completed with two clones that lacked pMHC multimer recognition, but still showed a clear TCR sequencing result.

Interestingly, many clones were identified with a second *alpha* chain, and rarely second *beta* chain. Mostly, the identified sequence for a second chain was out of frame, thus aborting adequate expression.

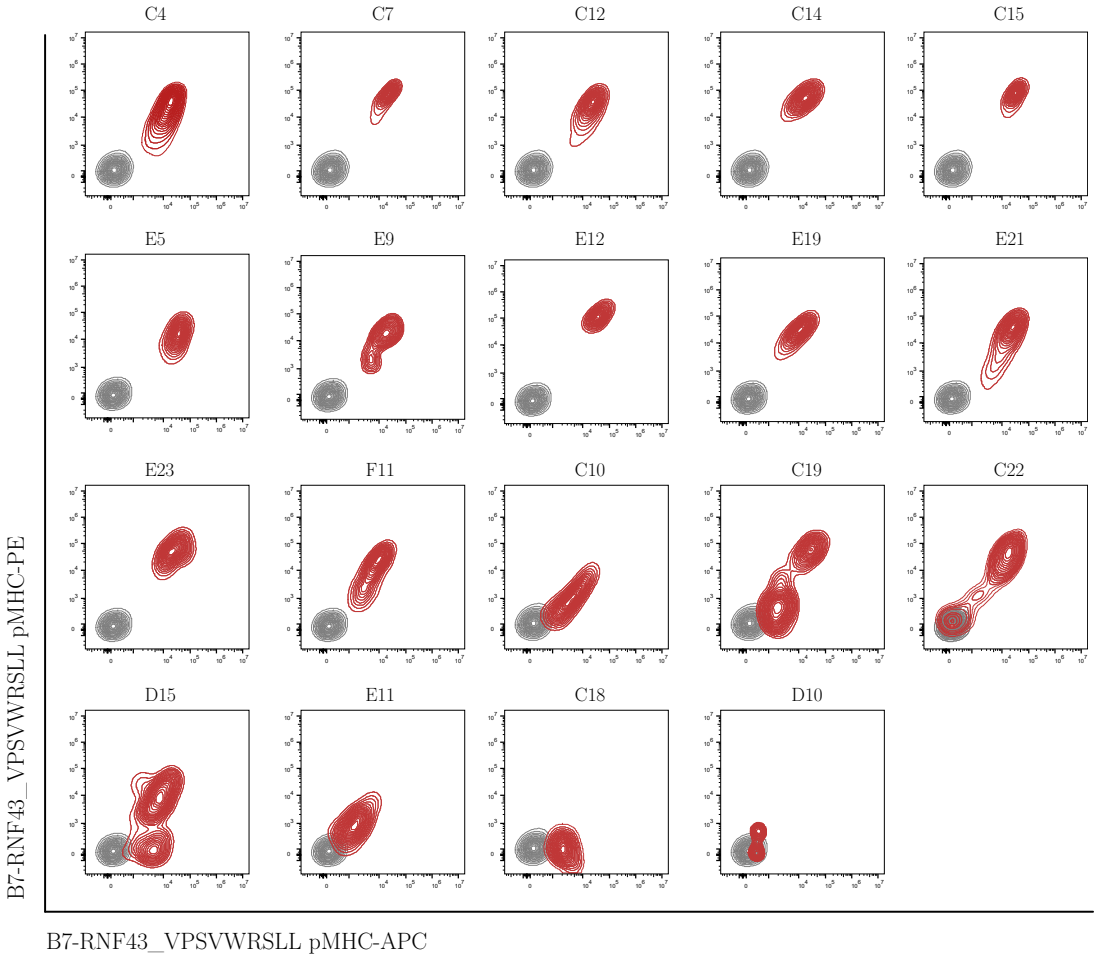

Figure 3.20: B7-RNF43_VPSVWRSLL pMHC multimer staining of expanded T cell clones. Clones derived from double multimer sort on putative neo-epitope-specific naive $CD8^+$ cells were split after 10 days of clonal expansion. Clone samples were stained with a CD45 color code, and pooled for multiplexed staining with PE- and APC-fluorochrome labeled B7-RNF43_VPSVWRSLL pMHC multimers. Labeling above the flow cytometry plots indicates the name given to each clone. Double multimer staining of expanded clones is shown in red, unrelated PBMCs as negative control for multimer recognition and color code artefacts are shown in shades of grey. Depicted are clones with positive sequencing result only. Pre-gated on lymphocytes, singlets, living, $CD8^+$, $CD45^+$ color code.

Table 3.3: TCR sequences of B7-RNF43_VPSVWRSLL sorted clones.

	all V Hits		aaSeqCDR3		Clone Count		MHC-staining*	
Clone name	**TRAV**	**TRBV**	**TRAV**	**TRBV**	**TRAV**	**TRBV**		**RNF43 TCR****
C4	TRAV8-2	TRBV6-2	CVVLNFNKFYF	CASSPPPRGLYLYEQYF	183	294	+	R17
	TRAV8-2		CVVLNFNKFYF		162			
C7	TRAV8-3	TRBV11-2	CAVGGNSGNTPLVF	CASSLPSQQYF	290	844	+	R18
	TRAV27		CAGVT_YKLSF		230			
C12	TRAV21	TRBV3-1	CAVKDYGGSQGNLIF	CASSQDRSLGNIQYF	319	146	+	R19
	TRAV8-3		CAVGASE_AGNMLTF		23			
C14	TRAV23DV6	TRBV7-6	CAASPMRRKAGSYQLTF	CASSRTLGSTGELFF	78	89	+	R20
	TRAV4		CLVGDGW_SNYQLIW		25			
C15	TRAV19	TRBV6-6	CALGTYGNNRLAF	CASTKGGPSSYEQYF	170	344	+	R21
	TRAV12-2		CAVPIW_NKLVF		15			
E5	TRAV12-2	TRBV7-2	CAVRGWTGKLIF	CASSYGKFEAFF	176	138	+	R22
	TRAV3		CAVRDTL_DYKLSF		24			
E9	TRAV21	TRBV27	CAVRPQGGSEKLVF	CASTVGGTQYF	321	83	+	R23
	TRAV29DV5		CAASATGL_SNTGKLIF		30			
E12	TRAV25	TRBV27	CAVHMNRDDKIIF	CASSLTSFYEQYF	265	169	+	R24
E19	TRAV13-1	TRBV27	CAAQKTSYDKVIF	CASSTPGSLNEQFF	1111	64	+	R25
E21	TRAV25	TRBV7-9	CAGQDYAGKSTF	CASSSGGRFYGYTF	1086	475	+	R26
	TRAV9-2		CALSPPELV_TSYGKLTF		111			
E23	TRAV21	TRBV7-6	CAVSGRNNNDMRF	CASSLATGGFYGYTF	1839	77	+	R27
F11	TRAV38-2DV8	TRBV5-4	CAYRSAGNQGAQKLVF	CASSLGRGTYEQYF	125	103	+	R28
		TRBV7-3		RASSLPWT_VYHEQYF		37		
C10	TRAV38-1	TRBV6-2	CAFMIGYGQNFVF	CASQESRRLNSPLHF	74	134	- / +	R29
	TRAV12-3		CAMNVRR_SQGNLIF		24			
C19	TRAV4	TRBV6-2	CLVGEVQAGTALIF	CASSYLQGVEEKLFF	138	59	- / +	R30
	TRAV1-2		CAVNIR_GQKLLF		29			
C22	TRAV26-1	TRBV7-9	CIVRAPRGYGNKLVF	CASSVTGTADNEQFF	592	318	- / +	R31
	TRAV38-1	TRBV7-4	CT*RNNARLMF	CASSLSAA_GGDQPQHF	62	45		
D15	TRAV1-2	TRBV25-1	CAVRDRDSNYQLIW	CASSEGAQGDEQFF	347	85	- / +	R32
	TRAV12-3		CAMLT_YKLSF		47			
E11	TRAV1-2	TRBV6-1	CAVRDRFSDGQKLLF	CASSPPMRRDEQYF	57	80	- / +	R33
C13	TRAV1-2	TRBV9	CAVPQGKGATNKLIF	CASSGGFDEQFF	14	216	?	R34
		TRBV20-1		CSARVTRD_GTYEQYF		13		
E8	TRAV26-1	TRBV11-2	CIVRVSNNNAGNMLTF	CASSLGHPYGYTF	161	257	?	R35
	TRAV9-2		CALSDTG_NTGKLIF		157			
C18	TRAV13-1	TRBV30	CAATPVHDMRF	CAWVQGASGANVLTF	585	100	-	R36
	TRAV29DV5		CAG*YW_GFKTIF		50			
D10	TRAV1-2	TRBV27	CAVRSRNDYKLSF	CASSPFGSEGLAGEQYF	205	79	-	R37
	TRAV26-2		CILSRAFRY_GTASKLTF		35			

* pMHC multimer re-staining is specified as positive (+), intermediate (+/-), negative (-) and not tested (?).

** Table is limited to selected clones for further functional characterization. Identifier of candidate B7-RNF43_VPSVWRSLL TCR for *in silico* assembly and re-expression is indicated.

3.1.6.2 pMHC multimer staining of TCR-engineered T cells for B7-RNF43_VPSVWRSLL-specificity

We selected a set of 21 candidate TCRs with different characteristics of pMHC multimer re-staining at the level of expanded clones for re-expression and subsequent *in vitro* functional characterization. All TCR sequences were *in silico* assembled in a fully humanized version with no further editing of the TCR chain constant region (Fig. 3.6 left). All of the 21 B7-RNF43_VPSVWRSLL neo-epitope-specific TCRs were re-expressed in healthy donor PBMCs via OTR.

Expression of the transgenic TCR can be assessed starting from five days post OTR editing via flow cytometry. Staining with mABs for the human TCR shows effective KO and loss of endogenous TCR expression. Successful KI of a fully humanized transgenic

TCR was assessed via staining with the respective pMHC multimer. All re-expressed candidate TCRs were re-stained with the relevant (B7-RNF43_VPSVWRSLL) pMHC multimer and an irrelevant (B7-pp65) pMHC multimer, which controlled for epitope specificity. We identified a clear recognition of the B7-RNF43_VPSVWRSLL multimer for 13 of the 21 TCRs in $CD8^+$ cells (Fig. 3.21 A). A positive pMHC multimer staining of the re-expressed TCR is a first validation of target specificity. We further identified all pMHC multimer positive T cells to specifically recognize the B7-RNF43_VPSVWRSLL pMHC multimer (Fig. 3.21 B), as the unspecific B7-pp65 pMHC multimer for a CMV virus epitope was not recognized. Two TCRs (R29 and R33) showed a rather weak multimer recognition, whereas for six TCRs, recognition of the pMHC multimer could not be detected. Inadequate transgene expression cannot be excluded, as pMHC multimer negative but human TCR positive transgenic cells cannot be discriminated from the human TCR positive population of unedited T cells. Here, surface mAB co-staining for TCR-V*beta* chains of the remaining $hTCR^+$ cell population could elucidate transgene expression. However, the selection of commercially available TCR-V*beta* did not cover all subtypes represented in this set of candidate TCRs, and the TCR-V*beta* in question could still be represented in the donor repertoire in the unedited T cell fraction. Thus, TCRs with lack of expression and/or pMHC multimer recognition were neglected for further analysis.

Altogether, we identified 15 TCRs specifically recognizing B7-RNF43_VPSVWRSLL pMHC multimers. From 12 clones that showed strong pMHC re-staining, all except for R18 confirmed to recognize the multimer upon TCR re-expression. Further, clones with an intermediate re-staining confirmed their multimer recognition also after re-expression, with the exception of R30. Generally, in this setting, we observed that an initial clone pMHC re-staining indicated a selection parameter for TCRs with high chances for pMHC recognition after TCR re-expression via OTR in healthy donor.

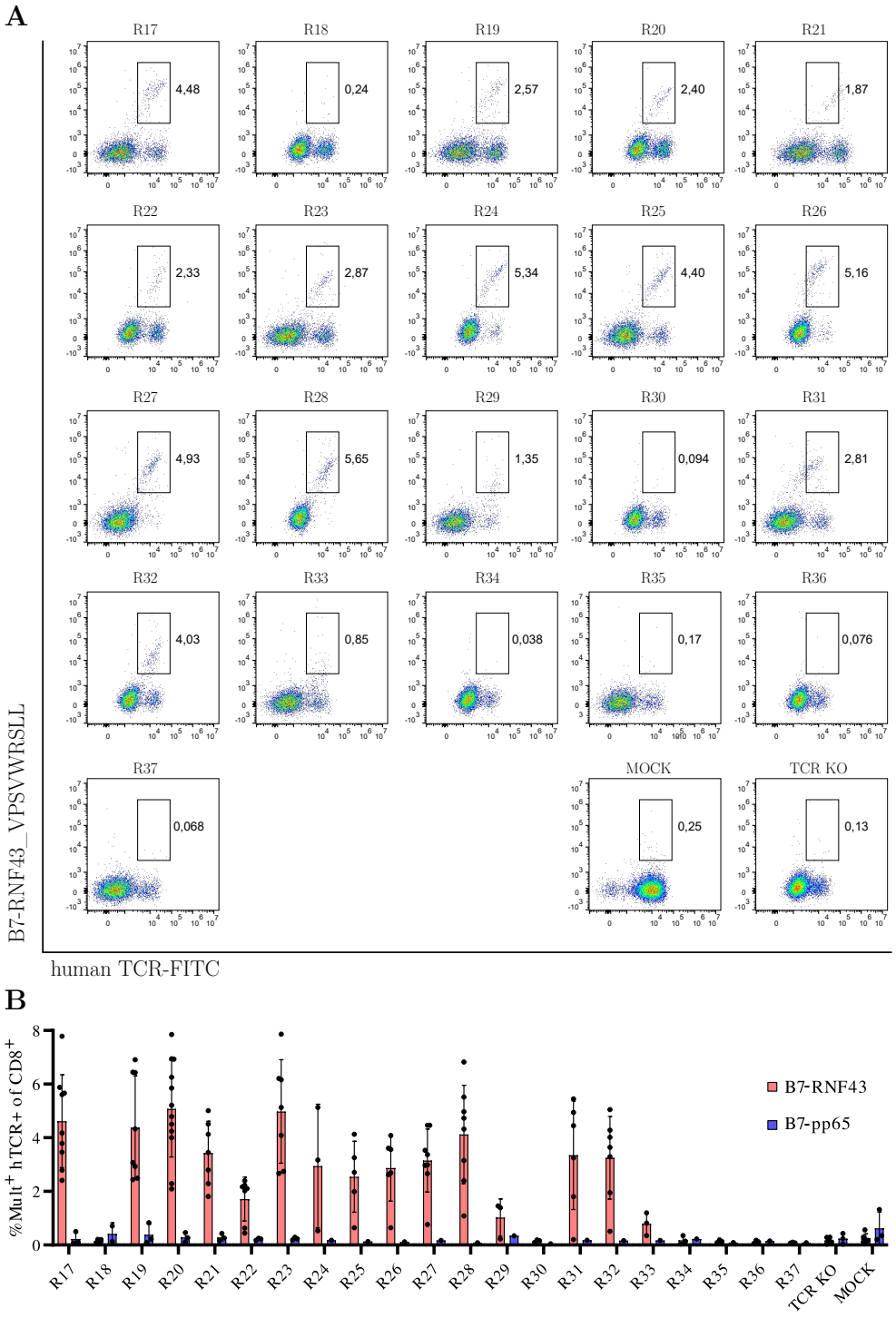

Figure 3.21: B7-RNF43_VPSVWRSLL-specific multimer recognition. A) Exemplary flow cytometric analysis of pMHC multimer reactivity and specificity of OTR-engineered PBMCs. Successful KI of the transgenic TCR is visualized via mAB staining for human TCR and B7-RNF43_VPSVWRSL pMHC multimer staining. Labeling above the flow cytometry plots indicates the name given to each TCR. B) Quantification of multimer staining with relevant B7-RNF43_VPSVWRSLL and irrelevant B7-pp65 pMHCs. Pre-gated on lymphocytes, singlets, living, $CD8^+$.

3.1.6.3 Measurement of B7-RNF43_VPSVWRSLL-specific TCR structural avidity

Re-expression of the B7-RNF43_VPSVWRSLL-specific candidate TCRs via OTR and subsequent pMHC multimer staining revealed efficient transgene expression and epitope recognition for 15 of 21 candidate TCRs. Similarly to how we proceeded in the process of TCR evaluation for A2-RNF43_SLLPTCWAL specific TCRs, we next measured the structural avidity of all 15 B7-RNF43_VPSVWRSLL-specific TCRs. To facilitate TCR:pMHC k_{off}-rate measurements for this high number of candidate TCRs, we did not follow the laborious approach of cell sorting and expansion of multimer positive cells, but rather used the engineered bulk population. To make this possible, we took advantage of a tethering approach to retain on the cell surface the StrepTactin-APC signal of the backbone upon D-Biotin incubation. In detail, cell samples were first CD45 color-barcoded for simultaneous sample acquisition. Then, cells were mixed and stained with a reversible B7-RNF43_VPSVWRSLL StrepTamer (pMHC-ATTO488 multimerized on an APC-conjugated StrepTactin backbone) as well as a CD8-APCeF780 antibody. In the step of tethering, the cell sample was stained with anti-APC mAB, thus connecting the StrepTactin-APC backbone to the cell surface bound CD8-APCeF780 mAB (Fig. 3.22 A). In this way, the neo-epitope-specific population can be continuously detected throughout the time of measurement also after D-Biotin addition, as the tethered backbone, and corresponding signal, is not lost (Fig. 3.22 B).

The set of B7-RNF43_VPSVWRSLL-specific TCRs showed a diverse range of structural avidities. TCR R20, R21, R23, R25 and R31 were characterized by high structural avidity due to a measured half-life TCR:pMHC k_{off}-rate of >100s (Fig. 3.22 C-D). TCR R17, R19, R22, R24 and R26 showed rather low structural avidities. TCRs with a low structural avidity have a fast release of pMHC-monomers from the TCR complex upon D-Biotin addition, and with a certain degree of variability on the assay, some measurements remain below the detection limit. Five TCRs followed this behavior and were identified with very fast TCR:pMHC k_{off}-rates, as the measurement of structural avidity remained below the detection limit.

Altogether, we identified 5 TCRs (R20, R21, R23, R25 and R31) with high structural avidity to the cognate B7-RNF43_VPSVWRSLL pMHC. This measurement suggested that these TCRs could also confer a certain degree of high functionality.

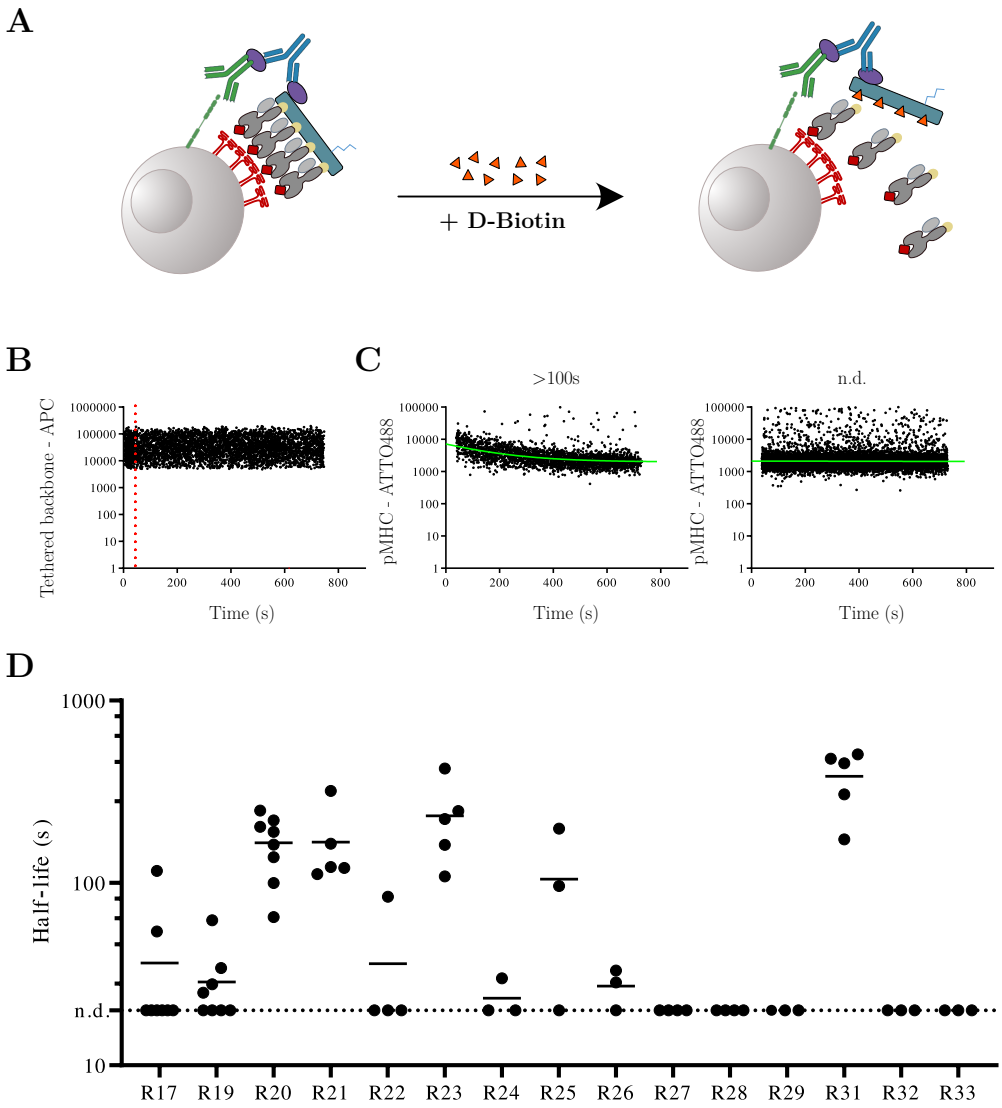

Figure 3.22: Structural avidity measurement of B7-RNF43_VPSVWRSLL pMHC multimer-reactive TCRs. A) Schematic depiction of the APC-tethering approach. Staining with anti-APC mAB links the StrepTactin-APC backbone to the cell surface bound CD8-APCeF780 mAB, and enables continuous detection of the multimer-specific cells throughout D-Biotin incubation and the time of measurement. B) Representative plot indicating the effect of backbone tethering for continuous measurement of StrepTactin-APC backbone signal. Red dotted line indicates the time point of D-Biotin addition. C) Representative plots for tracking of pMHC-ATTO488 fluorescence intensity over time for measurable (left) and non-detectable half-life measurements (right). Fitting a one-phase exponential curve through the decay of pMHC monomer signal yielded in the calculation of TCR:pMHC half-life for a TCR of interest. D) Quantification of pMHC-ATTO488 monomer dissociation. Pre-gated on lymphocytes, singlets, living, $CD8^+$, CD45 color code resolution. Half-life <20s remain non-detectable (n.d.).

3.1.6.4 Evaluation of peptide sensitivity of B7-RNF43_VPSVWRSLL-specific TCRs

Measurements of structural avidity determine the molecular binding strength between TCR and cognate pMHC, and can identify potentially functional TCR candidates. To validate this evidence, we next set out to determine the sensitivity of all 15 B7-RNF43_VPSVWRSLL-specific TCRs to the cognate peptide. Similarly to the peptide stimulation assay described above, we used a HLA-B*07:02-expressing K562 target cell line for peptide presentation to the TCR-engineered T cells. For precise measurements of functionality, we first purity sorted OTR-engineered $CD8^+$ T cells via pMHC multimer staining and rapidly expanded the sorted populations on feeder cells. Transgenic TCR-expressing cells were then incubated with HLA-B*07:02 K562 target cells pulsed with variable concentrations of VPSVWRSLL peptide. Peptide reactivity was measured by cytokine release and downregulation of the TCR.

In total, 9 out of 15 TCRs responded with release of IFN-γ to the highest epitope concentration of -4M (Fig. 3.23 A). TCR R21 and R23-R28 responded also to lower doses of peptide stimulation in a dose-dependent manner. TCR R17 and R19 did solely respond to maximum peptide stimulus. All TCR-expressing cells responded to the positive control of a strong TCR independent stimulus via PMA/Iono. EC_{50} values of the responsive TCRs indicated the most sensitive TCR candidates (Fig. 3.23 B-C). TCR R21 and R23 showed the lowest EC_{50} values with $10^{-6.1}$ M and $10^{-6.4}$ M respectively. Further, TCR R24, R25, R26, R27 and R28 showed slightly higher EC_{50} values, but remained in a comparable range. Additionally to the release of cytokines as a measure of TCR-peptide sensitivity, we analyzed also the level of TCR expression over the titration of peptide stimulation. Similarly to the results of cytokine release, the relative change of TCR downregulation upon peptide stimulation was strongest for TCR R21 and R23 (Fig. 3.23 D-E). The determination of EC_{50} values for TCR downregulation showed a more indistinct discrimination of the TCR potency, but supported the identification of most functional candidates via cytokine release. We concluded that in this assay IFN-γ release upon peptide stimulation provided the most sensitive readout for discrimination of TCR functionality.

Taken together, we identified R21 and R23 as highly functional TCRs. High peptide sensitivity confirmed initial measurements of high structural avidity and predicted functionality. Moreover TCR R24, R25, R26 and R28 responded with lower, but still strong, sensitivity to B7-RNF43_VPSVWRSLL peptide stimulation. The tendency of weaker reactivity was also reflected in the TCR:pMHC k_{off}-rate measurements, that partially remained below detection limit. TCR R17 and R19 showed low measurements of structural avidity and remained unresponsive to peptide stimulation apart from highest dosage. R32 and R33 represented TCRs with TCR:pMHC k_{off}-rates below the detection limit and were confirmed as non-functional in cytokine release upon peptide stimulation. The trend of correlation between a high TCR:pMHC k_{off}-rate value and strong peptide reactivity could not be confirmed for TCR R20 and R31. Despite high structural avidity, these TCRs remained unresponsive to peptide stimulation. A general correlation in this set of TCRs between measured structural avidity and peptide reactivity could not be identified.

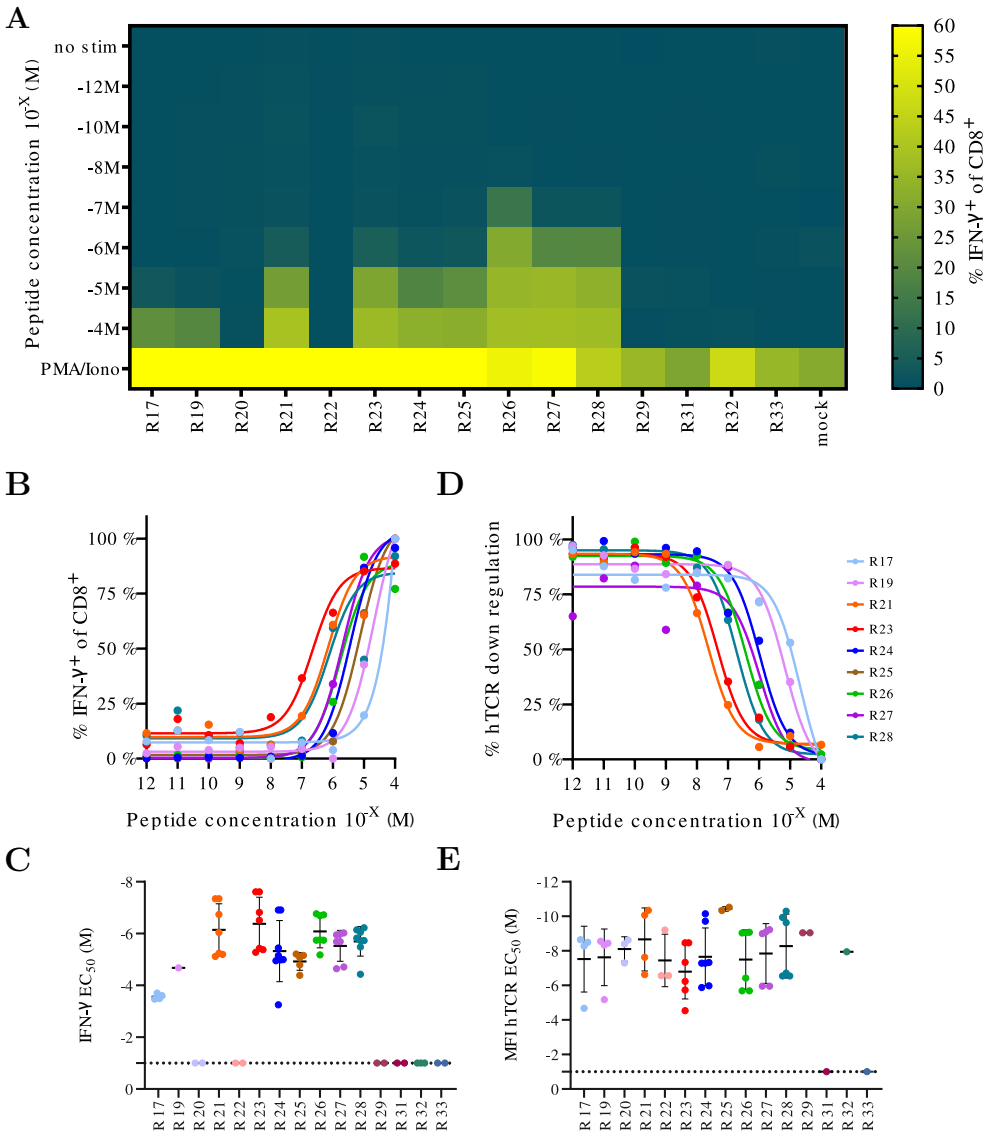

Figure 3.23: B7-RNF43_VPSVWRSLL-specific TCRs responded to peptide stimulation. OTR-engineered CD8$^+$ T cells were co-cultured with peptide-pulsed K562-HLA-B*07:02 target cells at equal T:E ratio (1:1) for 4 h of stimulation. Addition of a Brefeldin A containing protein transport inhibitor prevented cytokine release and enabled intracellular cytokine staining for detection via flow cytometry. A) Heatmap showing frequency of IFN-γ release of transgenic T cells upon dose-dependent stimulation with B7-RNF43_VPSVWRSLL peptide-pulsed HLA-B*07:02$^+$ K562 target cells. B) Relative release of IFN-γ upon range of peptide stimulation. C) Quantification of peptide concentration with half-maximum release of IFN-γ (EC_{50}). D) Relative TCR downregulation upon range of peptide stimulation. E) Quantification of peptide concentration with half-maximum TCR downregulation. Dotted line indicates non-measurable EC_{50} value due to lack of dose-dependent response. Flow cytometry analysis pre-gated on lymphocytes, living, singlets, CD8$^+$.

3.1.6.5 *In vitro* processing and presentation of B7-RNF43_VPSVWRSLL epitope in K562 cells

In the previous section, we could identify a number of B7-RNF43_VPSVWRSLL-specific TCRs with high response to peptide stimulation. In this experimental setup, we pulsed the target peptide on the surface of a HLA-B*07:02-expressing K562 target cell for epitope presentation to the T cells. Although this is an effective experimental approach to measure a TCR reactivity to the cognate peptide presented on the MHC Class I complex, it still does not validate the physiological presentation of the peptide. Therefore, to corroborate the initial findings of *in vitro* proteasomal processing, we established a cellular system for evaluating the endogenous epitope processing and presentation.

Similarly to the approach described above for the A2-RNF43_SLLPTCWAL epitope, we retrovirally transduced the HLA-B*07:02-expressing K562 target cell line for expression of the RNF43 A269fs-mutated protein (Fig. 3.13 A). The RNF43 A269fs-mutation leads to both of the epitopes - A2-RNF43_SLLPTCWAL and B7-RNF43_VPS-VWRSLL. Thus the construct designed previously, was also used for a proof of concept of physiological epitope processing in the HLA-B*07:02 setting. HLA-B*07:02-expressing K562 target cells were successfully transduced and RNF43 A269fs expressing cells were purity sorted via the co-expressed GFP signal (Fig. 3.24 A).

We selected the TCR with highest functionality, TCR R21, for preliminary experiments. TCR R21-expressing $CD8^+$ T cells were co-incubated with HLA-B*07:02 RNF43 A269fs-expressing K562 cells ($K562B7^+$ RNF43) and cytokine release was measured to indicate TCR stimulation. TCR R21-expressing cells responded with strong release of IFN-γ to the positive control of peptide-pulsed APCs. However, TCR R21-engineered T cells did not respond to stimulation with increasing T:E ratio of $K562B7^+$ RNF43 cells (Fig. 3.24 B), which should physiologically present the epitope of interest. Indeed, the signal of response remained at comparable levels to the background signal of the negative controls (unpulsed K562 cells, or an irrelevant TCR (SCoV34)).

We concluded that, despite the positive results from the *in vitro* proteasomal processing assay, we could not confirm physiological epitope processing and surface presentation in the established model system of the engineered K562 cells.

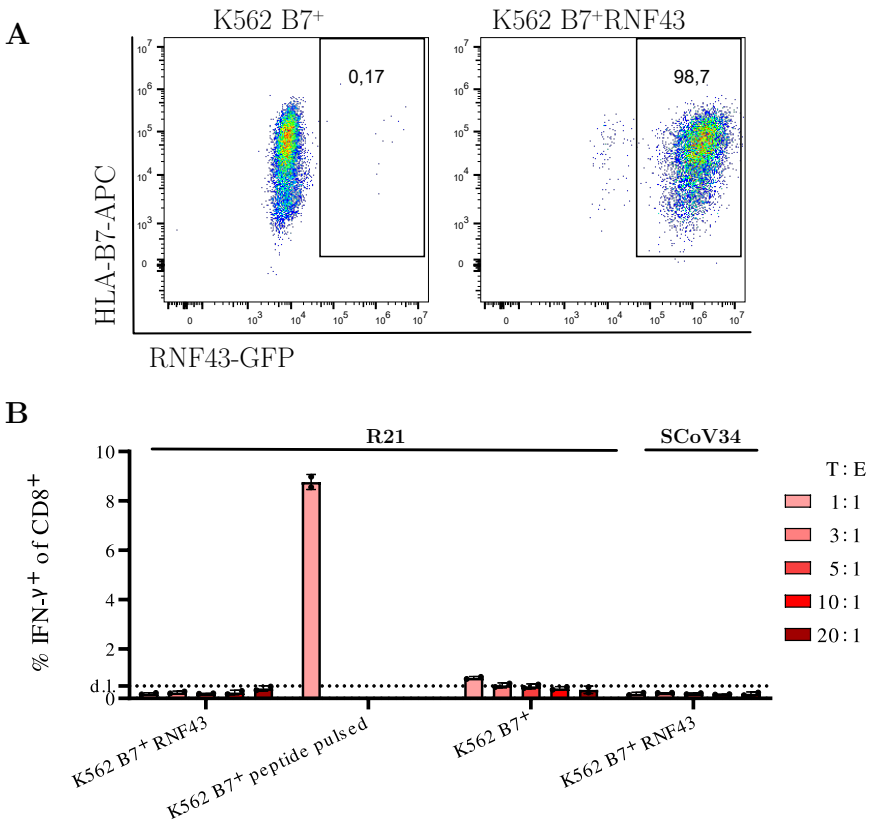

Figure 3.24: Engineering of K562 cells to model epitope processing. A) HLA-B*07:02$^+$ K562 cells (left) were retrovirally transduced for expression of RNF43 A269fs-mutated protein. Flow cytometry plots depict successfully edited and purity sorted HLA-B*07:02$^+$ K562 cells (right). GFP expression indicates RNF43 A269fs-mutated protein expression. B) IFN-γ cytokine release of OTR-engineered T cells co-cultured with indicated K562 target cells at specified T:E ratio for 4 h of stimulation. Inhibition of protein transport via Brefeldin A during co-culture time enabled intracellular mAB staining for IFN-γ and readout via flow cytometry. TCR R21-engineered T cells responding to VPSVWRSLL peptide-pulsed (-5M) K562 B7$^+$ target cells at 1:1 T:E ratio served as positive control. Non-target expressing K562 cells and T cells expressing irrelevant SCoV34 TCR served as negative control. Detection limit (d.l.) was set according to signal detection in the negative controls of TCR R21 responding to HLA-B*07:02-expressing K562 and an irrelevant SCoV34 TCR responding to HLA-B*07:02 RNF43 A269fs-expressing K562 cells. Flow cytometry analysis pre-gated on lymphocytes, living, singlets, CD8$^+$.

3.1.6.6 B7-RNF43_VPSVWRSLL-specific TCRs kill peptide-pulsed pancreatic cancer cell line

In the previous section, we concluded that the RNF43 fs-derived B7-RNF43_VPSVWRSLL epitope is not processed adequately on the surface of APCs. The screening of an avail-

able biobank of cancer cell lines did unfortunately not result in the identification of a HLA-B*07:02 positive cell line with a RNF43fs mutation leading to the generation of the B7-RNF43_VPSVWRSLL epitope.

Still, we finalized the *in vitro* characterization of the set of highly functional B7-RNF43_VPSVWRSLL-specific candidate TCRs with cytotoxicity measurements. We identified Panc28 as a pancreatic cancer cell line naturally expressing HLA-B*07:02, and we pulsed this target cell line with the B7-RNF43_VPSVWRSLL peptide. As described previously, the xCelligence technology represents a method for impedance-based real-time immune cell cytotoxicity assays. Target cells were seeded into the plate for impedance measurements and cell growth was monitored for 24 h. Next, purity sorted TCR-engineered $CD8^+$ T cells were added at equal T:E ratio and the impedance signal was followed for 48 h.

We observed strong killing of the peptide-pulsed Panc28 target cells by $CD8^+$ T cells expressing TCR R21, R23 and R26 (Fig. 3.25). TCR R24 showed a weaker effect on target cell lysis, but still induced a clear reduction of target cell line growth. TCR R28 did show limited cytotoxicity as Panc28 target cells continued growing similarly to the 'medium only' positive control. Panc28 cells without peptide presentation via pulsing, were not recognized by the effector cells. Thus, we concluded that B7-RNF43_VPSVWRSLL-specific TCRs specifically recognize and kill HLA-B*07:02 target cells presenting the cognate peptide on the surface. Undoubtedly, peptide pulsing leads to unphysiologically high peptide presentation of the target cells. In contrast to a cell system with physiological neo-epitope presentation, such as the Capan-2 $A2^+$ used for cytotoxicity assays of the previously described A2-RNF43_SLLPTCWAL-specific TCRs, a 1:1 T:E ratio already induced strong target cell killing.

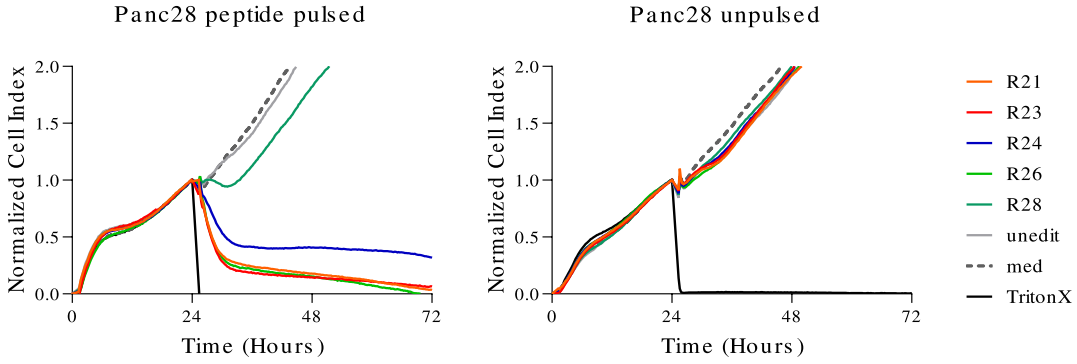

Figure 3.25: B7-RNF43_VPSVWRSLL-specific TCRs kill peptide-pulsed Panc28 cells. HLA-B*07:02 positive Panc28 cell line was pulsed with -5 M B7-RNF43_VPSVWRSLL peptide and cell growth was detected via impedance measurement. 24 h post target cell seeding, TCR-engineered $CD8^+$ T cells were added at 1:1 T:E ratio and cell lysis was monitored for 48 h. Unpulsed target cells served as negative control.

3.1.6.7 Evaluation of identification of B7-RNF43_VPSVWRSLL-specific TCRs

In the previous sections, we have characterized a set of 21 TCRs targeting the *in silico* predicted RNF43 fs-derived neo-epitope B7-RNF43_VPSVWRSLL. Only 15 of 21 re-expressed TCRs specifically, recognized the B7-RNF43_VPSVWRSLL pMHC multimer, and only 10 TCRs showed sufficient structural avidity for detectable measurements of TCR:pMHC k_{off}-rate. Further, only 9 TCRs were identified as highly functional according to cytokine release upon peptide stimulation. TCR R21 and R23 were identified as the most potent TCRs with also potent killing of peptide-presenting target cells, followed by TCR R24 and finally TCR R28.

Overall, the TCRs identified as highly functional were also found to be epitope-specific in the initial pMHC re-staining after sort and expansion. Evaluation of the functionality of the different TCRs and backgating to the original sort gate, brings the conclusion that highly functional TCRs are located at the top right corner of the double multimer sort gate (Fig. 3.26). Outliers of the compact multimer positive population were identified as non-functional TCRs. We conclude that the position in the double multimer sort gate can already suggest a selection of TCRs and reduce the number of candidates for laborious functional characterization.

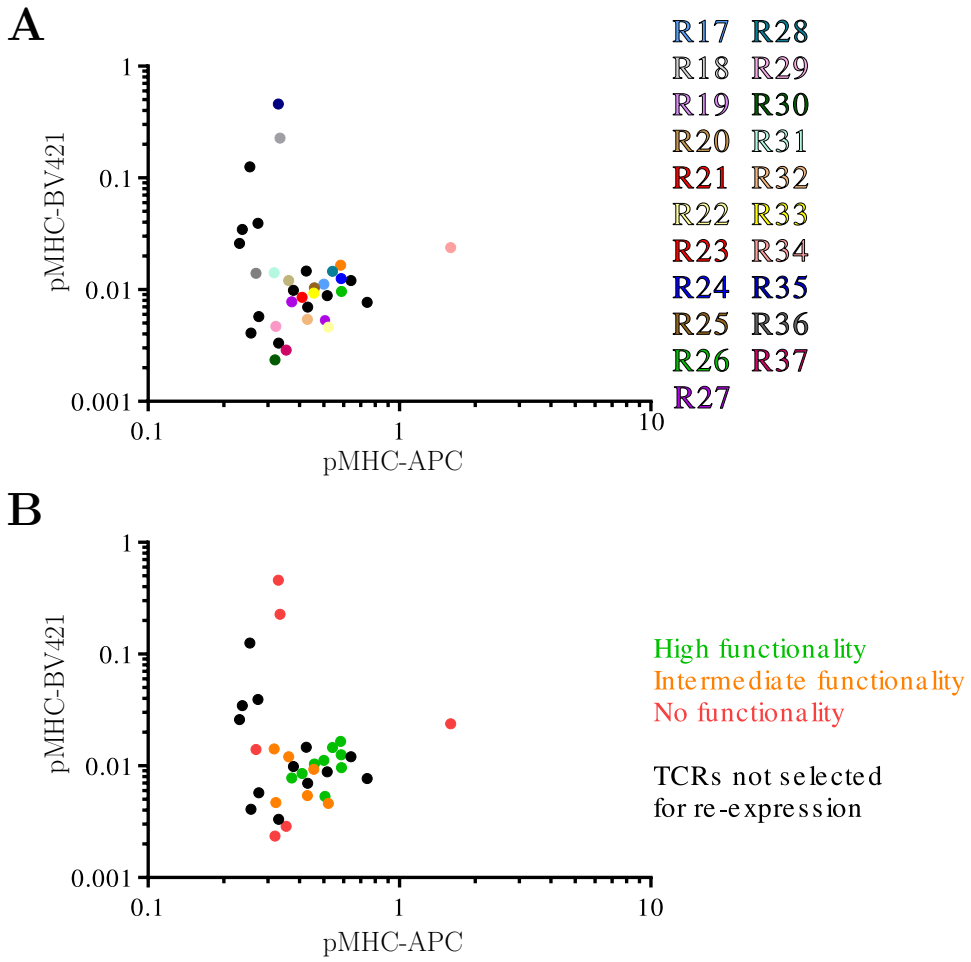

Figure 3.26: Evaluation of sorted B7-RNF43_VPSVWRSLL-specific TCRs. Initial double multimer sort gate with all sorted cells indicated as individual dots. Displayed are the pMHC multimer fluorescence intensities at the time of sorting (index data). A) Colored dots represent location of identified TCR candidates in the initial sort gate. B) Color scale indicates identified functionality. Black dots indicate an expanded clone excluded for functional characterization.

3.1.7 Characterization of TCRs targeting A2-RNF43_TQLARFFPI neo-epitope

3.1.7.1 Identification of TCRs specific for A2-RNF43_TQLARFFPI neo-epitope

In silico predictions of RNF43 fs-derived neo-epitopes revealed two peptides for the HLA-A*02:01 and HLA-B*07:02 that were selected as targets for TCR isolation. In addition, we included a published neo-epitope with high clinical relevance. RNF43_TQLARFFPI is a HLA-A*02:01 specific epitope derived from the most frequently occurring G659fs RNF43 mutation (Table 3.1). This neo-epitope has a predicted MHC binding affinity of 50 nM and we could further proof stable binding of the peptide to the HLA-A*02:01 by the successful *in vitro* re-folding of trimeric pMHCs (Fig. 3.2). We used the generated pMHC multimers to isolate neo-epitope-specific $CD8^+$ T cells from the naive repertoire of HLA-matched healthy donors. Similarly to the previous RNF43 fs-derived neo-epitopes, we used $CD8^+$ purified apheresis cells and accessed the A2-RNF43_TQLARFFPI-specific $CD8^+$ naive T cell population via SE and subsequent single cell sorting according to double multimer staining.

Here, we present data from three sorts from independent donors (Fig. 3.27). The double multimer positive population appeared very diverse in the different donors. In the first and second donor, the multimer positive population appeared surprisingly large. Moreover, the quality of the staining seemed suboptimal, as the majority of the putative antigen-specific T cells showed a single (BV421-conjugated multimer) rather than a double multimer staining, altogether speaking in favor of high background noise. On the contrary, a third donor showed a rather clean staining despite the very few events in the double multimer positive sort gate. As described previously, all cells with sufficient double multimer staining were single cell sorted and expanded in a feeder-cell-free system. Expansion and recovery rates of sorted cells were also diverse for the individual donors (Fig. 3.28). We expected from previous single cell expansion experiments a recovery rate of >50 %. However, despite the many events that were detected and sorted for donor #2, only 22 % of cells expanded, supporting the initial impression of many false-positive events in this donor. On the contrary, donor #1 and #3 showed a recovery rate comparable to other experiments.

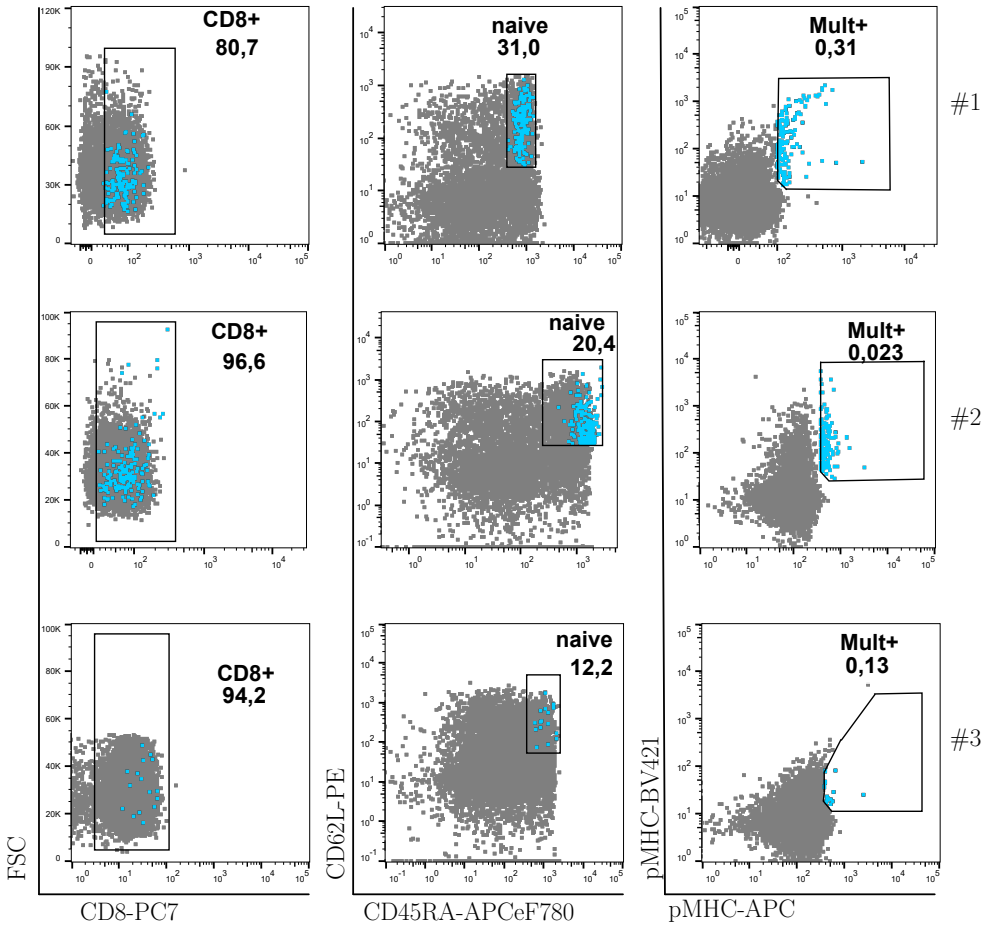

Figure 3.27: Isolation of A2-RNF43_TQLARFFPI neo-epitope-specific T cells. $CD8^+$ apheresis cells of three different HLA-A*02^+ healthy donors were stained with A2-RNF43_TQLARFFPI-specific pMHCs multimerized on a BV421-fluorochrome labeled Streptavidin backbone, and multimer positive cells were enriched through speed enrichment. Subsequently, enriched cells were stained with a second A2-RNF43_TQLARFFPI pMHCs multimerized on an APC-fluorochrome labeled backbone for higher specificity of the staining. Further, surface mAB staining for phenotypic markers allowed distinct detection of $CD8^+$ naive ($CD62L^+$ $CD45RA^+$) T cells. Sorted cells clearly originated from $CD8^+$ naive T cell population and are indicated in blue. Pre-gated on lymphocytes, singlets, living.

All clones growing to sufficient size for transfer into pMHC re-staining were evaluated for re-cognition of the A2-RNF43_TQLARFFPI pMHC multimer. Generally, most of the growing clones did not show a positive pMHC multimer re-staining post-expansion. Only few clones showed a dim pMHC multimer staining detectable above the signal of negative control (unrelated PBMCs) (Fig. 3.29). All growing clones were processed for *alpha* and *beta* TCR chain sequencing.

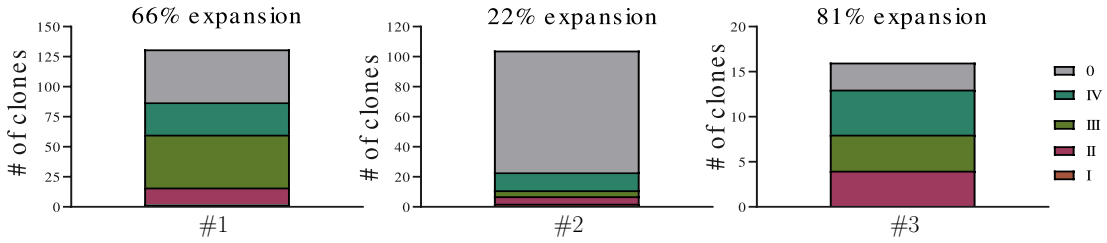

Figure 3.28: Expansion of A2-RNF43_TQLARFFPI neo-epitope sorted T cells. Sorted double pMHC multimer positive CD8$^+$ naive T cells of three independent donors were expanded in a feeder-cell-free system. After 12 days of expansion, clones were evaluated for clonal expansion in 384-well plate under the microscope. Scoring system defines 0=not expanded, I=few cells growing, II≤25 %, III≤50 % and IV≥50 % of the well covered with expanded clone population.

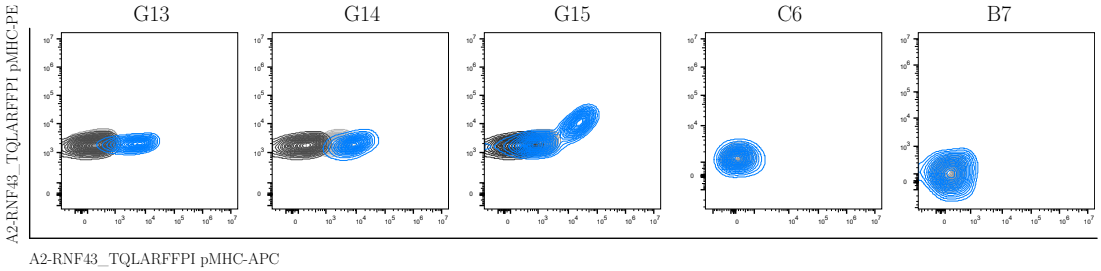

Figure 3.29: A2-RNF43_TQLARFFPI pMHC multimer staining of expanded T cell clones. Clones derived from double multimer sort on putative neo-epitope-specific naive CD8$^+$ cells were split after 10 days of clonal expansion. Clone samples were stained with a CD45 color-code, and pooled for multiplexed staining with PE- and APC-fluorochrome labeled A2-RNF43_TQLARFFPI pMHC multimers. Labeling above the flow cytometry plots indicates the name given to each clone. Depicted are only clones with positive sequencing result selected for re-expression. Double multimer staining of expanded clones is shown in blue, unrelated PBMCs as negative control for multimer recognition and color code artefacts are shown in shades of grey. Pre-gated on lymphocytes, singlets, living, CD8$^+$, CD45 color code.

Previous results of sorts for A2-RNF43_SLLPTCWAL and B7-RNF43_VPSVWRSLL specific TCRs indicated where highly functional TCRs are located in the initial double multimer sort gate. Further, the pMHC clone re-staining was identified as a reasonable indicator for pMHC multimer recognition after TCR re-expression. Thus, according to the position of a cell in the initial double multimer sort gate, the result of the pMHC multimer clone re-staining and the clear sequencing result of the TCR, in this set, we selected only seven TCRs from the sorts of the three individual donors for re-expression and further *in vitro* functional characterization (Table 3.4). Clone G15 was identified with two fully expressed TCR *alpha* chains with very similar clone count in the sequencing. Thus, we could not judge on the dominating *alpha* chain pairing with the expressed

beta chain and we re-assembled both versions as separate TCRs for re-expression (R40_a1 and R40_a2).

Table 3.4: TCR sequences of A2-RNF43_TQLARFFPI sorted clones.

		all V Hits		aaSeqCDR3		Clone Count		MHC-staining *	
Clone ID	**TCR Sort**	**TRAV**	**TRBV**	**TRAV**	**TRBV**	**TRAV**	**TRBV**		**RNF43 TCR****
G13	#1	TRAV20	TRBV6-2,TRBV6-3	CAGEQYNTDKLIF	CASSYSPVDMNTEAFF	3112	2137	+	R38
G14	#1	TRAV38-2DV8	TRBV7-9	CAYSGGGADGLTF	CASSLDPEIEAFF	3332	3249	+	R39
		TRAV13		CAASK*R_GNQFYF		1459			
G15	#1	TRAV8-6	TRBV11-2	CAVSLSGGYQKVTF	CASSLDTDTQYF	3854	681	+	R40_a1
	#1	TRAV12-1	TRBV11-2	CVPSRAPEDGNTPLVF	CASSLDTDTQYF	2821			R40_a2
C6	#2	TRAV20	TRBV19	CAVHPLQGGSEKLVF	CASSYGHYYEQYF	9490	42020	-	R41
B7	#3	TRAV10	TRBV9	CVVSGVGSDGQKLLF	CASSAGLLGTYEQYF	10980	27560	-	R42
B10	#3	TRAV23DV6	TRBV19	CAAGSGGSNYKLTF	CASSIRYNEQFF	27280	11320	?	R43

* pMHC multimer re-staining is specified as positive (+), intermediate (+/-), negative (-) and not tested (?).

** Table is limited to selected clones for further functional characterization. Identifier of candidate A2-RNF43_TQLARFFPI TCR for *in silico* assembly and re-expression is indicated.

3.1.7.2 pMHC multimer staining of TCR-engineered T cells for A2-RNF43_TQLARFFPI-specificity

To continue with the identification of functional TCRs, we selected seven candidate TCRs with a promising position in the initial double multimer sort gate and a positive or weak pMHC multimer recognition of the expanded clones.

Selected A2-RNF43_TQLARFFPI-specific TCR candidates were *in silico* assembled and synthesized for re-expression via CRISPR/Cas9-mediated OTR. This particular set of TCRs was edited in the constant region of the *alpha* and *beta* chain for a murine constant region with additional cysteine bridge (Fig. 3.6 right). In fact, this editing of the TCR facilitated detection of the transgenic TCR via surface mAB staining targeting the mTRBC.

About five days post editing, flow cytometry analysis confirmed the KO of the endogenous TCR of donor T cells and the expression of the transgenic TCR. Here, a successful KI of all seven candidate TCRs was shown by the mTRBC$^+$ population (Fig. 3.30). Further, we performed pMHC multimer staining to determine specificity of the transgenic TCRs. TCR R38 and R39 showed a clear recognition of the cognate multimer, as all cells identified with a successful TCR KI (mTRBC$^+$) also showed a positive staining for the A2-RNF43_TQLARFFPI pMHC multimer. All remaining candidates resulted in false-positive neo-epitope-specific TCRs.

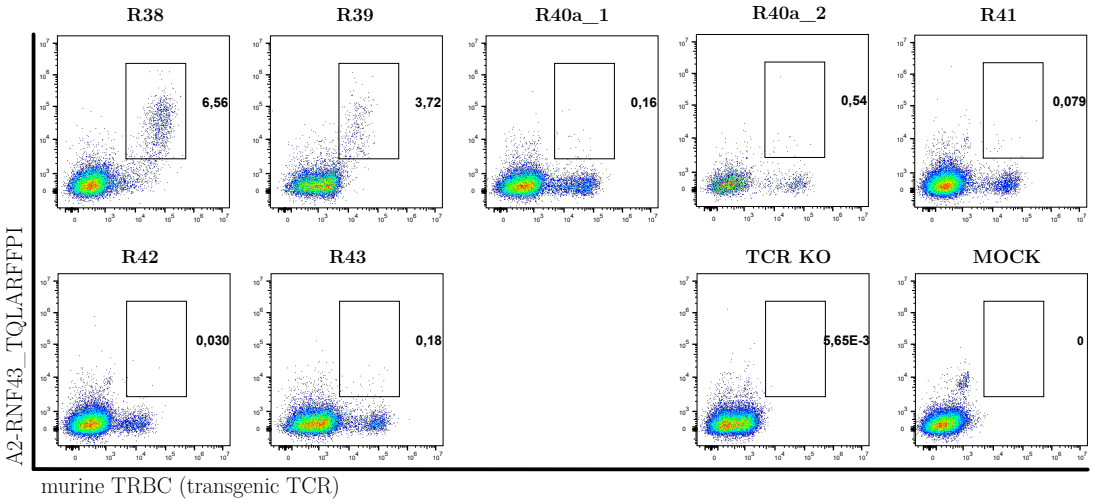

Figure 3.30: A2-RNF43_TQLARFFPI-specific multimer recognition. Exemplary flow cytometric analysis of pMHC multimer reactivity and specificity of OTR-engineered PBMCs. Efficient KI of the transgenic TCR is visualized via mAB staining for mTRBC. A2-RNF43_TQLARFFPI pMHC multimer staining of transgenic candidate TCRs is specific for mTRBC$^+$ population. Labeling above the flow cytometry plots indicates the name given to each TCR. Pre-gated on lymphocytes, singlets, living, CD8$^+$.

3.1.7.3 Evaluation of peptide sensitivity of A2-RNF43_TQLARFFPI-specific TCRs

To follow the above described flow of TCR *in vitro* characterization, we measured the structural avidity of the candidate TCRs with positive recognition of the A2-RNF43_TQLARFFPI. However, structural avidity remained below the detection limit for TCR R38 and R39. A half-life could not be determined due to the fast decay of the pMHC monomers.

Despite the lack of A2-RNF43_TQLARFFPI pMHC multimer recognition for five out of seven TCR candidates, all TCRs were characterized for cytokine release upon peptide stimulation. Transgenic TCRs expressing the murine constant regions can easily be tracked within a heterogeneous bulk population after genetic-editing. In addition, the murinized TCR is robustly expressed and still detectable upon TCR stimulation. Here, we stimulated A2-RNF43_TQLARFFPI neo-epitope-specific TCRs (bulk population) with HLA-A*02:01-expressing K562 cells that were pulsed with a titration of A2-RNF43_TQLARFFPI peptide concentration. T cell activity upon stimulation was detected via IFN-γ release. Gating on mTRBC$^+$ CD8$^+$ cells revealed the peptide responsive TCR-engineered subpopulation. All TCR-expressing cells responded to the positive control of a strong TCR independent stimulus via PMA/Iono. However, none of the candidate TCRs responded to peptide stimulation (Fig. 3.31). The absence of pMHC multimer recognition for most of the TCRs was then further corroborated by the lack of reactivity in the peptide stimulation assay. Even though TCR R38 and R39

showed a robust pMHC multimer staining, the low structural avidity to the cognate epitope presented on the MHC Class I molecule substantiated the deficiency in cytokine release upon peptide stimulation.

We concluded that highly functional A2-RNF43_TQLARFFPI neo-epitope-specific TCRs could so far not be identified.

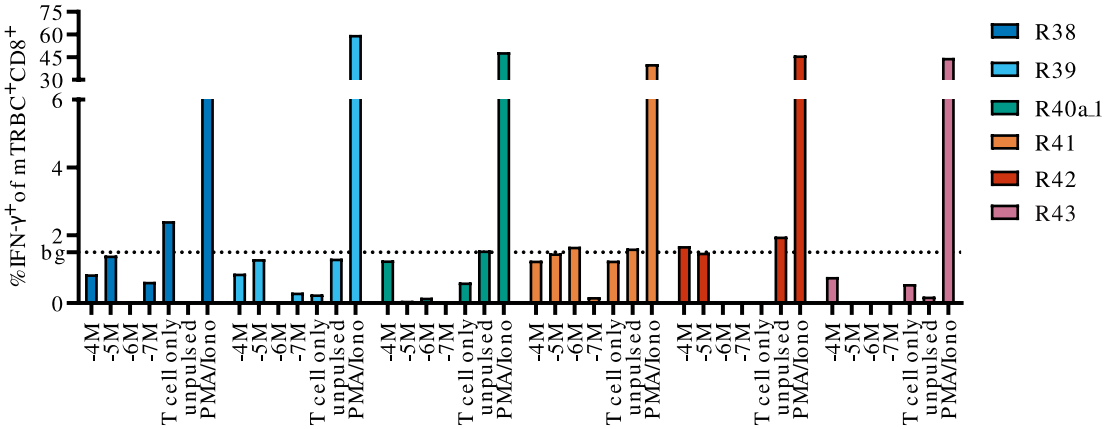

Figure 3.31: A2-RNF43_TQLARFFPI neo-epitope-specific T cells remain unresponsive to peptide stimulation. OTR-engineered $CD8^+$ T cells were co-cultured with peptide-pulsed K562 $A2^+$ target cells at equal T:E ratio (1:1) for 4 h of stimulation. Addition of a Brefeldin A containing protein transport inhibitor prevented cytokine release and enabled intracellular cytokine staining for detection via flow cytometry. Quantified IFN-γ release of $mTRBC^+$ $CD8^+$ T cells upon stimulation with target cell pulsed with peptide at indicated 10^{-X}M concentration. T cell only and unpulsed target cells served as negative controls and determine the indicated line for background signal (bg). PMA/Iono stimulation served as positive control. Flow cytometry analysis pre-gated on lymphocytes, living, singlets.

3.2 Identification and characterization of SARS-CoV-2-reactive T cells

In December 2019, first cases of infections with a novel corona virus strain SARS-CoV-2 were reported in the city of Wuhan in China [144]. Coronavirus Disease 2019 (COVID-19) patients showed symptoms of fever and severe respiratory illness potentially leading to a life threatening pneumonia [145, 146]. The disease quickly spread globally and was declared a pandemic by the World Health Organization (WHO) on March 11, 2020. The rapid spread of the virus with often severe course of disease and substantial number of deaths in the elderly population, presented a major threat to the worldwide economy and public health. The urgent need for effective treatment options and protective vaccination accelerated research at an unprecedented speed.

In the given angle of the situation, we urged to contribute to the research field with the knowledge and methodology we have on our hands for the identification and characterization of antigen-reactive T cells. Here, we describe the impact of the publications that resulted from this transfer of knowledge from the cancer therapy research field to the field of virus infection in times of the outbreak of SARS-CoV-2.

3.2.1 'Reverse Phenotyping' identified transcriptional signatures of SARS-CoV-2 reactive T cells

Early reports of immune response kinetics in a COVID-19 patient have promptly shown a strong induction of the adaptive immune system [147]. Most acute viral infections result in the development of T cell immunity, which can contribute to control and clearance of infection, but also establish long-term protection against secondary infection.

The previously described pMHC multimer technology that we use for detection and isolation of antigen-reactive T cells, is an elegant method to specifically detect T cells in an unperturbed manner [134]. This, however, requires a previous definition of specific epitopes and their restriction to the respective MHC Class I and II molecules. In early times of the pandemic, little was known about SARS-CoV-2-specific T cell epitopes. Commonly, virus-reactive T cells can be visualized by stimulation with peptide mixes covering large parts of the viral proteome and detection of effector cytokine release or activation marker upregulation. *Ex vivo* and *in vitro* T cell stimulation, however, introduces a certain bias in the cellular phenotype.

In our study, we present the method of 'reverse phenotyping' to specifically detect SARS-CoV-2 reactive T cells and their *ex vivo* unperturbed signature by single cell RNA sequencing (scRNAseq) [148]. In short, we collected PBMCs from two severely diseased patients and stimulated one half of the cells with a 15mer peptide mix covering large parts of the SARS-CoV-2 spike protein. The other half of the sample was left unstimulated. Flow cytometry-based cell sorting of $CD4^+$ and $CD8^+$ of the stimulated and unstimulated conditions provided material for subsequent scRNAseq (5'transcriptomics and VDJ). The transcriptional shifts induced in the cells of the peptide-stimulated sample clearly separated stimulated and unstimulated T cells from both donors into different

clusters. Using the TCR sequence as a barcode, we could identified individual clonotypes that showed a specific transcriptional shift in e.g. upregulation of Interferon-γ (gene) (IFNG) in the stimulated sample compared to the unstimulated sample, which is indicative of antigen specificity. For a proof of concept for the identification of truly antigen-reactive clonotypes, we re-expressed selected candidate TCRs via OTR, and stimulated TCR-engineered T cells with the SARS-CoV-2 spike peptide mix. Indeed, the identified reactive clonotypes responded to peptide stimulation with cytokine release. Further, the characterized transcriptional signatures of stimulated SARS-CoV-2-reactive T cells corresponded to T cell phenotypes observed in respiratory tract material of severely diseased patients. In conclusion, we identified 'reverse phenotyping' as a method to detect antigen-reactive T cells in an unperturbed manner and provide insights into their cellular states across tissue and activation status.

Single-cell RNA sequencing reveals ex vivo signatures of SARS-CoV-2-reactive T cells through 'reverse phenotyping'

Fischer DS*, Ansari M*, Wagner KI*, Jarosch S, Huang Y, Mayr CH, Strunz M, Lang NJ, D'Ippolito E, Hammel M, Mateyka L, Weber S, Wolff LS, Witter K, Fernandez IE, Leuschner G, Milger K, Frankenberger M, Nowak L, Heinig-Menhard K, Koch I, Stoleriu MG, Hilgendorff A, Behr J, Pichlmair A, Schubert B, Theis FJ, Busch DH, Schiller HB, Schober K.

* These authors contributed equally.

Published in: Nature Communications. 2021, Jul 26;12(1):4515.
doi: 10.1038/s41467-021-24730-4

3.2.2 Identification and characterization of SARS-CoV-2-specific cytotoxic CD8$^+$ T cells

In a second study on the identification of SARS-CoV-2-specific T cell responses, we set out to identify CD8$^+$-specific T cell epitopes. Commercially available peptide libraries mostly cover the viral proteome by 15mer sequences with 11aa overlap. Peptides of this length generally encourage stimulation of CD4$^+$ rather than CD8$^+$ T cells due to facilitated binding and presentation on the MHC Class II binding grove. A subsequent deconvolution of individual reactive peptides and HLA-type specificity remains difficult.

With the aim to elucidate SARS-CoV-2-specific cytotoxic responses, we used *in silico* prediction tools to identify 9mer peptides with high MHC Class I binding affinity to the most common HLA molecules. 40 candidate peptides were selected to build a peptide pool that we used to specifically stimulate CD8$^+$ T cells in a cohort of convalescent COVID-19 donors who experienced mild course of the disease without need of hospitalization. We collected blood samples over the course of several months from the infection and performed T cell stimulation assays using the entire peptide pool to detect SARS-CoV-2-specific reactive T cells via IFN-γ cytokine release. Additionally, IgG antibody levels were measured in the serum. As a first finding of our study, we observed that, despite decreasing antibody levels, SARS-CoV-2-specific T cells were still detectable up to 12 months after infection. Furthermore, we identified single-reactive peptides from the pool. Indeed, by deconvoluting the peptide responses and connecting the responsive peptides to the HLA-type of the donor, we identified 19 immunogenic peptides for various different HLA-types. The identification of epitopes with a high immunodominance and specificity to SARS-CoV-2 did now not only enable quantitative analysis, but also qualitative analysis of SARS-CoV-2-reactive CD8$^+$ T cells. For that, we flow cytometry-sorted for CD8$^+$ T cells with IFN-γ cytokine release upon single epitope stimulation and performed scRNAseq to access the TCR repertoire. Interestingly, we found a polyclonal response to the SARS-CoV-2-specific epitopes in the clusters of high IFNG expression and other signatures of recent T cell activation. Re-expression via OTR of selected TCRs in healthy donor cells allowed us to further functionally characterize the identified TCR clonotypes. Specificity of the transgenic TCRs was confirmed by pMHC multimer staining. Further, peptide stimulation assays with K562 cells expressing the relevant HLA-type revealed variable peptide sensitivity with high and low functional TCRs. Importantly, highly functional TCRs were found to specifically kill SARS-CoV-2-infected lung cancer target cells.

We concluded that convalescent donors of mild COVID-19 establish highly functional, polyclonal T cell responses that persist for longer time (up to 12 months followed). scRNAseq of single epitope reactive CD8$^+$ T cells revealed signatures of highly functional TCRs, which upon re-expression via OTR have proven cytotoxic potency on virus infected cells.

Recruitment of highly cytotoxic CD8$^+$ T cell receptors in mild SARS-CoV-2 infection

Wagner KI*, Mateyka LM*, Jarosch S*, Grass V, Weber S, Schober K, Hammel M, Burrell T, Kalali B, Poppert H, Beyer H, Schambeck S, Holdenrieder S, Strötges-Achatz A, Haselmann V, Neumaier M, Erber J, Priller A, Yazici S, Roggendorf H, Odendahl M, Tonn T, Dick A, Witter K, Mijočević H, Protzer U, Knolle PA, Pichlmair A, Crowell CS, Gerhard M, D'Ippolito E, Busch DH.

* These authors contributed equally.

Published in: Cell Reports. 2022, Jan 11;38(2):110214.
doi: 10.1016/j.celrep.2021.110214

4 Discussion

ACT in tumor diseases and viral infections has recently raised a lot of attention and has already proven astonishing clinical success. With this thesis work, a workflow for the identification of low-frequency, tumor neo-epitope-specific TCRs from the naive repertoire of healthy donors and a platform of *in vitro* screening to identify highly target-specific and functional TCRs have been established. Further, we described novel approaches for the high-throughput identification of virus-specific TCRs from the memory repertoire of SARS-CoV-2 exposed donors, and isolated TCRs specific for defined viral epitopes with high functionality in *in vitro* assays. Taken together, we provide a toolset to study antigen-specific T cell responses and isolate highly potent TCRs for potential therapeutic application.

4.1 Identification of candidate neo-epitopes by *in silico* predictions

The identification of disease-relevant epitopes by HLA ligandome analysis combined with mass spectrometry is most accurate, however, not always feasible. Alternatively, *in silico* prediction tools are largely used. In the work presented here, we used *in silico* prediction tools to identify peptides with high MHC Class I binding affinity and a high likelihood to be immunogenic from fs-derived neo-ORFs or viral ORFs. Despite the throughput and the easy usage, physiological processing and presentation of the predicted epitope could not further be validated with *in silico* tools. Thereby, the relevance of the selected candidate epitopes in the disease of interest has to be validated with alternative approaches.

In the case of viral epitopes, the *ex vivo* detection of epitope-reactive T cells in convalescent donors already represents a good indicator for a physiologically relevant epitope. Among a total of 40 selected epitopes specific for SARS-CoV-2, 19 were confirmed as immunogenic epitopes eliciting a $CD8^+$ T cell response in convalescent donor PBMCs [149]. Interestingly, the successful identification of immunogenic epitopes was skewed towards specific HLAs. Indeed, for some HLAs (e.g. HLA-A*01:01 and HLA-A*03:01) the majority of predicted peptides were truly immunogenic. Still, for other HLA class I molecules (e.g. HLA-A*24:02 and HLA-B*07:02) none of the predicted epitopes were found immunogenic. This demonstrates the limitation of such *in silico* tools for epitope prediction. As mentioned before, the level of accuracy strongly depends on the size and quality of the training data set for a given allele, and can be modeled with a moderate to high level of accuracy for common HLAs. Predictions for less frequent HLA-types often lack accuracy. Moreover, despite efficient cross-presentation of an immunogenic epitope

and the detection of T cells recognizing immunogenic epitopes, the presentation of an antigenic peptide in virus-infected cells is not self-understanding [150]. Thus, we experimentally validated that T cells engineered with a TCR specific for selected epitopes can effectively kill virus-infected target cells.

In the case of fs-derived tumor neo-epitopes, the naive repertoire theoretically holds a repertoire of TCRs targeting any non-self antigen, independent of its actual occurrence in immune presentation. Thereby, the isolation of even highly functional TCRs does not indicate whether the epitope of interest is expressed on target cells. Therefore, to validate the physiological relevance of the epitopes, we re-expressed the mutated protein leading to the peptides of interest in a K562 cell line-based system. HLA-transduced K562 cells have proven very efficient as artificial APCs, and can process the protein via its normal route through the proteasome and load peptide fragments via antigen peptide-transporter (TAP) in the endoplasmic reticulum on MHC Class I molecules for surface presentation [140,141]. In contrast to the K562 cells, other cancer cells often have intrinsic mechanisms of T cell escape like MHC deregulation or expression of inhibitory receptors, and thus present a less suitable model. Interestingly, *in vitro* cell culture treatment with IFN-γ has shown to restore TAP-dependent antigen processing and MHC Class I presentation competence in PDAC cell lines and induce T cell responses [151].

Among the two predicted RNF43 neo-epitopes, we identified the A2-RNF43_SLLPTCWAL epitope to be presented at the target cell surface and induce a response in epitope-specific TCR-engineered T cells. This was further confirmed in a PDAC cell line naturally harboring a fs-mutation leading to the neo-epitope. The second epitope, B7-RNF43_VPSVWRSLL did not show evidence of adequate processing and MHC Class I presentation reasoning from the lack of T cell response in co-culture assays with RNF43 fs-expressing K562 target cells. Even though, the B7-RNF43_VPSVWRSLL epitope was confirmed to be processed *in vitro* in a proteasomal processing assay, natural processing and presentation could not be confirmed. This finding supports other published studies that question the applicability and reliability of available algorithms simulating *in vivo* epitope splicing [152] and further emphasizes the need of high quality target identification.

4.2 Technological developments in TCR isolation

The isolation of tumor neo-epitope specific TCRs for therapy remains challenging, and as elucidated earlier, patient material often represents a T cell source with difficult availability, accessibility, as well as questionable quality. Thus, we focused on the peripheral blood of healthy donors as a potentially unlimited source of tumor neo-epitope-specific T cells. Yet, antigen-specific TCRs are of extremely low frequency in the naive repertoire of a healthy donor. Here, we have presented a platform to isolate such rare neo-epitope-specific TCRs via initial SE and subsequent combinatorial pMHC multimer staining for single cell sort. Sorted cells followed an additional step of *in vitro* expansion prior to TCR sequencing via canonical PCR-based TCR loci amplification and NGS. Interestingly, we have identified five identical clones for TCR R11 that all clearly originated

from the naive $CD8^+$ T cell population. Clonal expansion is not expected in the naive repertoire; however, uneven homeostatic proliferation leading to an increase of naive T cell clones without development of a memory cell phenotype has been found in the repertoires of elderly individuals [89].

With the developed platform, the naive repertoire has become easily accessible. However, we have no information on the functionality of the isolated TCRs at the time of sorting. This represents a relevant limitation to overcome in the near future as the naive TCR repertoire is mainly composed of low avidity and thus low functional TCRs [103]. We have successfully identified highly functional TCRs targeting the A2-RNF43_SLLPTCWAL and B7-RNF43_VPSVWRSLL neo-epitopes each from a single donor. For the A2-RNF43_SLLPTCWAL epitope, four out of six (66 %) candidate TCRs recognized the relevant pMHC, and three (50 %) were found responsive to peptide stimulation. Finally, only one TCR (17 %) was identified as highly functional. Similarly, for the B7-RNF43_VPSVWRSLL-specific TCRs, 15 of 21 (71 %) TCR candidates were identified with pMHC multimer recognition. Out of these, only 9 (43 %) responded with cytokine release to peptide stimulation but showed variable potency in a cytotoxicity assay. For the third epitope of interest (A2-RNF43_TQLARFFPI), however, the identification of functional TCRs was found to be more difficult. From three different donors, we only identified two TCRs with pMHC multimer recognition, yet, a lack of functionality in *in vitro* peptide stimulation assays. This highlights the need for an improved TCR isolation platform that can already reliably estimate functionality of a TCR before laborious re-expression.

To facilitate the selection of TCRs to re-express, we first looked whether the multimer staining at the time of sorting (index sorting data) could hold any information. After thorough *in vitro* functional characterization and tracing highly functional TCRs to their original position in the initial sort gate, we observed an enrichment in functional TCRs in cells showing high fluorescent intensities of pMHC multimers at the time of sorting. Still, this observation was not consistent enough to suggest the use of multimer staining as a reliable predictor for TCR functionality. Besides, we observed that an initial pMHC re-staining of single cell-derived clones indicated a selection parameter for TCRs with high chances for pMHC recognition after TCR re-expression. Although this may help the discrimination of false multimer-reactive TCRs at the time of sorting, it still does not provide information on functionality. In addition, the procedure remains tedious. Alternatively, potency of an expanded clone could be evaluated by assays of e.g. peptide stimulation, as has been described in many other studies [66, 71, 72, 80, 87]. However, such a T cell functionality readout requires the *in vitro* expansion of a clone, which can induce culture-related biases in T cell phenotype and peptide-reactivity. Furthermore, laborious expansion and peptide re-challenge protocols with a single peptide concentration cannot discriminate high and low functional TCRs. Development of a pMHC platform that simultaneously included a functional screen at the time of sort would solve the problems of precise selection of highly functional TCRs. Here, TCR avidity could be a pMHC-based parameter that, when implemented into a workflow for TCR isolation, could provide a reliable readout for TCR functionality [70].

Recent developments in scRNAseq have improved the field of antigen-reactive TCR identification by high-throughput target analysis and feasibility of TCR sequencing from multiplexed donors. Still, a functional readout is often not provided. By methods of transcriptional shifts induced by short-term peptide stimulation, antigen-reactive T cells can be detected and identified according to gene signatures of T cell activation [148]. In our study on SARS-CoV-2-specific $CD8^+$ T cells, we have stimulated T cells from convalescent COVID-19 donors and sorted IFN-γ positive cells for scRNAseq analysis. Re-expression of identified TCRs and connection of T cell activation and functionality signatures of the initial sorted clone, led us to define a transcriptional profile for the identification of highly functional SARS-CoV-2-specific $CD8^+$ T cells [149]. Recently, a study described a method for high-dimensional and high-throughput pMHC multimer-based single cell analysis of antigen-specific $CD8^+$ T cells [153]. Briefly, paired TCR sequences of antigen-specific cells were simultaneously profiled for selected surface-protein expression and targeted gene expression in tens of thousands of single cells from multiple biological samples. Further, this methods claims to validate antigen-specific T cells for potential cross-reactivity and broadens the horizon of high-precision/high-throughput TCR identification and isolation. Nevertheless, in stark contrast to reactive T cells from the memory population, a precise identification of naive epitope-reactive T cells will remain challenging due to low activation profiles.

Besides the need for a higher specificity in TCR isolation, a larger epitope library and a higher throughput for processing of donor material is of immediate relevance. Here, we have presented a platform focused on the isolation of TCRs specific for a single epitope from one donor. The development of fast and flexible pMHC libraries greatly influenced the rapid development of high-throughput applications for the identification of therapeutically valuable TCRs. Technologies enabling quick exchange of peptides bound to pMHCs by UV light-induced ligand exchange can circumvent tedious chain re-folding and provide a high-throughput production of many pMHCs for a wide set of epitopes [154]. Spectral overlap of fluorescent-labeled pMHCs limits the multiplexing for multi-epitope TCR isolation. However, methods of DNA-barcoding of pMHC backbones enable to link a TCR sequence to the cognate antigen in single cells at high throughput [155]. In this way libraries of about 1000 different pMHCs can simultaneously detect antigen-specific $CD8^+$ T cells in a single sample [156]. The implementation of scRNAseq to multiplexed pMHC-based TCR isolation platforms replaces the need for laborious TCR sequencing from a single cell or *in vitro* expanded clone. Sorts on low frequency neo-epitope reactive T cells from the naive repertoire often face the challenge of few sorted cells that remain below the capacity of a scRNAseq-run. However, sorted cells from individual donors can be pooled and later demultiplexed according to donor-specific single nucleotide polymorphisms or by barcoding donors with hash-tag mABs [157, 158]. In our study on SARS-CoV-2-specific $CD8^+$ T cell responses, we have shown successful donor discrimination for identified virus-specific T cells [149].

4.3 Advancing to high-throughput *in vitro* TCR characterization

Naive TCRs are often found with low functional avidity, and extensive characterization of the re-expressed candidate TCRs is crucial to identify best candidates for clinical application. Re-expression of candidate TCRs via OTR in human primary T cells is indeed physiological, but still a time- and cost-consuming process. In a first step of functional characterization, we stained for pMHC multimer recognition of OTR-engineered T cells. Similar to what was found in other studies on TCRs derived from the naive repertoire, our data also showed that pMHC multimer staining is not always predictive for antigen-specific reactivity and thorough analysis of functionality is needed [159]. TCR:pMHC k_{off}-rate measurements are particularly informative as the structural avidity is encoded in the TCR sequence and is independent of T cell physiology, phenotype and donor cell variability. Still, this parameter did not exclusively define the TCR candidates with highest functionality. TCR:pMHC k_{off}-rate measurements for the set of B7-RNF43_VPSVWRSLL-specific TCRs showed relatively good half-lives (100 s half-life is reported as minimal threshold for highly functional TCRs [160]). Still, this parameter required additional tests to identify most potent TCRs. Latest developments in the industry have launched instruments for precise measurements of cellular avidity, which defines the overall interactions that occur at the immunological synapse between effector and target cells (Lumicks). A technology based on resonant acoustic waves showed the potential to provide predictive, reproducible, and fast high-throughput measurement of avidity at a single cell resolution and could represent a more reliable readout to predict TCR functionality.

To further characterize the functionality of our identified candidate TCRs, we continued with an *in vitro* peptide stimulation assay. TCR-engineered T cells were first purity sorted on pMHC multimer recognition and expanded on feeder cells to reach feasible numbers for functional assays. Even though we used an antigen-unspecific expansion approach, the long expansion time strongly influences the cellular phenotype and brings a bias to the performance of the TCR-engineered $CD8^+$ T cells in functional assays. Upon peptide stimulation, we have measured release of IFN-γ and IL-2 cytokines. Despite IL-2 being a common marker for T cell activation, in this setting of *in vitro* expanded T cells, it did no longer represent a good indicator for peptide sensitivity. Further, we measured the level of TCR expression and downregulation upon peptide stimulation. However, this marker represented a variable readout and did not clearly resolve differences in high and low functional candidates, as indicated by the EC_{50} values determined for the B7-RNF43_VPSVWRSLL-specific TCRs. Specifically, highly functional TCR candidates TCR R21 and R23 were found with similar EC_{50} values for TCR downregulation compared to TCR R17 and R19 with low functionality. Calculation of EC_{50} values regards the relative change in TCR expression measured by fluorescent intensity, but does not account for the absolute change. With little variation in absolute TCR expression, EC_{50} values do not reflect a precise parameter. In the end, the release of IFN-γ demonstrated the most sensitive readout in this experimental setup

with long-term cultured primary CD8$^+$ T cells. Upon peptide stimulation, IFN-γ was released in a dose-dependent manner and the quantified EC_{50} values clearly discriminated TCRs with high reactivity (TCR R21 and R23) from low sensitivity TCRs (TCR R17 and R19) by about two log-scales. Despite a physiological way of TCR re-expression, this assay represents a laborious and time intensive manner of TCR characterization with partly variable quality of readout. Consequently, reporter cell lines expressing the TCRs of interest can be a promising tool for reliable, standardized and high-throughput TCR characterization. An optimal system is provided by the T cell lymphoma-derived Jurkat cell line engineered for a triple reporter model. The Jurkat triple parameter reporter (J-TPR) cell line is engineered for the expression of three different fluorescent protein-encoding genes, that become activated by TCR-triggered transcription factors.

Our group has demonstrated that TCR-engineered J-TPR cells exhibit reliable, highly epitope-specific pMHC multimer recognition and TCR functionality closely correlated with the potency of a TCR re-expressed in primary T cells [161]. The cell line model facilitates the generation of high-throughput TCR screening platforms for identification of TCRs with therapeutic value. Further, the cell line serves as a good model to study basic questions in TCR activation such as their functional dependency on co-receptors. Last but not least, the high-throughput compatibility of the cell line can also contribute to the generation of large data sets connecting a TCR sequence to antigen-specificity, epitope cross-reactivity and subsequent functionality for the development of improved prediction algorithms.

4.4 Optimize cell line models for *in vitro* TCR cytotoxicity

CD8$^+$ T cells can mediate highly epitope-specific cytotoxicity via the TCR and effectively kill target cells. The killing potential of a TCR-engineered CD8$^+$ T cell can be evaluated in *in vitro* cytotoxicity assays. For the study of SARS-CoV-2-specific TCRs, we infected a lung cancer cell line, expressing a red fluorescent protein, with a SARS-CoV-2 virus strain co-expressing a GFP. Upon co-culturing of infected targets cells with CD8$^+$ T cells expressing a SARS-CoV-2-specific TCR, we could follow target cell lysis via the fluorescent signal. This model represented a highly physiological model for epitope-presentation upon virus infection and epitope-specific T cell-mediated killing. However, working with a human pathogenic virus required sophisticated biosafety measurements. Alternatively, to simplify the model, lung cancer cell lines could be virally transduced with constructs for the expression of selected viral ORFs.

For the characterization of tumor neo-epitope-specific TCRs we needed to find an optimal target cell line model. For the set of A2-RNF43_SLLPTCWAL-specific TCRs, we had a PDAC cell line available that expressed an endogenous RNF43 fs-mutation, leading to the neo-epitope of interest. In a cytotoxicity assay, we observed that TCR R11, and to minor extend TCR R15, strongly recognized and killed the Capan-2 A2$^+$ target cell line. As a control for unspecific killing, we used the Capan-2 cell line that lacks HLA-A*02:01 expression. TCR-engineered T cells did not have an effect on target cell line growth. Nonetheless, this cell line remains questionable for an appropriate control,

as TCR recognition is completely impaired by the absence of the cognate HLA molecule. Notably, HLA-engineering by retroviral transduction of the Capan-2 cell line and positive selection for HLA-A*02:01 expression, changed the physiological behavior of the cell line. This can be clearly observed by the different shape of the growth curves after seeding and before T cell addition. We concluded that T cell-mediated killing is difficult to compare in different cell lines with divergent physiological behavior. Also, we controlled for unspecific target cell killing by co-incubating T cells engineered with the TCR of highest functionality (TCR R11) with the T3M4 target cell line. This cell line is HLA-A*02:01 positive but lacks an appropriate fs-mutation leading to the A2-RNF43_SLLPTCWAL neo-epitope. In this experimental setting, we did not observe neo-epitope unspecific, HLA-depend cytotoxicity by TCR R11-expressing $CD8^+$ T cells. Still, a negative control using a different target cell line does not represent the optimal system, as e.g. the expression of inhibitory molecules on the target cells can greatly influence the killing potency of a T cell. For an optimal target cell line system, the CRISPR/Cas9 technology could be used to specifically introduce the relevant fs-mutation for neo-epitope expression, and T cell cytotoxicity could be evaluated on the CRISPR/Cas9-engineered and wt-version of the same target cell line.

To keep the target cell line consistent among control settings, a target-specific killing can also be shown by a lack of killing by T cells devoid of the epitope-specific TCR. We used unedited mock T cells as a control for unspecific target cell killing. Importantly, we observed that the addition of high numbers of T cells with heterogeneous TCR expression (T:E 1:20) already induces growth inhibitory effects on the target cell lines. This indicates the importance of appropriate controls in this type of cytotoxicity assay to avoid misinterpretation of the data. Here, OTR-engineered T cells expressing a target irrelevant TCR (TCR SCoV34) represented a cleaner control.

4.5 Validation of TCR cross-reactivity

The sensitivity of a TCR is usually tightly connected to its specificity. Low affinity is connected to higher cross-reactivity. However, *in vitro* affinity enhancement could generate unpredictable reactivities and toxicities. Here, we have only superficially studied TCR specificity by staining TCR-engineered T cells with a target irrelevant pMHC multimer. We did not observe cross-reactivity of any of the TCRs to the cognate HLA molecule, but we could not exclude recognition of similar epitopes. Indeed, cross-reactivity of a TCR to more than one pMHC molecule and epitope is often found in T cell repertoires and even represents a biological necessity to cover protection against the vast diversity of foreign antigens.

TCRs identified from the naive repertoire and targeting self/tumor-epitopes are often of low target affinity, as the naive repertoire is skewed by central tolerance. Thus, when targeting TAAs such as MAGE-A3, low-affinity TCRs have been artificially enhanced. Methods of affinity-enhancement, conventionally performed by random mutagenesis of the TCR framework, can induce undesirable off-target events due to TCR cross-reactivity and it was reported with partially fatal outcome in several clinical studies [51, 162, 163].

Apart from detrimental cross-reactivity, affinity-enhanced TCRs are also susceptible to overstimulation and rapid exhaustion, and further flawed in cellular kinetics and signaling [164]. Such safety concerns raised with affinity-enhanced TCRs become neglectable for physiological TCRs derived from the naive repertoire, as they have passed thymic selection; thus, the likelihood of causing severe autoreactivity in recipient individuals is very low. Nevertheless, evaluation of cross-reactivity to related peptides remains a crucial part to finalize *in vitro* TCR characterization. *In silico* analysis tools for cross-reactivity can predict self-peptide similarity in human tissues [165]. Neo-epitopes derived from fs-mutations originate from a shift in the ORF, and a high homology with self peptides is not expected. Yet, the experimental validation of TCR reactivity to altered peptide ligands (APLs) remains crucial. A common approach to test for the cross-reactivity landscape is the design of APL libraries. Here, all possible aberrant target peptides are simulated by single aa substitution, or a combinatorial strategy that replaces all 20 naturally occurring aas at any position in the peptide sequence. In tedious peptide reactivity assays, single cross-reactive epitopes can be identified. Re-expression of TCRs in the previously mentioned J-TPR cell line can undoubtedly increase throughput in the number of TCRs analyzed. A major limitation of this approach remains clearly the need of a new peptide library for each analysis of pMHC specificity.

The pMHC multimer-based 'one-pot' strategy suggests a fast workflow to measure the relative affinities of TCRs to libraries of DNA-barcoded pMHCs variants and efficiently identify cross-recognized peptides [166].

5 Future perspectives

5.1 Combination therapies for successful treatment in solid tumors

Solid tumors have been difficult to successfully target with ACT so far. Especially treatment of PDAC, a cancer with a highly immunosuppressive TME, would benefit by simultaneous treatments that enable easier access of the T cells to the TME. The suppression of T cell activation by the TME can potentially be overcome by e.g. combination therapy with checkpoint inhibitors. Additionally, checkpoint inhibitor therapy can be further sensitized by the application of immunogenic chemotherapy drugs that have shown to trigger $CD8^+$ T cell anti-tumor immunity for durable cancer control [167, 168]. In mice treated with anti-ROR1 CAR T cells, such combination therapy has shown improved CAR T cell recruitment and survival in the tumor, indicating promising anti-tumor efficacy also for clinical application [169].

Another obstacle for persistence of the transferred transgenic receptor-engineered T cells is the potentially limited antigen expression. Here, mRNA vaccines, that have received first approval during the COVID-19 pandemic, have also been explored in the context of ACT. Studies of anti-CLDN6 CAR T cells in mice, but also a fist clinical trial, demonstrated that vaccination induced target presentation on APCs, and promoted CAR T cell expansion for improved engraftment [170,171]. In order to establish a heterogenous target expression in the tumor tissue, strengthening the T cell-mediated anti-tumor immunity, oncolytic viruses have been intensively studied. Several pre-clinical studies investigated the effect of CAR T cell-based ACT combined with oncolytic viruses in solid tumors and indicate this as a promising approach to overcome the currently low efficacy of therapeutic T cell products also in PDAC [172].

5.2 Advanced T cell engineering

As previously discussed, checkpoint inhibitors, or other immunotherapies can greatly influence the success of ACT. Still, many of these therapies act systemically with concomitant side effects; precise co-engineering of the therapeutic T cells can preserve the benefits of combinatorial therapy in potentiating T cell efficacy and survival in the TME but avoid systemic toxicity. For instance, CRISPR/Cas9-mediated KO of the inhibitory receptor PD-1 was found to improve anti-tumor T cell immunity in patients with refractory cancer [173]. Alternatively, T cell engineering attempts have been undertaken to modify inhibitory signaling domains of TIGIT with CD28 stimulatory domains to enhance T cell functionality [174]. Furthermore, T cells have been engineered with re-

ceptors for chemokines or cytokines abundant in the TME improving migration to the tumor site in pre-clinical models [175–178]. One of the most prominent examples that a single engineered T cell progeny can mediate protective tumor immunity is most likely the loss of TET2 function, which was found to enhance the proliferative ability of CAR T cells [179, 180]. From this oberservation, genome-wide CRISPR screens have been used to identify target genes crucial for improving T cell fitness.

Besides co-engineering, the phenotype of the edited T cell was found to play a crucial role. Senescent or exhausted CAR T cells were found with poor targeting and effector functions, and reduced persistence *in vivo* [181]. Further, memory T cells are less stringent in the requirements for activation with the co-receptors compared to naive T cells and are thus associated with improved potency. Especially, memory T cells with a weaker differentiated phenotype preserve a certain stemness, and can even from low cell numbers reconstitute a robust and long-term maintained immune response [182,183]. Thus it will be important to develop protocols for genetic engineering and manufacturing that preserve a stem-like phenotype and allow rapid re-infusion into the patient.

5.3 Outlook to clinical application

The TCRs identified in this thesis targeting tumor neo-antigens or virus-specific targets can be envisioned for clinical application. Early studies of T cell transfer have shown, that the transfer of virus-specific T cells from seropositive donors to immunocompromised patients after aHSCT enables protective effect from CMV, Epstein-Barr virus or adenovirus reactivation [184]. With the emergence of the novel SARS-CoV-2 virus and the development to an endemic persistence, SARS-CoV-2-specific T cells could become therapeutically relevant. Early clinical trials have registered the use of convalescent donor-derived virus-specific T cells to treat patients with severe course of diseases, but also a protective application to immune-vulnerable patients lies within the scope of possible therapeutic scenarios.

The urgent need for effective therapies in solid tumors, especially in PDAC, arises the possibility for novel treatment options and the future application of e.g. RNF43 fs-derived neo-epitope-specific TCRs in individual patients for compassionate use. Nevertheless, the implementation of such T cell based therapies in clinical use remains challenging mostly due to the highly personalized nature, but also obstacles in regulatory and manufacturing.

5.3.1 Safety profile of T cell engineered with CRISPR/Cas9-based editing

Non-viral, CRISPR/Cas9-based T cell engineering via OTR was shown to generate predictable and near to physiological engineered T cell products which are crucial aspects for clinical application in ACT [100, 102]. In the first in-human phase I clinical trial with CRISPR/Cas9-engineered T cells, both TCR chains were knocked-out along with PD-1. Further, a cancer-testis-antigen-specific TCR was co-transduced to treat patients with refractory cancer [173]. Promisingly, CRISPR/Cas9-edited T cells persisted in the

patient in the absence of clinical toxicities, and the study provided first evidence for safety and feasibility of such engineered T cell products in clinical use.

The CRISPR/Cas9-system is a highly targeted approach for genetic engineering, but still comes with possible effects of off-target double strand breaks, off-target template integration and chromosomal translocations through genetic editing of multiple loci. The choice of reagents for CRISPR-editing, such as high-fidelity RNPs, can greatly increase specificity and reduce the frequency of off-target effects [185]. Recent studies of whole-genome sequencing and targeted deep-sequencing of predicted off-target sites confirmed that off-target events are unlikely to be caused by CRISPR/Cas9-engineering in primary human T cells [186]. Further, by targeted locus amplification (TLA) analysis our group could show that TRAC-targeted integration of the donor DNA template showed only minor homology-independent integration in the T cell receptor *beta* chain (TRBC) locus [100]. Similarly, other studies on TLA sequencing have found no evidence for off-target integration above the detection limit of 1 % of alleles. Even at single cell level off-targets were detected at frequencies of 0.1 % and could be even further reduced with the selection of a single stranded DNA donor template [101]. Chromosomal translocations have been detected in CRISPR/Cas9-engineered T cells; however, the frequency decreased over time of the manufacturing process, conferring no evidence of further expansion and cell survival capacity [173]. Here, the use of Cas9 base editors that circumvent double strand breaks, could further decrease the risk of translocation in multiplexed editing.

5.3.2 A path to GMP-manufacturing

Recently, there has been immense progress in the industry to supply not only reagents needed for CRISPR/Cas9-engineering, but also electroporation devices in good manufacturing practice (GMP)-grade. Still, a major limitation is the low editing efficacy of OTR-engineered T cells. Wide efforts are currently undertaken to increase CRISPR/Cas9-mediated genome editing efficacy. For instance, the application of small molecule inhibitors interacting with the DNA-repair mechanisms after CRISPR/Cas9-editing have been reported to greatly elevate the editing efficacies [187]. Further, a pre-print published study (Shy *et.al.* 2021) reported on sophisticated designs of hybrid single strand DNA HDR templates and showed up to 62 % targeted KI of a CAR construct in a GMP-conform manufacturing setting.

As presented in this thesis, TCR-transgenic T cells can be easily expanded to high cell numbers within weeks. Also conventional T cell editing and manufacturing protocols usually include a step of *in vitro* culture and expansion. However, a short production and expansion process is believed to be key for the maintenance of a less differentiated cellular phenotype with effective *in vivo* engraftment and potency. This was demonstrated by a study showing that a limited *ex vivo* culture time of three to five days enhanced CAR T cell effector function with improved tumor control [188]. Recent advances in the industry e.g. the T-Charge™platform by Novartis focuses on the manufacturing engineered T cells that preserve T cell stemness. Such product retains a high *in vivo* proliferative potential and claims high tumor efficacy accompanied by reduced events of T cell exhaustion.

Despite the possibility to also easily scale up the CRISPR editing protocol to up to 1×10^9 T cells in the transfection step, possibly, extremely low cell numbers of OTR-engineered T cells might already be sufficient for effective transfer into a patient. In contrast to conventional virally transduced T cell products, OTR-engineered T cells show physiological activation and regulation of TCR triggering. Further, depending on the edited cellular phenotype, T cells can harbour high *in vivo* proliferative capacity and already the transfer of a single antigen-reactive cell has shown to be sufficient for robust protection in murine models of infection [182, 183, 189].

In summary, OTR-engineered T cell products with a high proliferative phenotype could already show high therapeutic effects when administered at low doses. Currently, the field of CRISPR/Cas9-mediated engineering of T cells for clinical application is developing fast and is addressing the remaining obstacles for safe and efficient manufacturing of a therapeutic cell product for clinical use.

References

[1] M. M. Davis, J. J. Boniface, Z. Reich, D. Lyons, J. Hampl, B. Arden, and Y. Chien. Ligand recognition by alpha beta T cell receptors. *Annu Rev Immunol*, 16:523–544, 1998.

[2] M. Malissen, J. Trucy, E. Jouvin-Marche, P. A. Cazenave, R. Scollay, and B. Malissen. Regulation of TCR alpha and beta gene allelic exclusion during T-cell development. *Immunol Today*, 13(8):315–322, Aug 1992.

[3] K. Kuida, M. Furutani-Seiki, T. Saito, H. Kishimoto, K. Sano, and T. Tada. Post-translational attainment of allelic exclusion of the T cell receptor alpha chain in a T cell clone. *Int Immunol*, 3(1):75–82, Jan 1991.

[4] M. Merkenschlager, D. Graf, M. Lovatt, U. Bommhardt, R. Zamoyska, and A. G. Fisher. How many thymocytes audition for selection? *J Exp Med*, 186(7):1149–1158, Oct 1997.

[5] V. I. Zarnitsyna, B. D. Evavold, L. N. Schoettle, J. N. Blattman, and R. Antia. Estimating the diversity, completeness, and cross-reactivity of the T cell repertoire. *Front Immunol*, 4:485, Dec 2013.

[6] T. Mora and A. M. Walczak. Quantifying lymphocyte receptor diversity. *Syst. Immunol*, 1:183–198, 2019.

[7] T. P. Arstila, A. Casrouge, V. Baron, J. Even, J. Kanellopoulos, and P. Kourilsky. A direct estimate of the human alphabeta T cell receptor diversity. *Science*, 286(5441):958–961, Oct 1999.

[8] M. Berard and D. F. Tough. Qualitative differences between naïve and memory T cells. *Immunology*, 106(2):127–138, Jun 2002.

[9] S. R. Riddell, K. S. Watanabe, J. M. Goodrich, C. R. Li, M. E. Agha, and P. D. Greenberg. Restoration of viral immunity in immunodeficient humans by the adoptive transfer of T cell clones. *Science*, 257(5067):238–241, Jul 1992.

[10] M. Saxena, S. H. van der Burg, C. J. M. Melief, and N. Bhardwaj. Therapeutic cancer vaccines. *Nat Rev Cancer*, 21(6):360–378, 06 2021.

[11] Y. Naito, K. Saito, K. Shiiba, A. Ohuchi, K. Saigenji, H. Nagura, and H. Ohtani. CD8+ T cells infiltrated within cancer cell nests as a prognostic factor in human colorectal cancer. *Cancer Res*, 58(16):3491–3494, Aug 1998.

[12] F. Prall, T. Dührkop, V. Weirich, C. Ostwald, P. Lenz, H. Nizze, and M. Barten. Prognostic role of CD8+ tumor-infiltrating lymphocytes in stage III colorectal cancer with and without microsatellite instability. *Hum Pathol*, 35(7):808–816, Jul 2004.

[13] O. Nakano, M. Sato, Y. Naito, K. Suzuki, S. Orikasa, M. Aizawa, Y. Suzuki, I. Shintaku, H. Nagura, and H. Ohtani. Proliferative activity of intratumoral CD8(+) T-lymphocytes as a prognostic factor in human renal cell carcinoma: clinicopathologic demonstration of antitumor immunity. *Cancer Res*, 61(13):5132–5136, Jul 2001.

[14] S. Kondratiev, E. Sabo, E. Yakirevich, O. Lavie, and M. B. Resnick. Intratumoral CD8+ T lymphocytes as a prognostic factor of survival in endometrial carcinoma. *Clin Cancer Res*, 10(13):4450–4456, Jul 2004.

[15] A. Fukunaga, M. Miyamoto, Y. Cho, S. Murakami, Y. Kawarada, T. Oshikiri, K. Kato, T. Kurokawa, M. Suzuoki, Y. Nakakubo, K. Hiraoka, T. Itoh, T. Morikawa, S. Okushiba, S. Kondo, and H. Katoh. CD8+ tumor-infiltrating lymphocytes together with CD4+ tumor-infiltrating lymphocytes and dendritic cells improve the prognosis of patients with pancreatic adenocarcinoma. *Pancreas*, 28(1):26–31, Jan 2004.

[16] T. Donnem, S. M. Hald, E. E. Paulsen, E. Richardsen, S. Al-Saad, T. K. Kilvaer, O. T. Brustugun, A. Helland, M. Lund-Iversen, M. Poehl, K. E. Olsen, H. J. Ditzel, O. Hansen, K. Al-Shibli, Y. Kiselev, T. M. Sandanger, S. Andersen, F. Pezzella, R. M. Bremnes, and L. T. Busund. Stromal CD8+ T-cell Density—A Promising Supplement to TNM Staging in Non-Small Cell Lung Cancer. *Clin Cancer Res*, 21(11):2635–2643, Jun 2015.

[17] S. A. Rosenberg, P. Spiess, and R. Lafreniere. A new approach to the adoptive immunotherapy of cancer with tumor-infiltrating lymphocytes. *Science*, 233(4770):1318–1321, Sep 1986.

[18] P. J. Spiess, J. C. Yang, and S. A. Rosenberg. In vivo antitumor activity of tumor-infiltrating lymphocytes expanded in recombinant interleukin-2. *J Natl Cancer Inst*, 79(5):1067–1075, Nov 1987.

[19] S. A. Rosenberg, B. S. Packard, P. M. Aebersold, D. Solomon, S. L. Topalian, S. T. Toy, P. Simon, M. T. Lotze, J. C. Yang, and C. A. Seipp. Use of tumor-infiltrating lymphocytes and interleukin-2 in the immunotherapy of patients with metastatic melanoma. A preliminary report. *N Engl J Med*, 319(25):1676–1680, Dec 1988.

[20] M. J. Besser, R. Shapira-Frommer, A. J. Treves, D. Zippel, O. Itzhaki, E. Schallmach, A. Kubi, B. Shalmon, I. Hardan, R. Catane, E. Segal, G. Markel, S. Apter, A. B. Nun, I. Kuchuk, A. Shimoni, A. Nagler, and J. Schachter. Minimally

cultured or selected autologous tumor-infiltrating lymphocytes after a lymphodepleting chemotherapy regimen in metastatic melanoma patients. *J Immunother*, 32(4):415–423, May 2009.

[21] M. E. Dudley, C. A. Gross, M. M. Langhan, M. R. Garcia, R. M. Sherry, J. C. Yang, G. Q. Phan, U. S. Kammula, M. S. Hughes, D. E. Citrin, N. P. Restifo, J. R. Wunderlich, P. A. Prieto, J. J. Hong, R. C. Langan, D. A. Zlott, K. E. Morton, D. E. White, C. M. Laurencot, and S. A. Rosenberg. CD8+ enriched "young" tumor infiltrating lymphocytes can mediate regression of metastatic melanoma. *Clin Cancer Res*, 16(24):6122–6131, Dec 2010.

[22] S. L. Goff, F. O. Smith, J. A. Klapper, R. Sherry, J. R. Wunderlich, S. M. Steinberg, D. White, S. A. Rosenberg, M. E. Dudley, and J. C. Yang. Tumor infiltrating lymphocyte therapy for metastatic melanoma: analysis of tumors resected for TIL. *J Immunother*, 33(8):840–847, Oct 2010.

[23] R. W. Joseph, V. R. Peddareddigari, P. Liu, P. W. Miller, W. W. Overwijk, N. B. Bekele, M. I. Ross, J. E. Lee, J. E. Gershenwald, A. Lucci, V. G. Prieto, J. D. McMannis, N. Papadopoulos, K. Kim, J. Homsi, A. Bedikian, W. J. Hwu, P. Hwu, and L. G. Radvanyi. Impact of clinical and pathologic features on tumor-infiltrating lymphocyte expansion from surgically excised melanoma metastases for adoptive T-cell therapy. *Clin Cancer Res*, 17(14):4882–4891, Jul 2011.

[24] E. Tran, S. Turcotte, A. Gros, P. F. Robbins, Y. C. Lu, M. E. Dudley, J. R. Wunderlich, R. P. Somerville, K. Hogan, C. S. Hinrichs, M. R. Parkhurst, J. C. Yang, and S. A. Rosenberg. Cancer immunotherapy based on mutation-specific CD4+ T cells in a patient with epithelial cancer. *Science*, 344(6184):641–645, May 2014.

[25] S. Kalaora, Y. Wolf, T. Feferman, E. Barnea, E. Greenstein, D. Reshef, I. Tirosh, A. Reuben, S. Patkar, R. Levy, J. Quinkhardt, T. Omokoko, N. Qutob, O. Golani, J. Zhang, X. Mao, X. Song, C. Bernatchez, C. Haymaker, M. A. Forget, C. Creasy, P. Greenberg, B. W. Carter, Z. A. Cooper, S. A. Rosenberg, M. Lotem, U. Sahin, G. Shakhar, E. Ruppin, J. A. Wargo, N. Friedman, A. Admon, and Y. Samuels. Combined Analysis of Antigen Presentation and T-cell Recognition Reveals Restricted Immune Responses in Melanoma. *Cancer Discov*, 8(11):1366–1375, 11 2018.

[26] S. A. Rosenberg, J. C. Yang, R. M. Sherry, U. S. Kammula, M. S. Hughes, G. Q. Phan, D. E. Citrin, N. P. Restifo, P. F. Robbins, J. R. Wunderlich, K. E. Morton, C. M. Laurencot, S. M. Steinberg, D. E. White, and M. E. Dudley. Durable complete responses in heavily pretreated patients with metastatic melanoma using T-cell transfer immunotherapy. *Clin Cancer Res*, 17(13):4550–4557, Jul 2011.

[27] R. Andersen, M. Donia, E. Ellebaek, T. H. Borch, P. Kongsted, T. Z. Iversen, L. R. Hoelmich, H. W. Hendel, O. Met, M. H. Andersen, P. Thor Straten, and I. M.

Svane. Long-Lasting Complete Responses in Patients with Metastatic Melanoma after Adoptive Cell Therapy with Tumor-Infiltrating Lymphocytes and an Attenuated IL2 Regimen. *Clin Cancer Res*, 22(15):3734–3745, 08 2016.

[28] D. S. Thommen and T. N. Schumacher. T Cell Dysfunction in Cancer. *Cancer Cell*, 33(4):547–562, 04 2018.

[29] W. Scheper, S. Kelderman, L. F. Fanchi, C. Linnemann, G. Bendle, M. A. J. de Rooij, C. Hirt, R. Mezzadra, M. Slagter, K. Dijkstra, R. J. C. Kluin, P. Snaebjornsson, K. Milne, B. H. Nelson, H. Zijlmans, G. Kenter, E. E. Voest, J. B. A. G. Haanen, and T. N. Schumacher. Low and variable tumor reactivity of the intratumoral TCR repertoire in human cancers. *Nat Med*, 25(1):89–94, 01 2019.

[30] Q. Li and Z. Y. Ding. The Ways of Isolating Neoantigen-Specific T Cells. *Front Oncol*, 10:1347, 2020.

[31] S. Seliktar-Ofir, E. Merhavi-Shoham, O. Itzhaki, S. Yunger, G. Markel, J. Schachter, and M. J. Besser. Selection of Shared and Neoantigen-Reactive T Cells for Adoptive Cell Therapy Based on CD137 Separation. *Front Immunol*, 8:1211, 2017.

[32] T. Inozume, K. Hanada, Q. J. Wang, M. Ahmadzadeh, J. R. Wunderlich, S. A. Rosenberg, and J. C. Yang. Selection of CD8+PD-1+ lymphocytes in fresh human melanomas enriches for tumor-reactive T cells. *J Immunother*, 33(9):956–964, 2010.

[33] M. Sadelain, R. Brentjens, and I. Rivière. The basic principles of chimeric antigen receptor design. *Cancer Discov*, 3(4):388–398, Apr 2013.

[34] J. N. Kochenderfer, W. H. Wilson, J. E. Janik, M. E. Dudley, M. Stetler-Stevenson, S. A. Feldman, I. Maric, M. Raffeld, D. A. Nathan, B. J. Lanier, R. A. Morgan, and S. A. Rosenberg. Eradication of B-lineage cells and regression of lymphoma in a patient treated with autologous T cells genetically engineered to recognize CD19. *Blood*, 116(20):4099–4102, Nov 2010.

[35] D. L. Porter, B. L. Levine, M. Kalos, A. Bagg, and C. H. June. Chimeric antigen receptor-modified T cells in chronic lymphoid leukemia. *N Engl J Med*, 365(8):725–733, Aug 2011.

[36] M. Kalos, B. L. Levine, D. L. Porter, S. Katz, S. A. Grupp, A. Bagg, and C. H. June. T cells with chimeric antigen receptors have potent antitumor effects and can establish memory in patients with advanced leukemia. *Sci Transl Med*, 3(95):95ra73, Aug 2011.

[37] R. Brentjens, R. Yeh, Y. Bernal, I. Riviere, and M. Sadelain. Treatment of chronic lymphocytic leukemia with genetically targeted autologous T cells: case report of an unforeseen adverse event in a phase I clinical trial. *Mol Ther*, 18(4):666–668, Apr 2010.

[38] S. S. Neelapu, S. Tummala, P. Kebriaei, W. Wierda, C. Gutierrez, F. L. Locke, K. V. Komanduri, Y. Lin, N. Jain, N. Daver, J. Westin, A. M. Gulbis, M. E. Loghin, J. F. de Groot, S. Adkins, S. E. Davis, K. Rezvani, P. Hwu, and E. J. Shpall. Chimeric antigen receptor T-cell therapy - assessment and management of toxicities. *Nat Rev Clin Oncol*, 15(1):47–62, Jan 2018.

[39] M. Chmielewski, A. Hombach, C. Heuser, G. P. Adams, and H. Abken. T cell activation by antibody-like immunoreceptors: increase in affinity of the single-chain fragment domain above threshold does not increase T cell activation against antigen-positive target cells but decreases selectivity. *J Immunol*, 173(12):7647–7653, Dec 2004.

[40] D. A. Schmid, M. B. Irving, V. Posevitz, M. Hebeisen, A. Posevitz-Fejfar, J. C. Sarria, R. Gomez-Eerland, M. Thome, T. N. Schumacher, P. Romero, D. E. Speiser, V. Zoete, O. Michielin, and N. Rufer. Evidence for a TCR affinity threshold delimiting maximal CD8 T cell function. *J Immunol*, 184(9):4936–4946, May 2010.

[41] S. Ghorashian, A. M. Kramer, S. Onuoha, G. Wright, J. Bartram, R. Richardson, S. J. Albon, J. Casanovas-Company, F. Castro, B. Popova, K. Villanueva, J. Yeung, W. Vetharoy, A. Guvenel, P. A. Wawrzyniecka, L. Mekkaoui, G. W. Cheung, D. Pinner, J. Chu, G. Lucchini, J. Silva, O. Ciocarlie, A. Lazareva, S. Inglott, K. C. Gilmour, G. Ahsan, M. Ferrari, S. Manzoor, K. Champion, T. Brooks, A. Lopes, A. Hackshaw, F. Farzaneh, R. Chiesa, K. Rao, D. Bonney, S. Samarasinghe, N. Goulden, A. Vora, P. Veys, R. Hough, R. Wynn, M. A. Pule, and P. J. Amrolia. Enhanced CAR T cell expansion and prolonged persistence in pediatric patients with ALL treated with a low-affinity CD19 CAR. *Nat Med*, 25(9):1408–1414, 09 2019.

[42] K. Newick, S. O'Brien, E. Moon, and S. M. Albelda. CAR T Cell Therapy for Solid Tumors. *Annu Rev Med*, 68:139–152, 01 2017.

[43] J. Foeng, I. Comerford, and S. R. McColl. Harnessing the chemokine system to home car-t cells into solid tumors. *Cell Reports Medicine*, 3(3):100543, 2022.

[44] X. Wang and I. Rivière. Clinical manufacturing of CAR T cells: foundation of a promising therapy. *Mol Ther Oncolytics*, 3:16015, 2016.

[45] J. Eyquem, J. Mansilla-Soto, T. Giavridis, S. J. van der Stegen, M. Hamieh, K. M. Cunanan, A. Odak, M. Gönen, and M. Sadelain. Targeting a CAR to the TRAC locus with CRISPR/Cas9 enhances tumour rejection. *Nature*, 543(7643):113–117, 03 2017.

[46] D. T. Harris, M. V. Hager, S. N. Smith, Q. Cai, J. D. Stone, P. Kruger, M. Lever, O. Dushek, T. M. Schmitt, P. D. Greenberg, and D. M. Kranz. Comparison of T Cell Activities Mediated by Human TCRs and CARs That Use the Same Recognition Domains. *J Immunol*, 200(3):1088–1100, 02 2018.

[47] F. Manfredi, B. C. Cianciotti, A. Potenza, E. Tassi, M. Noviello, A. Biondi, F. Ciceri, C. Bonini, and E. Ruggiero. TCR Redirected T Cells for Cancer Treatment: Achievements, Hurdles, and Goals. *Front Immunol*, 11:1689, 2020.

[48] R. A. Morgan, M. E. Dudley, J. R. Wunderlich, M. S. Hughes, J. C. Yang, R. M. Sherry, R. E. Royal, S. L. Topalian, U. S. Kammula, N. P. Restifo, Z. Zheng, A. Nahvi, C. R. de Vries, L. J. Rogers-Freezer, S. A. Mavroukakis, and S. A. Rosenberg. Cancer regression in patients after transfer of genetically engineered lymphocytes. *Science*, 314(5796):126–129, Oct 2006.

[49] P. F. Robbins, R. A. Morgan, S. A. Feldman, J. C. Yang, R. M. Sherry, M. E. Dudley, J. R. Wunderlich, A. V. Nahvi, L. J. Helman, C. L. Mackall, U. S. Kammula, M. S. Hughes, N. P. Restifo, M. Raffeld, C. C. Lee, C. L. Levy, Y. F. Li, M. El-Gamil, S. L. Schwarz, C. Laurencot, and S. A. Rosenberg. Tumor regression in patients with metastatic synovial cell sarcoma and melanoma using genetically engineered lymphocytes reactive with NY-ESO-1. *J Clin Oncol*, 29(7):917–924, Mar 2011.

[50] A. P. Rapoport, E. A. Stadtmauer, G. K. Binder-Scholl, O. Goloubeva, D. T. Vogl, S. F. Lacey, A. Z. Badros, A. Garfall, B. Weiss, J. Finklestein, I. Kulikovskaya, S. K. Sinha, S. Kronsberg, M. Gupta, S. Bond, L. Melchiori, J. E. Brewer, A. D. Bennett, A. B. Gerry, N. J. Pumphrey, D. Williams, H. K. Tayton-Martin, L. Ribeiro, T. Holdich, S. Yanovich, N. Hardy, J. Yared, N. Kerr, S. Philip, S. Westphal, D. L. Siegel, B. L. Levine, B. K. Jakobsen, M. Kalos, and C. H. June. NY-ESO-1-specific TCR-engineered T cells mediate sustained antigen-specific antitumor effects in myeloma. *Nat Med*, 21(8):914–921, Aug 2015.

[51] R. A. Morgan, N. Chinnasamy, D. Abate-Daga, A. Gros, P. F. Robbins, Z. Zheng, M. E. Dudley, S. A. Feldman, J. C. Yang, R. M. Sherry, G. Q. Phan, M. S. Hughes, U. S. Kammula, A. D. Miller, C. J. Hessman, A. A. Stewart, N. P. Restifo, M. M. Quezado, M. Alimchandani, A. Z. Rosenberg, A. Nath, T. Wang, B. Bielekova, S. C. Wuest, N. Akula, F. J. McMahon, S. Wilde, B. Mosetter, D. J. Schendel, C. M. Laurencot, and S. A. Rosenberg. Cancer regression and neurological toxicity following anti-MAGE-A3 TCR gene therapy. *J Immunother*, 36(2):133–151, Feb 2013.

[52] M. R. Parkhurst, J. C. Yang, R. C. Langan, M. E. Dudley, D. A. Nathan, S. A. Feldman, J. L. Davis, R. A. Morgan, M. J. Merino, R. M. Sherry, M. S. Hughes, U. S. Kammula, G. Q. Phan, R. M. Lim, S. A. Wank, N. P. Restifo, P. F. Robbins, C. M. Laurencot, and S. A. Rosenberg. T cells targeting carcinoembryonic antigen can mediate regression of metastatic colorectal cancer but induce severe transient colitis. *Mol Ther*, 19(3):620–626, Mar 2011.

[53] E. Tran, P. F. Robbins, Y. C. Lu, T. D. Prickett, J. J. Gartner, L. Jia, A. Pasetto, Z. Zheng, S. Ray, E. M. Groh, I. R. Kriley, and S. A. Rosenberg. T-Cell Transfer

Therapy Targeting Mutant KRAS in Cancer. *N Engl J Med*, 375(23):2255–2262, Dec 2016.

[54] N. Zacharakis, H. Chinnasamy, M. Black, H. Xu, Y. C. Lu, Z. Zheng, A. Pasetto, M. Langhan, T. Shelton, T. Prickett, J. Gartner, L. Jia, K. Trebska-McGowan, R. P. Somerville, P. F. Robbins, S. A. Rosenberg, S. L. Goff, and S. A. Feldman. Immune recognition of somatic mutations leading to complete durable regression in metastatic breast cancer. *Nat Med*, 24(6):724–730, 06 2018.

[55] L. B. Alexandrov, S. Nik-Zainal, D. C. Wedge, S. A. Aparicio, S. Behjati, A. V. Biankin, G. R. Bignell, N. Bolli, A. Borg, A. L. Børresen-Dale, S. Boyault, B. Burkhardt, A. P. Butler, C. Caldas, H. R. Davies, C. Desmedt, R. Eils, J. E. Eyfjörd, J. A. Foekens, M. Greaves, F. Hosoda, B. Hutter, T. Ilicic, S. Imbeaud, M. Imielinski, M. Imielinsk, N. Jäger, D. T. Jones, D. Jones, S. Knappskog, M. Kool, S. R. Lakhani, C. López-Otín, S. Martin, N. C. Munshi, H. Nakamura, P. A. Northcott, M. Pajic, E. Papaemmanuil, A. Paradiso, J. V. Pearson, X. S. Puente, K. Raine, M. Ramakrishna, A. L. Richardson, J. Richter, P. Rosenstiel, M. Schlesner, T. N. Schumacher, P. N. Span, J. W. Teague, Y. Totoki, A. N. Tutt, R. Valdés-Mas, M. M. van Buuren, L. van 't Veer, A. Vincent-Salomon, N. Waddell, L. R. Yates, J. Zucman-Rossi, P. A. Futreal, U. McDermott, P. Lichter, M. Meyerson, S. M. Grimmond, R. Siebert, E. Campo, T. Shibata, S. M. Pfister, P. J. Campbell, M. R. Stratton, A. Claviez, A. Rosenwald, A. Rosenwald, A. Borkhardt, B. Brors, B. Radlwimmer, C. Lawerenz, C. Lopez, D. Langenberger, D. Karsch, D. Lenze, D. Kube, E. Leich, G. Richter, J. Korbel, J. Hoell, J. Eils, K. Hezaveh, L. Trümper, M. Rosolowski, M. Weniger, M. Rohde, M. Kreuz, M. Loeffler, M. Schilhabel, M. Dreyling, M. L. Hansmann, M. Hummel, M. Szczepanowski, O. Ammerpohl, P. F. Stadler, P. Möller, R. Küppers, S. Haas, S. Eberth, S. Schreiber, S. H. Bernhart, S. Hoffmann, S. Radomski, U. Kostezka, W. Klapper, C. Sotiriou, D. Larsimont, D. Vincent, M. Maetens, O. Mariani, A. M. Sieuwerts, J. W. Martens, J. G. Jonasson, I. Treilleux, E. Thomas, G. Mac Grogan, C. Mannina, L. Arnould, L. Burillier, J. L. Merlin, M. Lefebvre, F. Bibeau, B. Massemin, F. Penault-Llorca, Q. Lopez, M. C. Mathieu, P. E. Lonning, M. Schlooz-Vries, J. Tol, H. van Laarhoven, F. Sweep, and P. Bult. Signatures of mutational processes in human cancer. *Nature*, 500(7463):415–421, Aug 2013.

[56] Z. R. Chalmers, C. F. Connelly, D. Fabrizio, L. Gay, S. M. Ali, R. Ennis, A. Schrock, B. Campbell, A. Shlien, J. Chmielecki, F. Huang, Y. He, J. Sun, U. Tabori, M. Kennedy, D. S. Lieber, S. Roels, J. White, G. A. Otto, J. S. Ross, L. Garraway, V. A. Miller, P. J. Stephens, and G. M. Frampton. Analysis of 100,000 human cancer genomes reveals the landscape of tumor mutational burden. *Genome Med*, 9(1):34, 04 2017.

[57] J. Wu, W. Zhao, B. Zhou, Z. Su, X. Gu, Z. Zhou, and S. Chen. TSNAdb: A Database for Tumor-specific Neoantigens from Immunogenomics Data Analysis. *Genomics Proteomics Bioinformatics*, 16(4):276–282, 08 2018.

[58] T. N. Schumacher, W. Scheper, and P. Kvistborg. Cancer Neoantigens. *Annu Rev Immunol*, 37:173–200, 04 2019.

[59] D. H. Busch and E. G. Pamer. MHC class I/peptide stability: implications for immunodominance, in vitro proliferation, and diversity of responding CTL. *J Immunol*, 160(9):4441–4448, May 1998.

[60] M. Harndahl, M. Rasmussen, G. Roder, I. Dalgaard Pedersen, M. Sørensen, M. Nielsen, and S. Buus. Peptide-MHC class I stability is a better predictor than peptide affinity of CTL immunogenicity. *Eur J Immunol*, 42(6):1405–1416, Jun 2012.

[61] C. Lundegaard, I. Hoof, O. Lund, and M. Nielsen. State of the art and challenges in sequence based T-cell epitope prediction. *Immunome Res*, 6 Suppl 2:S3, Nov 2010.

[62] K. Textoris-Taube, C. Keller, J. Liepe, P. Henklein, J. Sidney, A. Sette, P. M. Kloetzel, and M. Mishto. The T210M Substitution in the HLA-a*02:01 gp100 Epitope Strongly Affects Overall Proteasomal Cleavage Site Usage and Antigen Processing. *J Biol Chem*, 290(51):30417–30428, Dec 2015.

[63] U. Seifert, H. Liermann, V. Racanelli, A. Halenius, M. Wiese, H. Wedemeyer, T. Ruppert, K. Rispeter, P. Henklein, A. Sijts, H. Hengel, P. M. Kloetzel, and B. Rehermann. Hepatitis C virus mutation affects proteasomal epitope processing. *J Clin Invest*, 114(2):250–259, Jul 2004.

[64] A. Dalet, N. Vigneron, V. Stroobant, K. Hanada, and B. J. Van den Eynde. Splicing of distant peptide fragments occurs in the proteasome by transpeptidation and produces the spliced antigenic peptide derived from fibroblast growth factor-5. *J Immunol*, 184(6):3016–3024, Mar 2010.

[65] A. L. Creech, Y. S. Ting, S. P. Goulding, J. F. K. Sauld, D. Barthelme, M. S. Rooney, T. A. Addona, and J. G. Abelin. The Role of Mass Spectrometry and Proteogenomics in the Advancement of HLA Epitope Prediction. *Proteomics*, 18(12):e1700259, 06 2018.

[66] M. Bassani-Sternberg, E. Bräunlein, R. Klar, T. Engleitner, P. Sinitcyn, S. Audehm, M. Straub, J. Weber, J. Slotta-Huspenina, K. Specht, M. E. Martignoni, A. Werner, R. Hein, D. H Busch, C. Peschel, R. Rad, J. Cox, M. Mann, and A. M. Krackhardt. Direct identification of clinically relevant neoepitopes presented on native human melanoma tissue by mass spectrometry. *Nat Commun*, 7:13404, 11 2016.

[67] C. J. Cohen, Z. Zheng, R. Bray, Y. Zhao, L. A. Sherman, S. A. Rosenberg, and R. A. Morgan. Recognition of fresh human tumor by human peripheral blood lymphocytes transduced with a bicistronic retroviral vector encoding a murine anti-p53 TCR. *J Immunol*, 175(9):5799–5808, Nov 2005.

[68] M. R. Parkhurst, J. Joo, J. P. Riley, Z. Yu, Y. Li, P. F. Robbins, and S. A. Rosenberg. Characterization of genetically modified T-cell receptors that recognize the CEA:691-699 peptide in the context of HLA-A2.1 on human colorectal cancer cells. *Clin Cancer Res*, 15(1):169–180, Jan 2009.

[69] M. J. Moore, M. Zhong, J. Hansen, H. Gartner, C. Grant, M. Huang, F. M. Harris, N. Tu, N. A. Bowerman, K. H. Edelmann, T. Barry, O. Herbin, C. S. Tay, D. J. DiLillo, C. E. Decker, N. Levenkova, J. Shevchuk, A. Dhanik, K. A. Meagher, A. Karr, J. Roos, W. Y. Lee, D. Suh, M. Eckersdorff, T. C. Meagher, M. Koss, L. Esau, M. A. Sleeman, R. Babb, G. Chen, C. A. Kyratsous, W. T. Poueymirou, J. R. McWhirter, V. A. Voronina, C. Guo, C. Gurer, G. D. Yancopoulos, A. J. Murphy, and L. E. Macdonald. Humanization of T cell-mediated immunity in mice. *Sci Immunol*, 6(66):eabj4026, Dec 2021.

[70] E. D'Ippolito, K. I. Wagner, and D. H. Busch. Needle in a Haystack: The Naïve Repertoire as a Source of T Cell Receptors for Adoptive Therapy with Engineered T Cells. *Int J Mol Sci*, 21(21), Nov 2020.

[71] G. Cafri, R. Yossef, A. Pasetto, D. C. Deniger, Y. C. Lu, M. Parkhurst, J. J. Gartner, L. Jia, S. Ray, L. T. Ngo, M. Jafferji, A. Sachs, T. Prickett, P. F. Robbins, and S. A. Rosenberg. Memory T cells targeting oncogenic mutations detected in peripheral blood of epithelial cancer patients. *Nat Commun*, 10(1):449, 01 2019.

[72] P. Malekzadeh, R. Yossef, G. Cafri, B. C. Paria, F. J. Lowery, M. Jafferji, M. L. Good, A. Sachs, A. R. Copeland, S. P. Kim, S. Kivitz, M. R. Parkhurst, P. F. Robbins, S. Ray, L. Xi, M. Raffeld, Z. Yu, N. P. Restifo, R. P. T. Somerville, S. A. Rosenberg, and D. C. Deniger. Antigen Experienced T Cells from Peripheral Blood Recognize p53 Neoantigens. *Clin Cancer Res*, 26(6):1267–1276, 03 2020.

[73] R. Yossef, E. Tran, D. C. Deniger, A. Gros, A. Pasetto, M. R. Parkhurst, J. J. Gartner, T. D. Prickett, G. Cafri, P. F. Robbins, and S. A. Rosenberg. Enhanced detection of neoantigen-reactive T cells targeting unique and shared oncogenes for personalized cancer immunotherapy. *JCI Insight*, 3(19), 10 2018.

[74] P. Klenerman, V. Cerundolo, and P. R. Dunbar. Tracking T cells with tetramers: new tales from new tools. *Nat Rev Immunol*, 2(4):263–272, Apr 2002.

[75] J. D. Altman and M. M. Davis. MHC-peptide tetramers to visualize antigen-specific T cells. *Curr Protoc Immunol*, Chapter 17:Unit 17.3, May 2003.

[76] M. Effenberger, A. Stengl, K. Schober, M. Gerget, M. Kampick, T. R. Müller, D. Schumacher, J. Helma, H. Leonhardt, and D. H. Busch. FLEXamers: A Double Tag for Universal Generation of Versatile Peptide-MHC Multimers. *J Immunol*, 202(7):2164–2171, 04 2019.

[77] G. Dössinger, M. Bunse, J. Bet, J. Albrecht, P. J. Paszkiewicz, B. Weißbrich, I. Schiedewitz, L. Henkel, M. Schiemann, M. Neuenhahn, W. Uckert, and D. H.

Busch. MHC multimer-guided and cell culture-independent isolation of functional T cell receptors from single cells facilitates TCR identification for immunotherapy. *PLoS One*, 8(4):e61384, 2013.

[78] M. Neuenhahn, J. Albrecht, M. Odendahl, F. Schlott, G. Dössinger, M. Schiemann, S. Lakshmipathi, K. Martin, D. Bunjes, S. Harsdorf, E. M. Weissinger, H. Menzel, M. Verbeek, L. Uharek, N. Kröger, E. Wagner, G. Kobbe, T. Schroeder, M. Schmitt, G. Held, W. Herr, L. Germeroth, H. Bonig, T. Tonn, H. Einsele, D. H. Busch, and G. U. Grigoleit. Transfer of minimally manipulated CMV-specific T cells from stem cell or third-party donors to treat CMV infection after allo-HSCT. *Leukemia*, 31(10):2161–2171, 10 2017.

[79] M. D. Keller, K. M. Harris, M. A. Jensen-Wachspress, V. V. Kankate, H. Lang, C. A. Lazarski, J. Durkee-Shock, P. H. Lee, K. Chaudhry, K. Webber, A. Datar, M. Terpilowski, E. K. Reynolds, E. M. Stevenson, S. Val, Z. Shancer, N. Zhang, R. Ulrey, U. Ekanem, M. Stanojevic, A. Geiger, H. Liang, F. Hoq, A. A. Abraham, P. J. Hanley, C. R. Cruz, K. Ferrer, L. Dropulic, K. Gangler, P. D. Burbelo, R. B. Jones, J. I. Cohen, and C. M. Bollard. SARS-CoV-2-specific T cells are rapidly expanded for therapeutic use and target conserved regions of the membrane protein. *Blood*, 136(25):2905–2917, 12 2020.

[80] S. Bobisse, R. Genolet, A. Roberti, J. L. Tanyi, J. Racle, B. J. Stevenson, C. Iseli, A. Michel, M. A. Le Bitoux, P. Guillaume, J. Schmidt, V. Bianchi, D. Dangaj, C. Fenwick, L. Derré, I. Xenarios, O. Michielin, P. Romero, D. S. Monos, V. Zoete, D. Gfeller, L. E. Kandalaft, G. Coukos, and A. Harari. Sensitive and frequent identification of high avidity neo-epitope specific CD8+ T cells in immunotherapy-naive ovarian cancer. *Nat Commun*, 9(1):1092, 03 2018.

[81] S. Liu, J. Matsuzaki, L. Wei, T. Tsuji, S. Battaglia, Q. Hu, E. Cortes, L. Wong, L. Yan, M. Long, A. Miliotto, N. W. Bateman, S. B. Lele, T. Chodon, R. C. Koya, S. Yao, Q. Zhu, T. P. Conrads, J. Wang, G. L. Maxwell, A. A. Lugade, and K. Odunsi. Efficient identification of neoantigen-specific T-cell responses in advanced human ovarian cancer. *J Immunother Cancer*, 7(1):156, 06 2019.

[82] A. Gros, P. F. Robbins, X. Yao, Y. F. Li, S. Turcotte, E. Tran, J. R. Wunderlich, A. Mixon, S. Farid, M. E. Dudley, K. Hanada, J. R. Almeida, S. Darko, D. C. Douek, J. C. Yang, and S. A. Rosenberg. PD-1 identifies the patient-specific CD8+ tumor-reactive repertoire infiltrating human tumors. *J Clin Invest*, 124(5):2246–2259, May 2014.

[83] A. Gros, M. R. Parkhurst, E. Tran, A. Pasetto, P. F. Robbins, S. Ilyas, T. D. Prickett, J. J. Gartner, J. S. Crystal, I. M. Roberts, K. Trebska-McGowan, J. R. Wunderlich, J. C. Yang, and S. A. Rosenberg. Prospective identification of neoantigen-specific lymphocytes in the peripheral blood of melanoma patients. *Nat Med*, 22(4):433–438, Apr 2016.

[84] A. Gros, E. Tran, M. R. Parkhurst, S. Ilyas, A. Pasetto, E. M. Groh, P. F. Robbins, R. Yossef, A. Garcia-Garijo, C. A. Fajardo, T. D. Prickett, L. Jia, J. J. Gartner, S. Ray, L. Ngo, J. R. Wunderllich, J. C. Yang, and S. A. Rosenberg. Recognition of human gastrointestinal cancer neoantigens by circulating PD-1+ lymphocytes. *J Clin Invest*, 129(11):4992–5004, 11 2019.

[85] J. Zhu, P. F. Petit, and B. J. Van den Eynde. Apoptosis of tumor-infiltrating T lymphocytes: a new immune checkpoint mechanism. *Cancer Immunol Immunother*, 68(5):835–847, May 2019.

[86] S. A. Grossman, S. Ellsworth, J. Campian, A. T. Wild, J. M. Herman, D. Laheru, M. Brock, A. Balmanoukian, and X. Ye. Survival in Patients With Severe Lymphopenia Following Treatment With Radiation and Chemotherapy for Newly Diagnosed Solid Tumors. *J Natl Compr Canc Netw*, 13(10):1225–1231, Oct 2015.

[87] E. Strønen, M. Toebes, S. Kelderman, M. M. van Buuren, W. Yang, N. van Rooij, M. Donia, M. L. Böschen, F. Lund-Johansen, J. Olweus, and T. N. Schumacher. Targeting of cancer neoantigens with donor-derived T cell receptor repertoires. *Science*, 352(6291):1337–1341, Jun 2016.

[88] H. S. Robins, P. V. Campregher, S. K. Srivastava, A. Wacher, C. J. Turtle, O. Kahsai, S. R. Riddell, E. H. Warren, and C. S. Carlson. Comprehensive assessment of T-cell receptor beta-chain diversity in alphabeta T cells. *Blood*, 114(19):4099–4107, Nov 2009.

[89] Q. Qi, Y. Liu, Y. Cheng, J. Glanville, D. Zhang, J. Y. Lee, R. A. Olshen, C. M. Weyand, S. D. Boyd, and J. J. Goronzy. Diversity and clonal selection in the human T-cell repertoire. *Proc Natl Acad Sci U S A*, 111(36):13139–13144, Sep 2014.

[90] C. Alanio, F. Lemaitre, H. K. Law, M. Hasan, and M. L. Albert. Enumeration of human antigen-specific naive CD8+ T cells reveals conserved precursor frequencies. *Blood*, 115(18):3718–3725, May 2010.

[91] B. Engels, H. Cam, T. Schüler, S. Indraccolo, M. Gladow, C. Baum, T. Blankenstein, and W. Uckert. Retroviral vectors for high-level transgene expression in T lymphocytes. *Hum Gene Ther*, 14(12):1155–1168, Aug 2003.

[92] G. M. Bendle, C. Linnemann, A. I. Hooijkaas, L. Bies, M. A. de Witte, A. Jorritsma, A. D. Kaiser, N. Pouw, R. Debets, E. Kieback, W. Uckert, J. Y. Song, J. B. Haanen, and T. N. Schumacher. Lethal graft-versus-host disease in mouse models of T cell receptor gene therapy. *Nat Med*, 16(5):565–570, May 2010.

[93] M. M. van Loenen, R. de Boer, A. L. Amir, R. S. Hagedoorn, G. L. Volbeda, R. Willemze, J. J. van Rood, J. H. Falkenburg, and M. H. Heemskerk. Mixed T cell receptor dimers harbor potentially harmful neoreactivity. *Proc Natl Acad Sci U S A*, 107(24):10972–10977, Jun 2010.

[94] C. J. Cohen, Y. Zhao, Z. Zheng, S. A. Rosenberg, and R. A. Morgan. Enhanced antitumor activity of murine-human hybrid T-cell receptor (TCR) in human lymphocytes is associated with improved pairing and TCR/CD3 stability. *Cancer Res*, 66(17):8878–8886, Sep 2006.

[95] C. J. Cohen, Y. F. Li, M. El-Gamil, P. F. Robbins, S. A. Rosenberg, and R. A. Morgan. Enhanced antitumor activity of T cells engineered to express T-cell receptors with a second disulfide bond. *Cancer Res*, 67(8):3898–3903, Apr 2007.

[96] S. Thomas, F. Mohammed, R. M. Reijmers, A. Woolston, T. Stauss, A. Kennedy, D. Stirling, A. Holler, L. Green, D. Jones, K. K. Matthews, D. A. Price, B. M. Chain, M. H. M. Heemskerk, E. C. Morris, B. E. Willcox, and H. J. Stauss. Framework engineering to produce dominant T cell receptors with enhanced antigen-specific function. *Nat Commun*, 10(1):4451, 10 2019.

[97] A. G. Schrum, L. A. Turka, and E. Palmer. Surface T-cell antigen receptor expression and availability for long-term antigenic signaling. *Immunol Rev*, 196:7–24, Dec 2003.

[98] A. M. Gallegos, H. Xiong, I. M. Leiner, B. Sušac, M. S. Glickman, E. G. Pamer, and J. W. van Heijst. Control of T cell antigen reactivity via programmed TCR downregulation. *Nat Immunol*, 17(4):379–386, Apr 2016.

[99] M. M. van Loenen, R. S. Hagedoorn, R. de Boer, E. H. van Egmond, J. H. Falkenburg, and M. H. Heemskerk. Rapid re-expression of retrovirally introduced versus endogenous TCRs in engineered T cells after antigen-specific stimulation. *J Immunother*, 34(2):165–174, Mar 2011.

[100] K. Schober, T. R. Müller, F. Gökmen, S. Grassmann, M. Effenberger, M. Poltorak, C. Stemberger, K. Schumann, T. L. Roth, A. Marson, and D. H. Busch. Orthotopic replacement of T-cell receptor α- and β-chains with preservation of near-physiological T-cell function. *Nat Biomed Eng*, 3(12):974–984, 12 2019.

[101] T. L. Roth, C. Puig-Saus, R. Yu, E. Shifrut, J. Carnevale, P. J. Li, J. Hiatt, J. Saco, P. Krystofinski, H. Li, V. Tobin, D. N. Nguyen, M. R. Lee, A. L. Putnam, A. L. Ferris, J. W. Chen, J. N. Schickel, L. Pellerin, D. Carmody, G. Alkorta-Aranburu, D. Del Gaudio, H. Matsumoto, M. Morell, Y. Mao, M. Cho, R. M. Quadros, C. B. Gurumurthy, B. Smith, M. Haugwitz, S. H. Hughes, J. S. Weissman, K. Schumann, J. H. Esensten, A. P. May, A. Ashworth, G. M. Kupfer, S. A. W. Greeley, R. Bacchetta, E. Meffre, M. G. Roncarolo, N. Romberg, K. C. Herold, A. Ribas, M. D. Leonetti, and A. Marson. Reprogramming human T cell function and specificity with non-viral genome targeting. *Nature*, 559(7714):405–409, 07 2018.

[102] T. R. Müller, S. Jarosch, M. Hammel, J. Leube, S. Grassmann, B. Bernard, M. Effenberger, I. Andrä, M. Z. Chaudhry, T. Käuferle, A. Malo, L. Cicin-Sain, P. Steinberger, T. Feuchtinger, U. Protzer, K. Schumann, M. Neuenhahn, K. Schober, and

D. H. Busch. Targeted T cell receptor gene editing provides predictable T cell product function for immunotherapy. *Cell Rep Med*, 2(8):100374, 08 2021.

[103] T. M. Fahmy, J. G. Bieler, M. Edidin, and J. P. Schneck. Increased TCR avidity after T cell activation: a mechanism for sensing low-density antigen. *Immunity*, 14(2):135–143, Feb 2001.

[104] M. Corr, A. E. Slanetz, L. F. Boyd, M. T. Jelonek, S. Khilko, B. K. al Ramadi, Y. S. Kim, S. E. Maher, A. L. Bothwell, and D. H. Margulies. T cell receptor-MHC class I peptide interactions: affinity, kinetics, and specificity. *Science*, 265(5174):946–949, Aug 1994.

[105] M. Nauerth, C. Stemberger, F. Mohr, B. Weißbrich, M. Schiemann, L. Germeroth, and D. H. Busch. Flow cytometry-based TCR-ligand Koff -rate assay for fast avidity screening of even very small antigen-specific T cell populations ex vivo. *Cytometry A*, 89(9):816–825, 09 2016.

[106] S. I. Drew, P. I. Terasaki, R. J. Billing, O. J. Bergh, J. Minowada, and E. Klein. Group-specific human granulocyte antigens on a chronic myelogenous leukemia cell line with a Philadelphia chromosome marker. *Blood*, 49(5):715–718, May 1977.

[107] C. M. Britten, R. G. Meyer, T. Kreer, I. Drexler, T. Wölfel, and W. Herr. The use of HLA-A*0201-transfected K562 as standard antigen-presenting cells for CD8(+) T lymphocytes in IFN-gamma ELISPOT assays. *J Immunol Methods*, 259(1-2):95–110, Jan 2002.

[108] F. K. M. Lorenz, C. Ellinger, E. Kieback, S. Wilde, M. Lietz, D. J. Schendel, and W. Uckert. Unbiased Identification of T-Cell Receptors Targeting Immunodominant Peptide-MHC Complexes for T-Cell Receptor Immunotherapy. *Hum Gene Ther*, 28(12):1158–1168, 12 2017.

[109] M. Huang, W. Zhang, J. Guo, X. Wei, K. Phiwpan, J. Zhang, and X. Zhou. Improved Transgenic Mouse Model for Studying HLA Class I Antigen Presentation. *Sci Rep*, 6:33612, 09 2016.

[110] N. Harada, S. Fukaya, H. Wada, R. Goto, T. Osada, A. Gomori, K. Ikizawa, M. Sakuragi, and N. Oda. Generation of a Novel HLA Class I Transgenic Mouse Model Carrying a Knock-in Mutation at the β2-Microglobulin Locus. *J Immunol*, 198(1):516–527, 01 2017.

[111] Y. Lai, X. Wei, S. Lin, L. Qin, L. Cheng, and P. Li. Current status and perspectives of patient-derived xenograft models in cancer research. *J Hematol Oncol*, 10(1):106, 05 2017.

[112] M. Y. Want, A. Konstorum, R. Y. Huang, V. Jain, S. Matsueda, T. Tsuji, A. Lugade, K. Odunsi, R. Koya, and S. Battaglia. Neoantigens retention in patient derived xenograft models mediates autologous T cells activation in ovarian cancer. *Oncoimmunology*, 8(6):e1586042, 2019.

[113] B. Verma and A. Wesa. Establishment of Humanized Mice from Peripheral Blood Mononuclear Cells or Cord Blood CD34+ Hematopoietic Stem Cells for Immune-Oncology Studies Evaluating New Therapeutic Agents. *Curr Protoc Pharmacol*, 89(1):e77, 06 2020.

[114] J. T. Neal, X. Li, J. Zhu, V. Giangarra, C. L. Grzeskowiak, J. Ju, I. H. Liu, S. H. Chiou, A. A. Salahudeen, A. R. Smith, B. C. Deutsch, L. Liao, A. J. Zemek, F. Zhao, K. Karlsson, L. M. Schultz, T. J. Metzner, L. D. Nadauld, Y. Y. Tseng, S. Alkhairy, C. Oh, P. Keskula, D. Mendoza-Villanueva, F. M. De La Vega, P. L. Kunz, J. C. Liao, J. T. Leppert, J. B. Sunwoo, C. Sabatti, J. S. Boehm, W. C. Hahn, G. X. Y. Zheng, M. M. Davis, and C. J. Kuo. Organoid Modeling of the Tumor Immune Microenvironment. *Cell*, 175(7):1972–1988, 12 2018.

[115] R. L. Siegel, K. D. Miller, H. E. Fuchs, and A. Jemal. Cancer Statistics, 2021. *CA Cancer J Clin*, 71(1):7–33, 01 2021.

[116] L. Rahib, M. R. Wehner, L. M. Matrisian, and K. T. Nead. Estimated Projection of US Cancer Incidence and Death to 2040. *JAMA Netw Open*, 4(4):e214708, 04 2021.

[117] K. Panchal, R. K. Sahoo, U. Gupta, and A. Chaurasiya. Role of targeted immunotherapy for pancreatic ductal adenocarcinoma (PDAC) treatment: An overview. *Int Immunopharmacol*, 95:107508, Jun 2021.

[118] V. P. Balachandran, M. Łuksza, J. N. Zhao, V. Makarov, J. A. Moral, R. Remark, B. Herbst, G. Askan, U. Bhanot, Y. Senbabaoglu, D. K. Wells, C. I. O. Cary, O. Grbovic-Huezo, M. Attiyeh, B. Medina, J. Zhang, J. Loo, J. Saglimbeni, M. Abu-Akeel, R. Zappasodi, N. Riaz, M. Smoragiewicz, Z. L. Kelley, O. Basturk, M. Gönen, A. J. Levine, P. J. Allen, D. T. Fearon, M. Merad, S. Gnjatic, C. A. Iacobuzio-Donahue, J. D. Wolchok, R. P. DeMatteo, T. A. Chan, B. D. Greenbaum, T. Merghoub, S. D. Leach, A. L. Johns, R. S. Mead, A. J. Gill, D. K. Chang, S. H. McKay, L. A. Chantrill, V. T. Chin, A. Chou, J. L. Humphris, M. Pajic, A. Steinmann, M. Arshi, A. Drury, D. Froio, A. Morgan, P. Timpson, D. Hermann, C. Vennin, S. Warren, M. Pinese, J. Wu, A. V. Pinho, R. S. Mead, K. Tucker, L. Andrews, A. J. Gill, J. S. Samra, J. Arena, N. Pavlakis, H. A. High, A. Mittal, D. K. Chang, A. V. Biankin, P. Bailey, S. Martin, E. A. Musgrove, M. D. Jones, C. Nourse, N. B. Jamieson, A. Chou, L. A. Chantrill, A. Stoita, D. Williams, A. Spigelman, N. Waddell, J. V. Pearson, A. M. Patch, K. Nones, F. Newell, P. Mukhopadhyay, V. Addala, S. Kazakoff, O. Holmes, C. Leonard, S. Wood, C. Xu, S. M. Grimmond, O. Hofmann, P. J. Wilson, A. Christ, T. Bruxner, R. Asghari, N. D. Merrett, D. Pavey, A. Das, A. Goodwin, P. H. Cosman, K. Ismail, C. O'Connor, C. L. Cooper, A. Goodwin, P. Grimison, J. G. Kench, C. Sandroussi, V. W. Lam, D. McLeod, A. M. Nagrial, J. Kirk, V. James, M. Texler, C. Forest, K. P. Epari, M. Ballal, D. R. Fletcher, S. Mukhedkar, N. Zeps, M. Beilin, K. Feeney, N. Q. Nguyen, A. R. Ruszkiewicz, C. Worthley, J. Chen, M. E. Brooke-Smith, V. Papangelis, A. D. Clouston, P. Martin, A. P. Barbour, T. J. O'Rourke,

J. W. Fawcett, K. Slater, M. Hatzifotis, P. Hodgkinson, M. Nikfarjam, J. R. Eshleman, R. H. Hruban, C. L. Wolfgang, M. Hodgin, A. Scarpa, R. T. Lawlor, S. Beghelli, V. Corbo, M. Scardoni, C. Bassi, A. Scarpa, R. T. Lawlor, S. Beghelli, V. Corbo, M. Scardoni, and C. Bassi. Identification of unique neoantigen qualities in long-term survivors of pancreatic cancer. *Nature*, 551(7681):512–516, 11 2017.

[119] J. Bian and K. Almhanna. Pancreatic cancer and immune checkpoint inhibitors-still a long way to go. *Transl Gastroenterol Hepatol*, 6:6, 2021.

[120] V. P. Balachandran, G. L. Beatty, and S. K. Dougan. Broadening the Impact of Immunotherapy to Pancreatic Cancer: Challenges and Opportunities. *Gastroenterology*, 156(7):2056–2072, 05 2019.

[121] B. Salman, D. Zhou, E. M. Jaffee, B. H. Edil, and L. Zheng. Vaccine therapy for pancreatic cancer. *Oncoimmunology*, 2(12):e26662, Dec 2013.

[122] M. Hall, H. Liu, M. Malafa, B. Centeno, P. J. Hodul, J. Pimiento, S. Pilon-Thomas, and A. A. Sarnaik. Expansion of tumor-infiltrating lymphocytes (TIL) from human pancreatic tumors. *J Immunother Cancer*, 4:61, 2016.

[123] C. J. DeSelm, Z. E. Tano, A. M. Varghese, and P. S. Adusumilli. CAR T-cell therapy for pancreatic cancer. *J Surg Oncol*, 116(1):63–74, Jul 2017.

[124] I. M. Stromnes, T. M. Schmitt, A. Hulbert, J. S. Brockenbrough, H. Nguyen, C. Cuevas, A. M. Dotson, X. Tan, J. L. Hotes, P. D. Greenberg, and S. R. Hingorani. T Cells Engineered against a Native Antigen Can Surmount Immunologic and Physical Barriers to Treat Pancreatic Ductal Adenocarcinoma. *Cancer Cell*, 28(5):638–652, Nov 2015.

[125] P. Bailey, D. K. Chang, M. A. Forget, F. A. Lucas, H. A. Alvarez, C. Haymaker, C. Chattopadhyay, S. H. Kim, S. Ekmekcioglu, E. A. Grimm, A. V. Biankin, P. Hwu, A. Maitra, and J. Roszik. Exploiting the neoantigen landscape for immunotherapy of pancreatic ductal adenocarcinoma. *Sci Rep*, 6:35848, 10 2016.

[126] N. Waddell, M. Pajic, A. M. Patch, D. K. Chang, K. S. Kassahn, P. Bailey, A. L. Johns, D. Miller, K. Nones, K. Quek, M. C. Quinn, A. J. Robertson, M. Z. Fadlullah, T. J. Bruxner, A. N. Christ, I. Harliwong, S. Idrisoglu, S. Manning, C. Nourse, E. Nourbakhsh, S. Wani, P. J. Wilson, E. Markham, N. Cloonan, M. J. Anderson, J. L. Fink, O. Holmes, S. H. Kazakoff, C. Leonard, F. Newell, B. Poudel, S. Song, D. Taylor, N. Waddell, S. Wood, Q. Xu, J. Wu, M. Pinese, M. J. Cowley, H. C. Lee, M. D. Jones, A. M. Nagrial, J. Humphris, L. A. Chantrill, V. Chin, A. M. Steinmann, A. Mawson, E. S. Humphrey, E. K. Colvin, A. Chou, C. J. Scarlett, A. V. Pinho, M. Giry-Laterriere, I. Rooman, J. S. Samra, J. G. Kench, J. A. Pettitt, N. D. Merrett, C. Toon, K. Epari, N. Q. Nguyen, A. Barbour, N. Zeps, N. B. Jamieson, J. S. Graham, S. P. Niclou, R. Bjerkvig, R. Grützmann, D. Aust, R. H. Hruban, A. Maitra, C. A. Iacobuzio-Donahue, C. L. Wolfgang, R. A. Morgan, R. T. Lawlor, V. Corbo, C. Bassi, M. Falconi, G. Zamboni, G. Tortora, M. A. Tempero,

A. J. Gill, J. R. Eshleman, C. Pilarsky, A. Scarpa, E. A. Musgrove, J. V. Pearson, A. V. Biankin, S. M. Grimmond, A. V. Biankin, A. L. Johns, A. Mawson, D. K. Chang, C. J. Scarlett, M. A. Brancato, S. J. Rowe, S. H. Simpson, M. Martyn-Smith, M. T. Thomas, L. A. Chantrill, V. T. Chin, A. Chou, M. J. Cowley, J. L. Humphris, M. D. Jones, R. S. Mead, A. M. Nagrial, M. Pajic, J. Pettit, M. Pinese, I. Rooman, J. Wu, J. Tao, R. DiPietro, C. Watson, A. Steinmann, H. Ching Lee, R. Wong, A. V. Pinho, M. Giry-Laterriere, R. J. Daly, E. A. Musgrove, R. L. Sutherland, S. M. Grimmond, N. Waddell, K. S. Kassahn, D. K. Miller, P. J. Wilson, A. M. Patch, S. Song, I. Harliwong, S. Idrisoglu, C. Nourse, E. Nourbakhsh, S. Manning, S. Wani, M. Gongora, M. Anderson, O. Holmes, C. Leonard, D. Taylor, S. Wood, C. Xu, K. Nones, J. L. Fink, A. Christ, T. Bruxner, N. Cloonan, F. Newell, J. V. Pearson, P. Bailey, M. Quinn, S. Nagaraj, S. Kazakoff, N. Waddell, K. Krisnan, K. Quek, D. Wood, M. Z. Fadlullah, J. S. Samra, A. J. Gill, N. Pavlakis, A. Guminski, C. Toon, R. Asghari, N. D. Merrett, D. Pavey, A. Das, P. H. Cosman, K. Ismail, C. O'Connnor, V. W. Lam, D. McLeod, H. C. Pleass, A. Richardson, V. James, J. G. Kench, C. L. Cooper, D. Joseph, C. Sandroussi, M. Crawford, J. Gallagher, M. Texler, C. Forest, A. Laycock, K. P. Epari, M. Ballal, D. R. Fletcher, S. Mukhedkar, N. A. Spry, B. DeBoer, M. Chai, N. Zeps, M. Beilin, K. Feeney, N. Q. Nguyen, A. R. Ruszkiewicz, C. Worthley, C. P. Tan, T. Debrencini, J. Chen, M. E. Brooke-Smith, V. Papangelis, H. Tang, A. P. Barbour, A. D. Clouston, P. Martin, T. J. O'Rourke, A. Chiang, J. W. Fawcett, K. Slater, S. Yeung, M. Hatzifotis, P. Hodgkinson, C. Christophi, M. Nikfarjam, A. Mountain, J. R. Eshleman, R. H. Hruban, A. Maitra, C. A. Iacobuzio-Donahue, R. D. Schulick, C. L. Wolfgang, R. A. Morgan, M. Hodgin, A. Scarpa, R. T. Lawlor, S. Beghelli, V. Corbo, M. Scardoni, C. Bassi, M. A. Tempero, A. V. Biankin, S. M. Grimmond, D. K. Chang, E. A. Musgrove, M. D. Jones, C. Nourse, N. B. Jamieson, J. S. Graham, A. V. Biankin, D. K. Chang, N. B. Jamieson, J. S. Graham, K. Oien, and J. Hair. Whole genomes redefine the mutational landscape of pancreatic cancer. *Nature*, 518(7540):495–501, Feb 2015.

[127] E. Amato, M. D. Molin, A. Mafficini, J. Yu, G. Malleo, B. Rusev, M. Fassan, D. Antonello, Y. Sadakari, P. Castelli, G. Zamboni, A. Maitra, R. Salvia, R. H. Hruban, C. Bassi, P. Capelli, R. T. Lawlor, M. Goggins, and A. Scarpa. Targeted next-generation sequencing of cancer genes dissects the molecular profiles of intraductal papillary neoplasms of the pancreas. *J Pathol*, 233(3):217–227, Jul 2014.

[128] J. Tu, S. Park, W. Yu, S. Zhang, L. Wu, K. Carmon, and Q. J. Liu. The most common RNF43 mutant G659Vfs*41 is fully functional in inhibiting Wnt signaling and unlikely to play a role in tumorigenesis. *Sci Rep*, 9(1):18557, 12 2019.

[129] T. Zhan, N. Rindtorff, and M. Boutros. Wnt signaling in cancer. *Oncogene*, 36(11):1461–1473, 03 2017.

[130] B. K. Koo, M. Spit, I. Jordens, T. Y. Low, D. E. Stange, M. van de Wetering, J. H. van Es, S. Mohammed, A. J. Heck, M. M. Maurice, and H. Clevers. Tumour suppressor RNF43 is a stem-cell E3 ligase that induces endocytosis of Wnt receptors. *Nature*, 488(7413):665–669, Aug 2012.

[131] A. Loregger, M. Grandl, R. Mejías-Luque, M. Allgäuer, K. Degenhart, V. Haselmann, C. Oikonomou, P. Hatzis, K. P. Janssen, U. Nitsche, D. Gradl, O. van den Broek, O. Destree, K. Ulm, M. Neumaier, B. Kalali, A. Jung, I. Varela, R. M. Schmid, R. Rad, D. H. Busch, and M. Gerhard. The E3 ligase RNF43 inhibits Wnt signaling downstream of mutated β-catenin by sequestering TCF4 to the nuclear membrane. *Sci Signal*, 8(393):ra90, Sep 2015.

[132] V. Neumeyer, M. Grandl, A. Dietl, A. Brutau-Abia, M. Allgäuer, B. Kalali, Y. Zhang, K. F. Pan, K. Steiger, M. Vieth, M. Anton, R. Mejías-Luque, and M. Gerhard. Loss of endogenous RNF43 function enhances proliferation and tumour growth of intestinal and gastric cells. *Carcinogenesis*, 40(4):551–559, 06 2019.

[133] A. N. Hosein, G. Dangol, T. Okumura, J. Roszik, K. Rajapakshe, M. Siemann, M. Zaid, B. Ghosh, M. Monberg, P. A. Guerrero, A. Singhi, C. L. Haymaker, H. Clevers, L. Abou-Elkacem, S. M. Woermann, and A. Maitra. Loss of Rnf43 Accelerates Kras-Mediated Neoplasia and Remodels the Tumor Immune Microenvironment in Pancreatic Adenocarcinoma. *Gastroenterology*, Dec 2021.

[134] M. Knabel, T. J. Franz, M. Schiemann, A. Wulf, B. Villmow, B. Schmidt, H. Bernhard, H. Wagner, and D. H. Busch. Reversible MHC multimer staining for functional isolation of T-cell populations and effective adoptive transfer. *Nat Med*, 8(6):631–637, Jun 2002.

[135] C. Moosmann, T. R. Müller, D. H. Busch, and K. Schober. Orthotopic T-cell receptor replacement in primary human T cells using CRISPR-Cas9-mediated homology-directed repair. *STAR Protoc*, 3(1):101031, 03 2022.

[136] A. Sette, A. Vitiello, B. Reherman, P. Fowler, R. Nayersina, W. M. Kast, C. J. Melief, C. Oseroff, L. Yuan, J. Ruppert, J. Sidney, M. F. del Guercio, S. Southwood, R. T. Kubo, R. W. Chesnut, H. M. Grey, and F. V. Chisari. The relationship between class I binding affinity and immunogenicity of potential cytotoxic T cell epitopes. *J Immunol*, 153(12):5586–5592, Dec 1994.

[137] B. Engels, V. H. Engelhard, J. Sidney, A. Sette, D. C. Binder, R. B. Liu, D. M. Kranz, S. C. Meredith, D. A. Rowley, and H. Schreiber. Relapse or eradication of cancer is predicted by peptide-major histocompatibility complex affinity. *Cancer Cell*, 23(4):516–526, Apr 2013.

[138] M. Giannakis, E. Hodis, X. Jasmine Mu, M. Yamauchi, J. Rosenbluh, K. Cibulskis, G. Saksena, M. S. Lawrence, Z. R. Qian, R. Nishihara, E. M. Van Allen, W. C. Hahn, S. B. Gabriel, E. S. Lander, G. Getz, S. Ogino, C. S. Fuchs, and L. A.

Garraway. RNF43 is frequently mutated in colorectal and endometrial cancers. *Nat Genet*, 46(12):1264–1266, Dec 2014.

[139] J. P. McCoy, W. H. Chambers, R. Lakomy, J. A. Campbell, and C. C. Stewart. Sorting minor subpopulations of cells: use of fluorescence as the triggering signal. *Cytometry*, 12(3):268–274, 1991.

[140] N. Hirano, M. O. Butler, Z. Xia, S. Ansén, M. S. von Bergwelt-Baildon, D. Neuberg, G. J. Freeman, and L. M. Nadler. Engagement of CD83 ligand induces prolonged expansion of CD8+ T cells and preferential enrichment for antigen specificity. *Blood*, 107(4):1528–1536, Feb 2006.

[141] N. Hirano, M. O. Butler, Z. Xia, A. Berezovskaya, A. P. Murray, S. Ansén, and L. M. Nadler. Efficient presentation of naturally processed HLA class I peptides by artificial antigen-presenting cells for the generation of effective antitumor responses. *Clin Cancer Res*, 12(10):2967–2975, May 2006.

[142] S. Rosskopf, S. Jutz, A. Neunkirchner, M. R. Candia, B. Jahn-Schmid, B. Bohle, W. F. Pickl, and P. Steinberger. Creation of an engineered APC system to explore and optimize the presentation of immunodominant peptides of major allergens. *Sci Rep*, 6:31580, 08 2016.

[143] X. Jiang, H. X. Hao, J. D. Growney, S. Woolfenden, C. Bottiglio, N. Ng, B. Lu, M. H. Hsieh, L. Bagdasarian, R. Meyer, T. R. Smith, M. Avello, O. Charlat, Y. Xie, J. A. Porter, S. Pan, J. Liu, M. E. McLaughlin, and F. Cong. Inactivating mutations of RNF43 confer Wnt dependency in pancreatic ductal adenocarcinoma. *Proc Natl Acad Sci U S A*, 110(31):12649–12654, Jul 2013.

[144] N. Zhu, D. Zhang, W. Wang, X. Li, B. Yang, J. Song, X. Zhao, B. Huang, W. Shi, R. Lu, P. Niu, F. Zhan, X. Ma, D. Wang, W. Xu, G. Wu, G. F. Gao, and W. Tan. A Novel Coronavirus from Patients with Pneumonia in China, 2019. *N Engl J Med*, 382(8):727–733, 02 2020.

[145] C. Huang, Y. Wang, X. Li, L. Ren, J. Zhao, Y. Hu, L. Zhang, G. Fan, J. Xu, X. Gu, Z. Cheng, T. Yu, J. Xia, Y. Wei, W. Wu, X. Xie, W. Yin, H. Li, M. Liu, Y. Xiao, H. Gao, L. Guo, J. Xie, G. Wang, R. Jiang, Z. Gao, Q. Jin, J. Wang, and B. Cao. Clinical features of patients infected with 2019 novel coronavirus in Wuhan, China. *Lancet*, 395(10223):497–506, 02 2020.

[146] W. J. Guan, Z. Y. Ni, Y. Hu, W. H. Liang, C. Q. Ou, J. X. He, L. Liu, H. Shan, C. L. Lei, D. S. C. Hui, B. Du, L. J. Li, G. Zeng, K. Y. Yuen, R. C. Chen, C. L. Tang, T. Wang, P. Y. Chen, J. Xiang, S. Y. Li, J. L. Wang, Z. J. Liang, Y. X. Peng, L. Wei, Y. Liu, Y. H. Hu, P. Peng, J. M. Wang, J. Y. Liu, Z. Chen, G. Li, Z. J. Zheng, S. Q. Qiu, J. Luo, C. J. Ye, S. Y. Zhu, N. S. Zhong, N. S. Zhong, L. J. Li, G. Zeng, G. F. Gao, and K. Y. Yuen. Clinical Characteristics of Coronavirus Disease 2019 in China. *N Engl J Med*, 382(18):1708–1720, 04 2020.

[147] I. Thevarajan, T. H. O. Nguyen, M. Koutsakos, J. Druce, L. Caly, C. E. van de Sandt, X. Jia, S. Nicholson, M. Catton, B. Cowie, S. Y. C. Tong, S. R. Lewin, and K. Kedzierska. Breadth of concomitant immune responses prior to patient recovery: a case report of non-severe COVID-19. *Nat Med*, 26(4):453–455, 04 2020.

[148] D. S. Fischer, M. Ansari, K. I. Wagner, S. Jarosch, Y. Huang, C. H. Mayr, M. Strunz, N. J. Lang, E. D'Ippolito, M. Hammel, L. Mateyka, S. Weber, L. S. Wolff, K. Witter, I. E. Fernandez, G. Leuschner, K. Milger, M. Frankenberger, L. Nowak, K. Heinig-Menhard, I. Koch, M. G. Stoleriu, A. Hilgendorff, J. Behr, A. Pichlmair, B. Schubert, F. J. Theis, D. H. Busch, H. B. Schiller, and K. Schober. Single-cell RNA sequencing reveals ex vivo signatures of SARS-CoV-2-reactive T cells through 'reverse phenotyping'. *Nat Commun*, 12(1):4515, 07 2021.

[149] K. I. Wagner, L. M. Mateyka, S. Jarosch, V. Grass, S. Weber, K. Schober, M. Hammel, T. Burrell, B. Kalali, H. Poppert, H. Beyer, S. Schambeck, S. Holdenrieder, A. Strötges-Achatz, V. Haselmann, M. Neumaier, J. Erber, A. Priller, S. Yazici, H. Roggendorf, M. Odendahl, T. Tonn, A. Dick, K. Witter, H. Mijočević, U. Protzer, P. A. Knolle, A. Pichlmair, C. S. Crowell, M. Gerhard, E. D'Ippolito, and D. H. Busch. T cell receptors in mild SARS-CoV-2 infection. *Cell Rep*, 38(2):110214, 01 2022.

[150] R. Holtappels, J. Podlech, M. F. Pahl-Seibert, M. Jülch, D. Thomas, C. O. Simon, M. Wagner, and M. J. Reddehase. Cytomegalovirus misleads its host by priming of CD8 T cells specific for an epitope not presented in infected tissues. *J Exp Med*, 199(1):131–136, Jan 2004.

[151] K. Stifter, J. Krieger, L. Ruths, J. Gout, M. Mulaw, A. Lechel, A. Kleger, T. Seufferlein, M. Wagner, and R. Schirmbeck. Pancreatic tumor cells selectively restores their TAP-mediated presentation competence and CD8 T-cell priming potential. *J Immunother Cancer*, 8(2), 08 2020.

[152] G. Willimsky, C. Beier, L. Immisch, G. Papafotiou, V. Scheuplein, A. Goede, H. G. Holzhütter, T. Blankenstein, and P. M. Kloetzel. In vitro proteasome processing of neo-splicetopes does not predict their presentation in vivo. *Elife*, 10, 04 2021.

[153] K. Y. Ma, A. A. Schonnesen, C. He, A. Y. Xia, E. Sun, E. Chen, K. R. Sebastian, Y. W. Guo, R. Balderas, M. Kulkarni-Date, and N. Jiang. High-throughput and high-dimensional single-cell analysis of antigen-specific CD8+ T cells. *Nat Immunol*, 22(12):1590–1598, 12 2021.

[154] B. Rodenko, M. Toebes, S. R. Hadrup, W. J. van Esch, A. M. Molenaar, T. N. Schumacher, and H. Ovaa. Generation of peptide-MHC class I complexes through UV-mediated ligand exchange. *Nat Protoc*, 1(3):1120–1132, 2006.

[155] S. Q. Zhang, K. Y. Ma, A. A. Schonnesen, M. Zhang, C. He, E. Sun, C. M. Williams, W. Jia, and N. Jiang. High-throughput determination of the antigen specificities of T cell receptors in single cells. *Nat Biotechnol*, Nov 2018.

[156] A. K. Bentzen, A. M. Marquard, R. Lyngaa, S. K. Saini, S. Ramskov, M. Donia, L. Such, A. J. Furness, N. McGranahan, R. Rosenthal, P. T. Straten, Z. Szallasi, I. M. Svane, C. Swanton, S. A. Quezada, S. N. Jakobsen, A. C. Eklund, and S. R. Hadrup. Large-scale detection of antigen-specific T cells using peptide-MHC-I multimers labeled with DNA barcodes. *Nat Biotechnol*, 34(10):1037–1045, Oct 2016.

[157] H. M. Kang, M. Subramaniam, S. Targ, M. Nguyen, L. Maliskova, E. McCarthy, E. Wan, S. Wong, L. Byrnes, C. M. Lanata, R. E. Gate, S. Mostafavi, A. Marson, N. Zaitlen, L. A. Criswell, and C. J. Ye. Multiplexed droplet single-cell RNA-sequencing using natural genetic variation. *Nat Biotechnol*, 36(1):89–94, 01 2018.

[158] M. Stoeckius, S. Zheng, B. Houck-Loomis, S. Hao, B. Z. Yeung, W. M. Mauck, P. Smibert, and R. Satija. Cell Hashing with barcoded antibodies enables multiplexing and doublet detection for single cell genomics. *Genome Biol*, 19(1):224, 12 2018.

[159] P. Hombrink, Y. Raz, M. G. Kester, R. de Boer, B. Weißbrich, P. A. von dem Borne, D. H. Busch, T. N. Schumacher, J. H. Falkenburg, and M. H. Heemskerk. Mixed functional characteristics correlating with TCR-ligand koff -rate of MHC-tetramer reactive T cells within the naive T-cell repertoire. *Eur J Immunol*, 43(11):3038–3050, Nov 2013.

[160] M. Nauerth, B. Weißbrich, R. Knall, T. Franz, G. Dössinger, J. Bet, P. J. Paszkiewicz, L. Pfeifer, M. Bunse, W. Uckert, R. Holtappels, D. Gillert-Marien, M. Neuenhahn, A. Krackhardt, M. J. Reddehase, S. R. Riddell, and D. H. Busch. TCR-ligand koff rate correlates with the protective capacity of antigen-specific CD8+ T cells for adoptive transfer. *Sci Transl Med*, 5(192):192ra87, Jul 2013.

[161] T. R. Müller, C. Schuler, M. Hammel, A. Köhler, S. Jutz, J. Leitner, K. Schober, D. H. Busch, and P. Steinberger. A T-cell reporter platform for high-throughput and reliable investigation of TCR function and biology. *Clin Transl Immunology*, 9(11):e1216, 2020.

[162] B. J. Cameron, A. B. Gerry, J. Dukes, J. V. Harper, V. Kannan, F. C. Bianchi, F. Grand, J. E. Brewer, M. Gupta, G. Plesa, G. Bossi, A. Vuidepot, A. S. Powlesland, A. Legg, K. J. Adams, A. D. Bennett, N. J. Pumphrey, D. D. Williams, G. Binder-Scholl, I. Kulikovskaya, B. L. Levine, J. L. Riley, A. Varela-Rohena, E. A. Stadtmauer, A. P. Rapoport, G. P. Linette, C. H. June, N. J. Hassan, M. Kalos, and B. K. Jakobsen. Identification of a Titin-derived HLA-A1-presented peptide as a cross-reactive target for engineered MAGE A3-directed T cells. *Sci Transl Med*, 5(197):197ra103, Aug 2013.

[163] G. P. Linette, E. A. Stadtmauer, M. V. Maus, A. P. Rapoport, B. L. Levine, L. Emery, L. Litzky, A. Bagg, B. M. Carreno, P. J. Cimino, G. K. Binder-Scholl, D. P. Smethurst, A. B. Gerry, N. J. Pumphrey, A. D. Bennett, J. E. Brewer, J. Dukes, J. Harper, H. K. Tayton-Martin, B. K. Jakobsen, N. J. Hassan, M. Kalos, and C. H. June. Cardiovascular toxicity and titin cross-reactivity of affinity-enhanced T cells in myeloma and melanoma. *Blood*, 122(6):863–871, Aug 2013.

[164] T. T. Spear, B. D. Evavold, B. M. Baker, and M. I. Nishimura. Understanding TCR affinity, antigen specificity, and cross-reactivity to improve TCR gene-modified T cells for cancer immunotherapy. *Cancer Immunol Immunother*, 68(11):1881–1889, Nov 2019.

[165] V. Jaravine, A. Mösch, S. Raffegerst, D. J. Schendel, and D. Frishman. Expitope 2.0: a tool to assess immunotherapeutic antigens for their potential cross-reactivity against naturally expressed proteins in human tissues. *BMC Cancer*, 17(1):892, 12 2017.

[166] A. K. Bentzen, L. Such, K. K. Jensen, A. M. Marquard, L. E. Jessen, N. J. Miller, C. D. Church, R. Lyngaa, D. M. Koelle, J. C. Becker, C. Linnemann, T. N. M. Schumacher, P. Marcatili, P. Nghiem, M. Nielsen, and S. R. Hadrup. T cell receptor fingerprinting enables in-depth characterization of the interactions governing recognition of peptide-MHC complexes. *Nat Biotechnol*, Nov 2018.

[167] C. Pfirschke, C. Engblom, S. Rickelt, V. Cortez-Retamozo, C. Garris, F. Pucci, T. Yamazaki, V. Poirier-Colame, A. Newton, Y. Redouane, Y. J. Lin, G. Wojtkiewicz, Y. Iwamoto, M. Mino-Kenudson, T. G. Huynh, R. O. Hynes, G. J. Freeman, G. Kroemer, L. Zitvogel, R. Weissleder, and M. J. Pittet. Immunogenic Chemotherapy Sensitizes Tumors to Checkpoint Blockade Therapy. *Immunity*, 44(2):343–354, Feb 2016.

[168] C. Wang, P. Kulkarni, and R. Salgia. Combined Checkpoint Inhibition and Chemotherapy: New Era of 1st-Line Treatment for Non-Small-Cell Lung Cancer. *Mol Ther Oncolytics*, 13:1–6, Jun 2019.

[169] S. Srivastava, S. N. Furlan, C. A. Jaeger-Ruckstuhl, M. Sarvothama, C. Berger, K. S. Smythe, S. M. Garrison, J. M. Specht, S. M. Lee, R. A. Amezquita, V. Voillet, V. Muhunthan, S. Yechan-Gunja, S. P. S. Pillai, C. Rader, A. M. Houghton, R. H. Pierce, R. Gottardo, D. G. Maloney, and S. R. Riddell. Immunogenic Chemotherapy Enhances Recruitment of CAR-T Cells to Lung Tumors and Improves Antitumor Efficacy when Combined with Checkpoint Blockade. *Cancer Cell*, 39(2):193–208, 02 2021.

[170] K. Reinhard, B. Rengstl, P. Oehm, K. Michel, A. Billmeier, N. Hayduk, O. Klein, K. Kuna, Y. Ouchan, S. Wöll, E. Christ, D. Weber, M. Suchan, T. Bukur, M. Birtel, V. Jahndel, K. Mroz, K. Hobohm, L. Kranz, M. Diken, K. Kuehlcke, O. Tuereci, and U. Sahin. An RNA vaccine drives expansion and efficacy of claudin-CAR-T cells against solid tumors. *Science*, 367(6476):446–453, 01 2020.

[171] A. Mackensen, C. Koenecke, J. Haanen, W. Alsdorf, A. Desuki, E. Wagner-Drouet, D. Heudobler, P. Borchmann, E. Wiegert, C. Schulz, B. Rengstl, L. Preussner, O. Tuereci, and U. Sahin. 958 bnt211: a phase i/ii trial to evaluate safety and efficacy of cldn6 car-t cells and vaccine-mediated in vivo expansion in patients with cldn6-positive advanced solid tumors. *Journal for ImmunoTherapy of Cancer*, 9(Suppl 2):A1008–A1008, 2021.

[172] K. Watanabe, Y. Luo, T. Da, S. Guedan, M. Ruella, J. Scholler, B. Keith, R. M. Young, B. Engels, S. Sorsa, M. Siurala, R. Havunen, S. Tähtinen, A. Hemminki, and C. H. June. Pancreatic cancer therapy with combined mesothelin-redirected chimeric antigen receptor T cells and cytokine-armed oncolytic adenoviruses. *JCI Insight*, 3(7), 04 2018.

[173] E. A. Stadtmauer, J. A. Fraietta, M. M. Davis, A. D. Cohen, K. L. Weber, E. Lancaster, P. A. Mangan, I. Kulikovskaya, M. Gupta, F. Chen, L. Tian, V. E. Gonzalez, J. Xu, I. Y. Jung, J. J. Melenhorst, G. Plesa, J. Shea, T. Matlawski, A. Cervini, A. L. Gaymon, S. Desjardins, A. Lamontagne, J. Salas-Mckee, A. Fesnak, D. L. Siegel, B. L. Levine, J. K. Jadlowsky, R. M. Young, A. Chew, W. T. Hwang, E. O. Hexner, B. M. Carreno, C. L. Nobles, F. D. Bushman, K. R. Parker, Y. Qi, A. T. Satpathy, H. Y. Chang, Y. Zhao, S. F. Lacey, and C. H. June. CRISPR-engineered T cells in patients with refractory cancer. *Science*, 367(6481), 02 2020.

[174] S. Hoogi, V. Eisenberg, S. Mayer, A. Shamul, T. Barliya, and C. J. Cohen. A TIGIT-based chimeric co-stimulatory switch receptor improves T-cell anti-tumor function. *J Immunother Cancer*, 7(1):243, 09 2019.

[175] S. Garetto, C. Sardi, E. Martini, G. Roselli, D. Morone, R. Angioni, B. C. Cianciotti, A. E. Trovato, D. G. Franchina, G. F. Castino, D. Vignali, M. Erreni, F. Marchesi, C. Rumio, and M. Kallikourdis. Tailored chemokine receptor modification improves homing of adoptive therapy T cells in a spontaneous tumor model. *Oncotarget*, 7(28):43010–43026, Jul 2016.

[176] I. Siddiqui, M. Erreni, M. van Brakel, R. Debets, and P. Allavena. Enhanced recruitment of genetically modified CX3CR1-positive human T cells into Fractalkine/CX3CL1 expressing tumors: importance of the chemokine gradient. *J Immunother Cancer*, 4:21, 2016.

[177] T. Shum, B. Omer, H. Tashiro, R. L. Kruse, D. L. Wagner, K. Parikh, Z. Yi, T. Sauer, D. Liu, R. Parihar, P. Castillo, H. Liu, M. K. Brenner, L. S. Metelitsa, S. Gottschalk, and C. M. Rooney. Constitutive Signaling from an Engineered IL7 Receptor Promotes Durable Tumor Elimination by Tumor-Redirected T Cells. *Cancer Discov*, 7(11):1238–1247, 11 2017.

[178] S. Lesch, V. Blumenberg, S. Stoiber, A. Gottschlich, J. Ogonek, B. L. Cadilha, Z. Dantes, F. Rataj, K. Dorman, J. Lutz, C. H. Karches, C. Heise, M. Kurzay, B. M. Larimer, S. Grassmann, M. Rapp, A. Nottebrock, S. Kruger, N. Tokarew,

P. Metzger, C. Hoerth, M. R. Benmebarek, D. Dhoqina, R. Grünmeier, M. Seifert, A. Oener, O. Umut, S. Joaquina, L. Vimeux, T. Tran, T. Hank, T. Baba, D. Huynh, R. T. A. Megens, K. P. Janssen, M. Jastroch, D. Lamp, S. Ruehland, M. Di Pilato, J. N. Pruessmann, M. Thomas, C. Marr, S. Ormanns, A. Reischer, M. Hristov, E. Tartour, E. Donnadieu, S. Rothenfusser, P. Duewell, L. M. König, M. Schnurr, M. Subklewe, A. S. Liss, N. Halama, M. Reichert, T. R. Mempel, S. Endres, and S. Kobold. T cells armed with C-X-C chemokine receptor type 6 enhance adoptive cell therapy for pancreatic tumours. *Nat Biomed Eng*, 5(11):1246–1260, 11 2021.

[179] J. A. Fraietta, C. L. Nobles, M. A. Sammons, S. Lundh, S. A. Carty, T. J. Reich, A. P. Cogdill, J. J. D. Morrissette, J. E. DeNizio, S. Reddy, Y. Hwang, M. Gohil, I. Kulikovskaya, F. Nazimuddin, M. Gupta, F. Chen, J. K. Everett, K. A. Alexander, E. Lin-Shiao, M. H. Gee, X. Liu, R. M. Young, D. Ambrose, Y. Wang, J. Xu, M. S. Jordan, K. T. Marcucci, B. L. Levine, K. C. Garcia, Y. Zhao, M. Kalos, D. L. Porter, R. M. Kohli, S. F. Lacey, S. L. Berger, F. D. Bushman, C. H. June, and J. J. Melenhorst. Disruption of TET2 promotes the therapeutic efficacy of CD19-targeted T cells. *Nature*, 558(7709):307–312, 06 2018.

[180] N. Jain, Z. Zhao, A. S. Iyer, M. Lopez, J. Feucht, R. P. Koche, Y. Zhan, and M. Sadelain. Loss of TET2 Uncouples Proliferative and Effector Functions in CAR T Cells. *Blood*, 136(Supplement 1):1–1, 11 2020.

[181] K. Beider, O. Itzhaki, J. Schachter, A. H. Grushchenko-Polaq, V. Voevoda-Dimenshtein, E. Rosenberg, O. Ostrovsky, O. Devillers, R. Shapira Frommer, L. A. Zeltzer, A. Toren, E. Jacoby, A. Shimoni, A. Avigdor, A. Nagler, and M. J. Besser. Molecular and Functional Signatures Associated with CAR T Cell Exhaustion and Impaired Clinical Response in Patients with B Cell Malignancies. *Cells*, 11(7), Mar 2022.

[182] P. Graef, V. R. Buchholz, C. Stemberger, M. Flossdorf, L. Henkel, M. Schiemann, I. Drexler, T. Höfer, S. R. Riddell, and D. H. Busch. Serial transfer of single-cell-derived immunocompetence reveals stemness of CD8(+) central memory T cells. *Immunity*, 41(1):116–126, Jul 2014.

[183] C. Stemberger, P. Graef, M. Odendahl, J. Albrecht, G. Dössinger, F. Anderl, V. R. Buchholz, G. Gasteiger, M. Schiemann, G. U. Grigoleit, F. R. Schuster, A. Borkhardt, B. Versluys, T. Tonn, E. Seifried, H. Einsele, L. Germeroth, D. H. Busch, and M. Neuenhahn. Lowest numbers of primary CD8(+) T cells can reconstitute protective immunity upon adoptive immunotherapy. *Blood*, 124(4):628–637, Jul 2014.

[184] T. Kaeuferle, R. Krauss, F. Blaeschke, S. Willier, and T. Feuchtinger. Strategies of adoptive T -cell transfer to treat refractory viral infections post allogeneic stem cell transplantation. *J Hematol Oncol*, 12(1):13, 02 2019.

[185] C. A. Vakulskas, D. P. Dever, G. R. Rettig, R. Turk, A. M. Jacobi, M. A. Collingwood, N. M. Bode, M. S. McNeill, S. Yan, J. Camarena, C. M. Lee, S. H. Park,

V. Wiebking, R. O. Bak, N. Gomez-Ospina, M. Pavel-Dinu, W. Sun, G. Bao, M. H. Porteus, and M. A. Behlke. A high-fidelity Cas9 mutant delivered as a ribonucleoprotein complex enables efficient gene editing in human hematopoietic stem and progenitor cells. *Nat Med*, 24(8):1216–1224, 08 2018.

[186] T. Kaeuferle, T. A. Stief, S. Canzar, N. N. Kutlu, S. Willier, D. Stenger, P. Ferrada-Ernst, N. Habjan, A. E. Peters, D. H. Busch, and T. Feuchtinger. Genome-wide off-target analyses of CRISPR/Cas9-mediated T-cell receptor engineering in primary human T cells. *Clin Transl Immunology*, 11(1):e1372, 2022.

[187] D. N. Nguyen, T. L. Roth, P. J. Li, P. A. Chen, R. Apathy, M. R. Mamedov, L. T. Vo, V. R. Tobin, D. Goodman, E. Shifrut, J. A. Bluestone, J. M. Puck, F. C. Szoka, and A. Marson. Polymer-stabilized Cas9 nanoparticles and modified repair templates increase genome editing efficiency. *Nat Biotechnol*, 38(1):44–49, 01 2020.

[188] S. Ghassemi, S. Nunez-Cruz, R. S. O'Connor, J. A. Fraietta, P. R. Patel, J. Scholler, D. M. Barrett, S. M. Lundh, M. M. Davis, F. Bedoya, C. Zhang, J. Leferovich, S. F. Lacey, B. L. Levine, S. A. Grupp, C. H. June, J. J. Melenhorst, and M. C. Milone. Reducing Ex Vivo Culture Improves the Antileukemic Activity of Chimeric Antigen Receptor (CAR) T Cells. *Cancer Immunol Res*, 6(9):1100–1109, 09 2018.

[189] C. Stemberger, K. M. Huster, M. Koffler, F. Anderl, M. Schiemann, H. Wagner, and D. H. Busch. A single naive CD8+ T cell precursor can develop into diverse effector and memory subsets. *Immunity*, 27(6):985–997, Dec 2007.

A Publications

Parts of this thesis have already been published or are submitted for publication.

First-author publications

- **Wagner KI***, Mateyka LM*, Jarosch S*, Grass V, Weber S, Schober K, Hammel M, Burrell T, Kalali B, Poppert H, Beyer H, Schambeck S, Holdenrieder S, Strötges-Achatz A, Haselmann V, Neumaier M, Erber J, Priller A, Yazici S, Roggendorf H, Odendahl M, Tonn T, Dick A, Witter K, Mijočević H, Protzer U, Knolle PA, Pichlmair A, Crowell CS, Gerhard M, D'Ippolito E, Busch DH. *Recruitment of highly cytotoxic CD8+ T cell receptors in mild SARS-CoV-2 infection.* Cell Rep. 2022 Jan 11;38(2):110214. doi: 10.1016/j.celrep.2021.110214. PMID: 34968416.

- Fischer DS*, Ansari M*, **Wagner KI***, Jarosch S, Huang Y, Mayr CH, Strunz M, Lang NJ, D'Ippolito E, Hammel M, Mateyka L, Weber S, Wolff LS, Witter K, Fernandez IE, Leuschner G, Milger K, Frankenberger M, Nowak L, Heinig-Menhard K, Koch I, Stoleriu MG, Hilgendorff A, Behr J, Pichlmair A, Schubert B, Theis FJ, Busch DH, Schiller HB, Schober K. *Single-cell RNA sequencing reveals ex vivo signatures of SARS-CoV-2-reactive T cells through 'reverse phenotyping'.* Nat Commun. 2021 Jul 26;12(1):4515. doi: 10.1038/s41467-021-24730-4. PMID: 34312385.

Review

- D'Ippolito E, **Wagner KI**, Busch DH. *Needle in a Haystack: The Naïve Repertoire as a Source of T Cell Receptors for Adoptive Therapy with Engineered T Cells.* Int J Mol Sci. 2020 Nov 6;21(21):8324. doi: 10.3390/ijms21218324. PMID: 33171940.

Collaborations

- Schambeck SE, Crowell CS, **Wagner KI**, D'Ippolito E, Burrell T, Mijočević H, Protzer U, Busch DH, Gerhard M, Poppert H, Beyer H. *Phantosmia, Parosmia, and Dysgeusia Are Prolonged and Late-Onset Symptoms of COVID-19.* J Clin Med. 2021 Nov 12;10(22):5266. doi: 10.3390/jcm10225266. PMID: 34830550.

- Weber S, Kehl V, Erber J, **Wagner KI**, Jetzlsperger A, Burrell T, Schober K, Schommers P, Augustin M, Crowell CS, Gerhard M, Winter C, Moosmann A,

Spinner CD, Protzer U, Hoffmann D, D'Ippolito E, Busch DH. *CMV seropositivity is a potential novel risk factor for severe COVID-19 in non-geriatric patients.* PLoS One. 2022 May 25;17(5)::e0268530. doi: 10.1371/journal.pone.0268530. PMID: 35613127.

- Purcarea A, Jarosch S, Barton J, Grassmann S, Pachmayr L, D'Ippolito E, Hammel M, Hochholzer A,**Wagner KI**, van den Berg JH, Buchholz VR, Haanen JBAG, Busch DH, Schober K. *Signatures of recent activation identify a circulating T cell compartment containing tumor-specific antigen receptors with high avidity.* Sci Immunol. 2022 Aug 12;7(74):eabm2077. doi: 10.1126/sciimmunol.abm2077. PMID: 35960818.

Conference Abstract

International Conference on Lymphocyte Engineering, Munich 2022

- **Wagner KI***, D'Ippolito E, Brutau-Abia A, Albert A, Sonntag R, Mejias-Luque R, Gerhard M, Busch DH. *Isolation and characterization of RNF43 neo-epitope specific TCRs for T cell therapy in gastrointestinal cancer.* Human Gene Therapy. 2022 Apr 30(4), pp. A26. doi: 10.1089/hum.2022.29200.abstracts

B Acknowledgements

In this section I would like to emphasize that the work presented in this thesis has been tremendously supported by many different people over the years. I thrived in the ambitious and highly collaborative research environment provided to me at the Institute for Medical Microbiology, Immunology and Hygiene at the Technical University of Munich.
First of all, I would like to thank Prof. Dr. Dirk Busch for accepting me as a Ph.D. student in his laboratory and providing me with continuous mentoring and support in the diverse projects I have been involved in. I would like to thank my other Ph.D. mentors Prof. Dr. Markus Gerhard and Prof. Dr. Roland Rad for valuable discussions, feedback and support for a smooth conduction of my thesis work.
I would like to acknowledge PD Dr. Kilian Schober who initially supervised my early Ph.D. work and was initiating the 'Reverse Phenotyping' project. Succeeding, I would like to express my gratitude to Dr. Elvira D'Ippolito who has been tremendously supportive to my work. With close team work on various projects, she helped in developing ideas, provided guidance and feedback. Her consistent support truly enhanced the process of finishing my thesis work.
A number of students have been working with me and supporting my projects during their internships and master theses. Especially, I would like thank Alexander Albert and Rachel Sonntag for their dedicated experimental work. I very much enjoyed the teaching experience. It has been a pleasure working in the Busch laboratory. Especially, Laura Mateyka and Sebastian Jarosch have had great impact on the success of the SARS-CoV-2 project work. I think we have proven the point that a team in research always succeeds in more than each individual person, and I truly valued working with them. Further, I would like to thank everyone being part of the group over the years: Sarah Dötsch, Thomas Müller, Pascal Winterhalter, Simone Weber, Adrian Straub, Linda Warmuth, Jack Barton, Sebastian Scheu, Jan Köhlen, Julius Schütz, Mortimer Svec, Anna Purcarea, Sabrina Wagner, Dr. Johannes Pettmann, Karl Moukarzel and Andreas Carr. Besides the support among the group of Ph.D. students, I am very thankful for the technical support from the lab technicians. Special thanks are dedicated to Monika Hammel who has supported my projects with her precise work and excellent technical experience. I would like to thank Franziska Graml, Anna Hochholzer and Noomen Hamed for the support on pMHC refolding and functionalization, as well as Füsun Gökmen, Laura Valentiner and Andrea Werner for general everyday lab work support.
I highly appreciate the work of the in-house sort facility run by Dr. Matthias Schiemann, Dr. Immanuel Andrä and the technicians Corinne Angerpointer, Lynette Henkel, Kerstin

Killisperger and Dharshini Raju for their dedicated work to provide high quality cell sorting.
I would like to thank PD Dr. Raquel-Mejias Luque and Anna Brutau-Abia for their support in the RNF43 project within the CRC1321 and continuous work in the TCR *in vivo* characterization.
The projects described in this thesis have been supported by a number of external collaborators. I would like to thank the clinical staff at the study sites for thorough blood sample collection during the COVID-19 pandemic.
Finally, I would like to thank my family who has encouraged me over the years. I am thankful for the financial support I received from my parents over the years of my university studies. My younger siblings Laura, Lars and Antonia have continuously supported with a strong familiar emotional backing. Further, I am grateful to my partner Jouke for his unconditional support and endowment to provide me an environment of calmness and sense of belonging.
Many thanks to my friends inside and outside of Munich who have been very understanding in times with longer working hours and always provided the right amount of distraction and recreation.